

**DANISH METEOROLOGICAL INSTITUTE**

————— **SCIENTIFIC REPORT** —————

**99-11**

**Inversion Methods for Atmospheric  
Profiling with GPS Occultations**

**Mette Dahl Meincke**



**COPENHAGEN 1999**

**ISSN-Nr. 0905-3263**  
**ISSN-Nr. 1399-1949 (Online)**  
**ISBN-Nr. 87-7478-400-5**

# Inversion Methods for Atmospheric Profiling with GPS Occultations

Ph.D. Thesis

Mette Dahl Meincke

November, 1999

The work presented in this thesis was carried out at the Department of Automation, Technical University of Denmark and at the Atmosphere Ionosphere Research Division, Danish Meteorological Institute in partial fulfilment of the requirements for the Ph.D. degree from the Technical University of Denmark.

This is a revised version of the original thesis on which basis the Ph.D. degree was awarded. A number of typographical errors has been corrected and minor editorial changes have been implemented relative to the original thesis.

Mette Dahl Meincke (formerly Mortensen),  
November 1999

## Abstract

Two high vertical resolution methods for inversion of Global Positioning System (GPS) radio occultation data are described: The Fresnel transform inversion method and the back-propagation inversion method. Both methods are specifically designed to provide accurate inversions of occultation data in the troposphere and around the tropopause of the Earth.

The resolution properties of the methods are characterized both from theoretical considerations and from numerical tests. Also the accuracy of the methods is assessed. The numerical tests are performed on simulated occultation data and on occultation measurements from the GPS/MET experiment. The results are compared to the results obtained with the geometrical optics inversion method, and in the cases of real measurements to data from the European Center for Medium Range Weather Forecasting (ECMWF).

One of the main findings is that the back-propagation inversion method is clearly superior to the Fresnel inversion method. The Fresnel inversion method has a limited average accuracy in comparison to the back-propagation inversion method. The back-propagation inversion method is also found to be superior to the geometrical optics inversion method. The lower limit of the vertical resolution of the back-propagation inversion method is  $\approx 100$  m while the horizontal resolution is  $\approx 250$  km. Noise and horizontal variations on a smaller scale than the horizontal resolution are shown to limit the accuracy of the inversion results.

The two thin screen inversion method is presented. This is a new method for inversion of GPS radio occultation data. The method extends the principles used for deriving the Fresnel transform inversion method. As the atmosphere is approximated using two thin screens instead of only one, as is done in the Fresnel transform inversion method, the two thin screen inversion method can model the troposphere more accurately. Also horizontal variation can be introduced. It is shown how to implement the method using a nonlinear iterative algorithm. An initial test result, of inversion of a simulated occultation data set in a spherically symmetric atmosphere, is shown. This test result shows that still some modifications are necessary to optimized the method. Primarily it is important to implement bend thin screens in the model, but also the numerical algorithm for performing the nonlinear inversion should be modified to reduce the level of numerical noise in the results. From the test result it is judged that when the method is optimized, high vertical resolution inversion results can be obtained with an accuracy better than 1 K in the lower troposphere and with a horizontal resolution of about 125 km.

## Dansk Resume

To højopløsningsmetoder til inversion af radio okkultations data fra det globale positioneringssystem (GPS) er beskrevet: Fresnel transformationsinversionsmetoden og tilbageudbredelsesinversionsmetoden. Begge metoder er blevet designet specielt med henblik på at give nøjagtige resultater ved inversion af okkultationsdata i jordens troposfære og tropopause.

Metodernes opløsningsegenskaber er karakteriseret både ud fra teoretiske overvejelser og ud fra numeriske tests. Yderligere er nøjagtigheden af metoderne beskrevet. De numeriske test er udført på simulerede okkultationsdata og på okkultationsmålinger fra GPS/MET eksperimentet. Resultaterne er sammenlignet med de resultater, der kan opnåes ved at anvende den geometrisk optiske inversionsmetode, og i tilfældene med rigtige måledata er der blevet sammenlignet med data fra det Europæiske Center for Vejrforudsigelser (ECMWF).

Et af de primære resultater af undersøgelserne er, at tilbageudbredelsesinversionsmetoden er overlegen set i forhold til Fresnel transformationsinversionsmetoden. Fresnel transformationsinversionsmetoden har en begrænset middelnøjagtighed sammenlignet med tilbageudbredelsesinversionsmetoden. Tilbageudbredelsesinversionsmetoden er også fundet overlegen set i forhold til den geometriske optiske inversionsmetode. Den nedre grænse for den vertikale opløsning af tilbageudbredelsesinversionsmetoden er  $\approx 100$  m, mens den horisontale opløsning er  $\approx 250$  km. Det er vist, at støj og horisontale variationer af en mindre størrelsesorden end den horisontale opløsning begrænser nøjagtigheden af inversionsresultaterne.

To-tyndskærmsinversionsmetoden er præsenteret. Dette er en ny metode til inversion af GPS radio okkultations data. Metoden udvider de principper, der blev anvendt til at udvikle Fresnel transformationsinversionsmetoden. Da atmosfæren bliver approksimeret ved hjælp af to tynde skærme i stedet for kun en, som det blev gjort i Fresnel transformationsinversionsmetoden, kan to-tyndskærms inversionsmetoden modellere troposfæren mere nøjagtigt. Endvidere kan horisontale variationer blive introduceret. Det er vist, hvordan metoden implementeres ved hjælp af en ikke-lineær iterativ algoritme. Et første testresultat, i form af inversion af et simuleret okkultationsdatasæt i en sfærisk symmetrisk atmosfære, er vist. Dette testresultat viser, at det stadig er nødvendigt at indføre visse modifikationer i implementeringen for at optimere inversionsmetoden. Primært er det vigtigt at implementere bøjede tynde skærme i modellen, men det er også nødvendigt at modificere den numeriske algoritme, der anvendes i den ikke-lineære inversion for at reducere niveauet af numerisk støj i resultaterne. Fra testresultatet vurderes det, at når metoden er optimeret, kan inversionsresultater med høj vertikal opløsning opnåes med en nøjagtighed bedre end 1 K i den lave del af troposfæren med en horisontal opløsning omkring 125 km.

## Preface

The work presented in this thesis was carried out at the Department of Automation, Technical University of Denmark (DTU) and at the Danish Meteorological Institute (DMI). Part of the work was carried out during a 5 months visit at the Jet Propulsion Laboratory (JPL), California, USA. The supervisors of the study have been Associate Professor Per Høeg, from the DMI and Associate Professor Ib Laursen and Senior Researcher Fritz Primdahl, from DTU.

I thank Per Høeg for involving me in the research in radio occultations performed at DMI. I got my initial experience with the subject of radio occultations and high resolution inversion methods for radio occultations during a one year study at DMI funded by the European Space Agency contract no. ESA/11930/96/NL/CN and ESA/11818/96/NL/CN. From this study I gained the interest in the subject of inversion methods for radio occultation data that has carried me through my Ph.D. work. I am grateful to everyone who were involved in these contracts.

I owe thanks to Ib Laursen and Fritz Primdahl for taking an interest in this project and neglecting that it is only remotely connected to their normal areas of research.

I thank Dr. Stephen Leroy for arranging my stay at JPL. During this stay I performed the validation tests of the Fresnel transform inversion method and of the back-propagation inversion method. I thank Dr. Rob Kursinski and Dr. Roger Linfield, JPL for the discussions on the results.

I am grateful to Dr. Stig Syndergaard, DMI and to Rob Kursinski and Roger Linfield for providing the simulated occultation data sets used for testing of the inversion methods. I am also grateful to the GPS/MET team at University Cooperation for Atmospheric Research, Boulder for providing the GPS/MET occultation data sets.

I sincerely thank Stig Syndergaard for undertaking the task of critically reading through this manuscript, and for many discussions about the value of the high vertical resolution inversion methods. Finally, I am also very grateful to Dr. Peter Meincke, DTU for his thorough reading of the last part of the manuscript, and for his support and comments while I was working on developing the two thin screen inversion method.

# Contents

<b>1</b>	<b>Introduction</b>	<b>1</b>
1.1	The Radio Occultation Principle . . . . .	1
1.2	Radio Occultation Measurements of the Atmosphere of the Earth . . . . .	2
1.3	The Importance of Accuracy and Resolution . . . . .	4
1.4	Content of the Thesis . . . . .	6
<b>2</b>	<b>Inversion Using the Geometrical Optics Approximation</b>	<b>7</b>
2.1	The Geometrical Optics Approximation . . . . .	7
2.2	Resolution and Error Aspects . . . . .	12
2.3	Derivation of Atmospheric Parameters . . . . .	16
2.4	Summary . . . . .	18
<b>3</b>	<b>Inversion Using the Fresnel Transform</b>	<b>19</b>
3.1	The Thin Screen Approximation . . . . .	20
3.2	The Fresnel Transform . . . . .	24
3.3	Resolution and Approximations . . . . .	29
3.4	Summary . . . . .	32
<b>4</b>	<b>Inversion Using the Back-Propagation Inversion Method</b>	<b>33</b>
4.1	2-D Wave Propagation . . . . .	34
4.2	Back-Propagation . . . . .	36
4.3	Resolution and Approximations . . . . .	41
4.4	Summary . . . . .	43

<b>5</b>	<b>Validation and Comparisons: Simulated Data</b>	<b>45</b>
5.1	Inversion Tests using Simulated Data . . . . .	45
5.2	Inversion Tests using Simulated Data with Noise . . . . .	54
5.3	Inversion Tests of the Importance of the Sampling Rate . . . . .	58
5.4	Summary . . . . .	60
<b>6</b>	<b>Validation and Comparisons: GPS/MET Data</b>	<b>61</b>
6.1	Comparing the Results from the Inversion Methods . . . . .	61
6.2	Comparisons with Independent Data . . . . .	64
6.3	Summary . . . . .	68
<b>7</b>	<b>The Fresnel Transform using Two Thin Screens</b>	<b>69</b>
7.1	Two Thin Screens versus one Thin Screen . . . . .	70
7.2	Wave Propagation with two Thin Screens . . . . .	72
7.3	Nonlinear Inversion . . . . .	74
7.4	An Example of the Inversion . . . . .	81
7.5	Discussion . . . . .	88
7.6	Summary . . . . .	90
<b>8</b>	<b>Conclusions</b>	<b>91</b>
8.1	High Vertical Resolution Inversion Methods . . . . .	91
8.2	A new Inversion Method . . . . .	93
8.3	Future Research . . . . .	94
<b>A</b>	<b>The Phase Modulation in a Spherically Symmetric Atmosphere</b>	<b>95</b>
<b>B</b>	<b>Papers</b>	<b>97</b>
	<b>References</b>	<b>115</b>



# Chapter 1

## Introduction

### 1.1 The Radio Occultation Principle

The radio occultation technique is a remote sensing method for profiling of planetary atmospheres. The principles for performing radio occultation measurements of planetary atmospheres was developed in the 1960's [e.g., *Fjeldbo and Eshleman, 1965; Phinney and Anderson, 1968*].

Figure 1.1 illustrates the occultation principle as it is applied in the planetary missions. A satellite is sent in orbit around the planet or passes by the planet. Onboard the satellite is a phase coherent radio transmitter which transmits signals to a receiver on Earth. That the signal is phase coherent means that the phase difference between the transmitter and the receiver can be measured accurately. In Figure 1.1 the signal propagation is illustrated with rays. The signal propagation is described by rays in the geometrical optics approximation which is valid when the signal frequency is high and the density of the medium, the signal propagates through, is low. On its way to the receiver, the radio signal will propagate through a part of the atmosphere of the planet. Which part of the atmosphere, the signal will propagate through, will depend on the position of the satellite relative to the receiver on Earth. In free space the radio signal

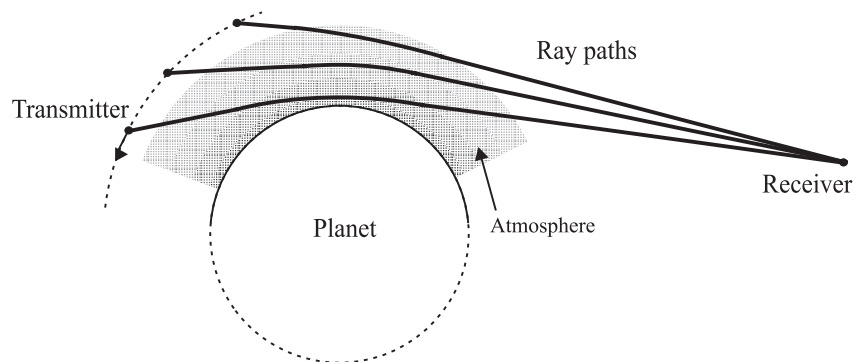


Figure 1.1: *The radio occultation principle as applied to planetary atmospheres.*

propagates as a ray in a straight line with the speed of light. In an atmosphere the ray will be bend, delayed, and attenuated due to the non-zero density of particles. The amplitude and phase of the radio signal measured at the receiver will thus be perturbed compared to a signal that has propagated through free space. The perturbations depend on both the density of particles and the type and state of the particles in the atmosphere. If the positions of the satellite and the receiver are known, the perturbations caused by the atmosphere can be extracted from the measured, phase coherent signal, and information on the atmosphere can be derived from the measurement.

In Figure 1.1 three ray paths have been shown to illustrate the increased bending of the ray path as the ray paths approach the planet. This situation occurs for an atmosphere which has neutral particles and an increasing density as the surface of the planet is approached. In general, planetary atmospheres have a relatively low density of particles and the density vary primarily in the radial direction [Fälthammar, 1994]. In the outer part of planetary atmospheres the particles will be ionized by radiation from space. When passing through an ionized layer the ray path will be bend in the direction away from the planet.

If the orbiting satellite with the transmitter is placed outside the atmosphere of the planet a measurement sequence can be started as the transmitter is in direct sight of the receiver, where the signal will not have to propagate through the atmosphere of the planet. The measurement sequence consists of a series of samples taken as the orbiting satellite sets behind the limb of the planet seen relative to the receiver. As the satellite sets, the received signal will have propagated through parts of the atmosphere closer and closer to the planet on the way to the receiver. The measurement sequence stops when the signal is lost because of blockage by the Earth. This measurement sequence constitutes a setting radio occultation measurement. Rising occultations where the measurement sequence is performed in reversed order are also possible.

The occultation measurement divides the atmosphere into successive layers, as each sample in the measurement represents one layer. The measurement starts outside the atmosphere, and ends at the surface of the Earth. Thus a single occultation measurement contains sufficient information about the atmosphere to be inverted to a vertical profile of the atmosphere using an assumption of spherical symmetry of the atmosphere. The radio occultation principle has been used with great success to probe the atmospheres of most of the planets in the solar system [e.g., Fjeldbo and Eshleman, 1968; Fjeldbo et al., 1971; Kliore et al., 1976; Tyler, 1987; Tyler et al., 1989; Lindal, 1992]

## 1.2 Radio Occultation Measurements of the Atmosphere of the Earth

Numerical weather forecasting and climate research have high demands for accurate and dense measurements of the atmosphere of the Earth. Measurements of the atmosphere primarily

consist of pressure, temperature, humidity and density distribution measurements and of wind measurements. The atmosphere is constantly changing its state, i.e., it is dynamic. The set of equations describing the changes in the state of the atmosphere are thus called dynamic equations [Holton, 1992]. Numerical models of the dynamic atmosphere is the basis for forecasting and climate research. The numerical models predict the future state of the atmosphere from knowledge of its present state by use of numerical approximations to the dynamic equations [Holton, 1992]. The time period, in which the state of the atmosphere can be accurately predicted from the numerical models, is limited by the density and accuracy of the measurements describing the present state of the atmosphere. At the moment weather forecasts are useful at most 5-6 days ahead. To improve this the global density of measurements of the atmosphere must be increased. For climate research, accurate mean values of the atmospheric state are the important inputs to predict trends. Thus this also requires highly accurate, globally distributed measurements.

Radio occultation measurements of the atmosphere of the Earth have for a long time been considered an option for achieving an unprecedented density of atmospheric measurements covering the entire Earth. An early suggestion was made by *Fischback* [1965], and the form in which the measurements are performed today was developed by, e.g., *Gurvich and Sokolovskiy* [1985]; *Hardy et al.* [1992]; and *Hajj et al.* [1994].

The Global Positioning System (GPS) which has been functioning since the 1980's provides the highly accurate phase coherent signal which is necessary for achieving sufficient accuracy in occultation measurements of the atmosphere of the Earth. As the name indicates the system is designed for precise positioning [Hofmann-Wellenhof et al., 1993]. The GPS satellite system is a constellation of 24 satellites deployed at a radius of  $\approx 26000$  km. The GPS system transmits signals at two frequencies: 1.57542 GHz and 1.22760 GHz. The phase coherence is obtained by using a ultra stable oscillator to generate the signals.

When the GPS system is used for occultation measurements of the atmosphere of the Earth, a low orbiting satellite (LEO) is used to receive the signals. When comparing with the radio occultation situation as it is illustrated in Figure 1.1 the receiver and the transmitter has been swapped but this has no influence on the principle. Figure 1.2 shows the occultation situation as it looks for the atmosphere of the Earth. The LEO satellite will typically be orbiting at a

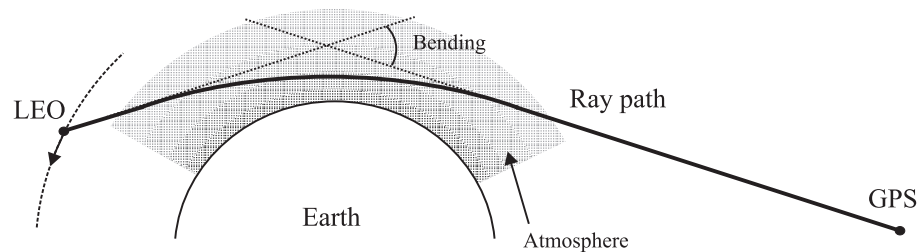


Figure 1.2: *The radio occultation principle as applied to the atmosphere of the Earth.*

height of approximately 600-800 km. At this height the satellite can almost be considered to be outside the atmosphere of the Earth. The total bending of the signal which has been indicated in Figure 1.2 reaches its maximum of approximately  $1^\circ$  just before the signal is lost as the LEO sets behind the limb of the Earth.

The primary inversion product from an occultation measurement is the refractive index of the atmosphere. From the refractive index, information on temperature, pressure, density, water vapor, and in the upper atmosphere electron density, can be derived. Currently the radio occultation principle for measurements of the atmosphere of the Earth has only been tested by one LEO satellite experiment: In 1995 the MicroLab-1 satellite carrying the GPS/MET experiment was launched. The GPS/MET experiment was meant as a proof of concept experiment and was very successful in that context [Ware *et al.*, 1996]. Statistical analysis of the GPS/MET data shows that a mean accuracy in the obtained temperature profiles better than 1 K is obtainable in the height range from  $\approx 1$  km to  $\approx 40$  km [Kursinski *et al.*, 1996; Rocken *et al.*, 1997; Steiner *et al.*, 1999]. The standard deviation of the results is 2-3 K. This is in comparison to acknowledged measurement methods like for example radiosonde measurements. These results are in agreement with the theoretical predictions [Kursinski *et al.*, 1997]. The corresponding vertical resolution varies from  $\approx 0.4$  km at the height 1 km to  $\approx 1.5$  km at the height 40 km. The horizontal resolution is  $\approx 250$  km.

Follow-up missions to the GPS/MET experiment on Microlab-1 are the Danish Ørsted satellite and the South-African SUNSAT which were launched in February 1999. Unfortunately the occultation data from these missions are not yet available. Due to the success of the GPS/MET experiment many other missions carrying a GPS occultation experiment, like the German CHAMP, the Argentinian SAC-C and the European METOP, will follow soon.

### 1.3 The Importance of Accuracy and Resolution

The inversion method which was initially used for inversion of the GPS/MET radio occultation data is based on a geometrical optics (GO) approximation of the propagation of the radio signals. The atmosphere of the Earth is horizontally stratified, i.e., the scale sizes in the horizontal direction is much larger than the scale sizes in the vertical direction. The resolution of the GO inversion method complies well with the scale sizes seen in the atmosphere of the Earth [McIlveen, 1986]. The primary exceptions from this occur in the lower troposphere, where water vapor and temperature inversion layers cause horizontal and vertical variations on a significantly smaller scale than what can be resolved by the GO inversion method. For weather forecasting purposes the limitations in the resolution as such is not an important problem as long as the errors introduced by the averaging can be determined [Zou *et al.*, 1998a, b]. Particularly the vertical resolution of the occultation data is significantly better than the vertical resolution used in the numerical weather prediction models. For climatological research, on the other hand, it is of interest to study for example the fine vertical scale structure of the tropopause and upper

troposphere [Leroy, 1997; Høeg and Jensen, 1998] and to resolve gravity waves [Steiner and Kirchengast, 1999].

Even if it is not of interest to resolve the small scale structures in the atmosphere, these structures can cause problems for the GO inversion method. The GO approximation is not valid in areas where small scale vertical and horizontal variations occur. Primarily, small scale vertical variations are known to be a problem [Gorbunov and Gurvich, 1998a]. Furthermore, the GO approximation is not valid near boundaries like for example the surface of the Earth. The result of the problems encountered for the GO inversion method can be errors of several degrees in the temperature profiles in a height range around the small scale variations.

Although the requirements on accuracy and resolution are generally lower in the planetary missions, problems with using the GO inversion method in connection with small scale vertical variations has been discovered. Thus, alternative inversion methods have been developed [Hubbard et al., 1978; Haugstad, 1978; Marouf et al., 1986]. The methods are high vertical resolution inversion methods. These methods are valid in the presence of small scale vertical variations and they can take the surface of the Earth into account. The methods cannot be used directly on the occultation measurements of the atmosphere of the Earth as they have been based on an assumption of the atmosphere being thin. This assumption is not valid for the lower part of the atmosphere of the Earth. Recently, it has gained much attention to adapt these methods to the case of occultation measurements of the atmosphere of the Earth [Gorbunov et al., 1996; Karayel and Hinson, 1997; Melbourne et al., 1994; Mortensen and Høeg, 1998b; Hocke et al., 1999]. The impact on the inversion results from the GPS/MET experiment has been found to be significant, primarily in the sense of reducing errors due to the approximations in the GO inversion method [Gorbunov and Gurvich, 1998a; Rocken et al., 1997; Mortensen and Høeg, 1998b]. If the noise level in the occultation data sets is low and there is no horizontal variations, the methods furthermore enhance the vertical resolution significantly [Karayel and Hinson, 1997; Gorbunov and Gurvich, 1998a; Mortensen et al., 1999; Mortensen and Høeg, 1998b].

The GO inversion method as well as the high vertical resolution inversion methods are all based on an assumption of spherical symmetry in the atmosphere. This assumption leads to a low horizontal resolution of the inversion results. An estimate is  $\approx 250$  km. It has been shown, that small scale horizontal variations will map into the vertical profile, which is the inversion result, and thus introduce errors [Belloul and Hauchecorne, 1997; Ahmad and Tyler, 1998a, b]. On the other hand, others have shown examples of frontal systems, which have relatively large horizontal gradients, being well retrieved [Kuo et al., 1997, 1998; Hardy et al., 1994].

This thesis is devoted to the description of high resolution inversion methods for radio occultation data. Emphasis is placed on determining the obtainable resolution and accuracy of the inversion methods. The inversion products that will be described are refractive index profiles and temperature profiles of the lower atmosphere, i.e., from a height of approximately 30 km and down to the surface of the Earth.

## 1.4 Content of the Thesis

The thesis is organized into 8 chapters. The main body of the thesis is the chapters 2-7.

The first part of the thesis consists of the chapters 2-6. These chapters concentrate on three different methods for inversion of radio occultation data.

Chapter 2 gives an overview of the GO inversion method. As this method is the original and most well known method used for inversion of occultation data, the chapter is only included as background material for the subsequent chapters. In Chapter 3, an inversion method termed the Fresnel transform inversion method is described. The method is a high vertical resolution inversion method for thin atmospheres. The method was developed for the planetary missions and adapted to the atmosphere of the Earth by *Melbourne et al.* [1994] and *Mortensen and Høeg* [1998a]. Chapter 4 describes the back-propagation inversion method, which is another high vertical resolution inversion method that has been developed recently [*Gorbunov et al.*, 1996; *Karayel and Hinson*, 1997; *Gorbunov and Gurvich*, 1998b]. The method has by now been relatively extensively tested and gives very good results [*Mortensen et al.*, 1999; *Rocken et al.*, 1997; *Hinson et al.*, 1997; *Gorbunov and Gurvich*, 1998a; *Hinson et al.*, 1998]. In each of the chapters 2-4 the theoretical limitations of the inversion methods with respect to accuracy and resolution are described.

Chapter 5 presents comparisons between the three inversion methods. On the basis of inversion of simulated occultation data the potentials and limitations of the methods are discussed. The results are related to the theoretical predictions. The methods are applied to occultation data from the GPS/MET experiment in Chapter 6. These results are furthermore compared to numerical weather prediction data.

The second part of the thesis consists of Chapter 7. This chapter is about a new inversion method. The method has been developed on the basis of the experience from the other inversion methods, and is a compromise between the methods presented in the first part. Particularly, the method contains the possibility to include horizontal information, i.e., improving the horizontal resolution. At the same time, the method keeps the high vertical resolution seen in the high vertical resolution methods presented in the first part of the thesis. The Chapter shows an initial result from inversion of a simulated occultation data set. The inversion method still needs some refinement before it can be applied routinely. On the basis of the test result the potentials of the method is discussed and compared to the results of the first part of the thesis.

Chapter 8 gives the conclusions and prospect for future work. Finally, copies of the papers [*Mortensen and Høeg*, 1998b] and [*Mortensen et al.*, 1999] are included in Appendix B.

## Chapter 2

# Inversion Using the Geometrical Optics Approximation

In the planetary missions, the original model used for describing the signal propagation in an occultation measurement was based on a geometrical optics (GO) approximation. When the radio occultation method was first used on the atmosphere of the Earth the same model was applied. The GO approximation is used to derive an inversion scheme for finding the refractive index from the measured data. A model for the refractive index dependence on the constituents of the atmosphere and the meteorological parameters is then used to derive the meteorological parameters.

Inversion of data from the GPS/MET experiment and statistical comparisons with other measurement methods has demonstrated the capabilities of the GO based inversion method to derive accurate profiles of the Earth's atmosphere [Ware *et al.*, 1996; Rocken *et al.*, 1997]. The statistics show an average error in the retrieved temperature of less than 1 K when compared to other measurements [Kursinski *et al.*, 1996; Rocken *et al.*, 1997; Steiner *et al.*, 1999].

This chapter about the GO inversion method has been included as background for the rest of the thesis. In Section 2.1 the GO inversion method will be described for occultation measurements of the atmosphere of the Earth. The limitations it imposes on the inversion results will be discussed in Section 2.2. In Section 2.3 the conversion of the refractive index to meteorological parameters will be described. Most of the conversion from refractive index to meteorological parameters is common to all the inversion methods to be described in this thesis.

### 2.1 The Geometrical Optics Approximation

The radio signals transmitted from the GPS satellite are electromagnetic waves and thus the propagation will be determined by Maxwell's equations. When the frequency of a transmitted

wave is sufficiently high the geometrical optics (GO) approximation may be used for describing the wave propagation.

The GO approximation is obtained by considering Maxwell's equations in the limiting case where the vacuum wavelength  $\lambda_0 \rightarrow 0$  [Born and Wolf, 1993, ch. 3]. This leads to the electromagnetic wave propagating as rays and these rays can, as will be shown below, be determined by geometrical considerations. The GO description of the electromagnetic wave is valid only under certain restrictions of the first and second order derivative of the electromagnetic field [Born and Wolf, 1993, sec. 3.1]. Also, the electromagnetic field itself must be finite. This implies that the GO approximation is not valid at shadow boundaries and caustics. For larger wavelengths the GO approximation will give a good description of the electromagnetic waves when the linear dimensions in a propagation problem are very large compared to the wavelength, outside areas close to caustics and shadow boundaries.

The frequencies of the two signals transmitted from the GPS satellites are  $f_1 = 1.57542$  GHz and  $f_2 = 1.22760$  GHz which gives a vacuum wavelength of the order of 20 cm. This dimension is very small compared to both the dimension of the occultation geometry and the features in the atmosphere which are ordinarily studied. Thus the GO approximation will in many cases be a good approximation for the wave propagation in an occultation measurement of the atmosphere of the Earth. The exceptions are in the vicinity of the limb of the Earth and in regions of very large refractive index gradients.

The GO approximation of the wave propagation in an occultation measurement is illustrated in Figure 2.1. Herein, the thick solid line illustrates the signal ray path from the GPS to the

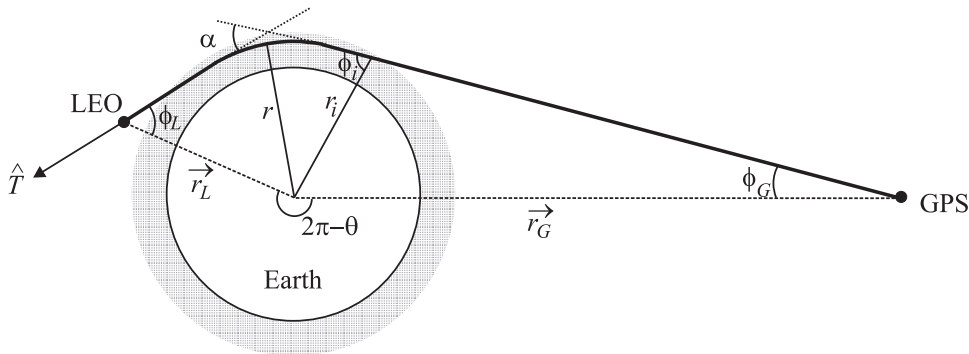


Figure 2.1: *Bending of a ray path in an occultation.*

LEO satellite. The direction of the ray path at any point is given by the unit tangent vector  $\hat{T}$ . The length of the radius vector  $\vec{r}_G$  from the center of the Earth to the GPS is  $r_G$ , and the length of the radius vector  $\vec{r}_L$  from the center of the Earth to the LEO is  $r_L$ . The angle between the radius vectors to the two satellites is given by  $\theta$ . The angle between the negative radius vector and the tangent to the ray path is at the GPS satellite denoted by  $\phi_G$ , and at the LEO satellite by  $\phi_L$ . At any given point on the ray path a radius vector with length  $r_i$ , and an angle between the negative radius vector and the tangent to the ray path  $\phi_i$  can be defined. The

closest distance to the center of the Earth is denoted by  $r$ . The total bending encountered by the signal during propagation from the GPS to the LEO satellite can be characterized by the angle  $\alpha$  between the initial direction of the ray at the GPS, and the direction of the ray at the LEO. This will be considered in Section 2.1.1.

Figure 2.1 only illustrates the ray path for a single sample in an occultation measurement. A complete occultation measurement consists of the sequence of samples obtained while the LEO sets behind or rises from the limb of the Earth seen with respect to the occulting GPS satellite. The occultation measurement starts when the signal from the GPS begins to propagate through the atmosphere, reaching values of  $r$  lower than  $r_G$  on the path to the LEO. The measurement stops when the signal is lost because it is blocked by the Earth.

The ray path in a geometrical optics approximation must follow the principle of Fermat. The principle of Fermat states, that the ray path between any two points  $P_1$  and  $P_2$  is defined by the optical path length having a stationary value [Born and Wolf, 1993, sec. 3.3]. If  $n$  denotes the refractive index then the ray path from  $P_1$  to  $P_2$  is determined from

$$\int_{P_1}^{P_2} n d\tau = \text{stationary value} \quad (2.1)$$

where  $d\tau$  denotes the infinitesimal length along the propagation path. In the limiting case of a boundary with a non-continuous variation of  $n$ , Fermat's principle results in Snell's law:

$$n_2 \sin \phi_2 = n_1 \sin \phi_1 \quad (2.2)$$

where indices 1,2 denotes the two different sides of the boundary, and the incident angle  $\phi$  is defined as the angle between the normal to the boundary and the ray tangent vector. Snell's law expresses that the refracted ray at a boundary lies in the same plane as the plane defined by the incident ray and the normal to the boundary surface. Furthermore, Snell's law expresses that the ratio of the sine of the angle of refraction to the sine of the angle of incidence is equal to the ratio between the refractive indices.

In an occultation measurement Fermat's principle and Snell's law can be used to derive the expressions for the ray path propagation. This can be used to derive an inversion scheme using the Abel transform which is the subject of the next subsection.

### 2.1.1 The Abel Transform

If the atmosphere of the Earth is assumed to be spherically symmetric, the atmosphere can be seen as consisting of a sequence of infinitesimal thin spherical layers to each of which Snell's law applies. In this case Snell's law results in [Born and Wolf, 1993, sec. 3.2]

$$n(r_i)r_i \sin \phi_i = \text{constant} \quad (2.3)$$

where  $r_i$  and  $\phi_i$  are defined in Figure 2.1. This is also known as Bouger's rule. In a spherically symmetric atmosphere the ray path will be a curve situated in a plane through the center of the Earth.

For a signal transmitted from outside the atmosphere, an initial ray path asymptote  $a$ , called the impact parameter, is defined. This denotes the perpendicular distance from the center of the Earth to the tangent of the ray. From Bouger's rule it follows that for a ray with impact parameter  $a$  the closest distance  $r$  to the center of the Earth for the ray will be given by [Fjeldbo *et al.*, 1971]

$$a = n(r)r. \quad (2.4)$$

This is because the closest distance to the Earth is obtained for  $\phi_i = 90^\circ$  and thus  $r$  is also called the tangent radius.

From geometrical considerations in Figure 2.1 it can be seen that the differential bending angle  $d\alpha$  and the angle  $\phi_i$  are connected as

$$d\alpha = -d\phi_i - \tan \phi_i \frac{1}{r} dr \quad (2.5)$$

which together with Bouger's rule (2.3) can be used to derive an expression for the total bending angle  $\alpha$  as a function of the impact parameter  $a$  [Fjeldbo *et al.*, 1971]

$$\alpha(a) = -2a \int_r^\infty \frac{1}{\sqrt{r'^2 n(r')^2 - a^2}} \frac{d \ln(n(r'))}{dr'} dr'. \quad (2.6)$$

In this,  $a$  and the tangent radius  $r$  are connected via (2.4). An expression for  $n(r)$  in terms of  $\alpha$  can be obtained from (2.6) using the Abel transform [Fjeldbo *et al.*, 1971]

$$\ln n(r) = \frac{1}{\pi} \int_a^\infty \frac{\alpha(a')}{\sqrt{a'^2 - a^2}} da'. \quad (2.7)$$

Thus if the bending angle as a function of the impact parameter can be derived for an occultation measurement, the radial refractive index profile can be derived from the Abel transform (2.7) with  $r = \frac{a}{n(r)}$  (2.4).

### 2.1.2 The Derivation of Bending Angles from an Occultation Measurement

In order to derive the bending angle from the occultation measurement, Fermat's principle (2.1) is applied. Fermat's principle provides a connection between the measured signal and the ray path. The illustration of a ray path for a sample in an occultation measurement which was shown in Figure 2.1 is repeated in Figure 2.2. Additionally, Figure 2.2 shows the geometry and the basic parameters characterizing the occultation in the GO approximation. The ray path is

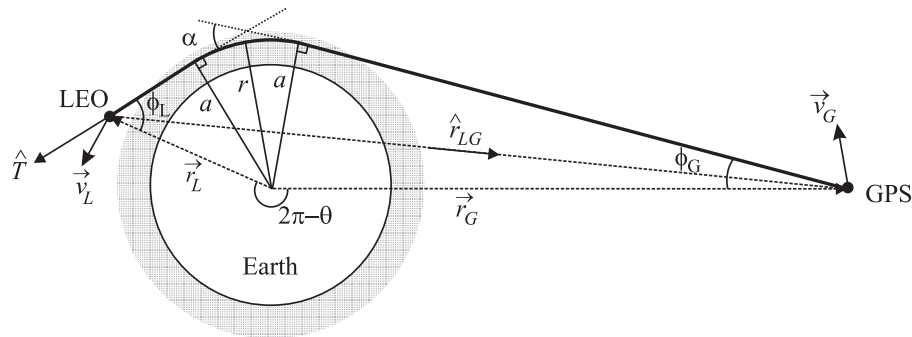


Figure 2.2: Occultation geometry.

again characterized by the direction vector  $\hat{T}$ . It is assumed that both the LEO and the GPS satellite are in an orbit outside the atmosphere of the Earth. Thus, the impact parameter  $a$  is defined by the ray path asymptotes at the satellites. The situation illustrated in Figure 2.2, where the impact parameter is the same on both sides of the atmosphere, is valid for a spherically symmetric atmosphere. The figure also shows the tangent radius  $r$ , as well as the bending angle  $\alpha$  for the ray path. The unit vector  $\hat{r}_{LG}$  denote the direction for the direct distance from the LEO to the GPS satellite. The vectors  $\vec{v}_L$  and  $\vec{v}_G$  denote the velocity vectors for the two satellites, respectively. The angles  $\theta$ ,  $\phi_G$ , and  $\phi_L$  have been defined previously.

The parameters  $\vec{r}_L$ ,  $\vec{r}_G$ ,  $\vec{v}_L$ , and  $\vec{v}_G$  are known from the orbit information of the satellites. From these, the direction vector  $\hat{r}_{LG}$  and the angle  $\theta$  can be found directly.

In accordance with Fermat's principle the phase of the signal measured at the LEO is per definition equal to the optical path length in a GO approximation. Thus, subtracting the phase due to the direct distance between the satellites, the measured excess phase  $\Delta\phi$  will be given by

$$\Delta\phi = k_T \left( \int_T n(r) d\tau - r_{LG} \right) = \text{stationary value} \quad (2.8)$$

where  $d\tau$  is the infinitesimal length along the ray path  $T$  and  $k_T$  denotes the vacuum wave number corresponding to the GPS signal with frequency either  $f_1$  or  $f_2$ . The excess phase  $\Delta\phi$  is dependent on both the LEO position and on time, as the occultation measurement consists of a series of samples measured as the LEO sets or rises seen with respect to the GPS satellite. Differentiating the expression (2.8) with respect to time, and invoking the endpoint transversality conditions from the calculus of variations, an expression for the measured Doppler residual is obtained [Melbourne *et al.*, 1994]

$$\frac{d(\Delta\phi)}{dt} = k_T [\vec{v}_L \cdot \hat{T}(\vec{r}_L) - \vec{v}_G \cdot \hat{T}(\vec{r}_G) - (\vec{v}_L \cdot \hat{r}_{LG} - \vec{v}_G \cdot \hat{r}_{LG})]. \quad (2.9)$$

In the relation (2.9) for the Doppler residual it is assumed that  $\Delta\phi$  has already been corrected for relativistic effects [Kursinski, 1997]. If the velocity vectors are projected onto the plane of the ray path and split into a radial component  $v^r$ , and a tangential component  $v^\tau$ , then the

Doppler residual can be written as

$$\frac{d(\Delta\phi)}{dt} = k_T[v_G^r \sin\phi_G - v_L^r \sin\phi_L + v_G^r \cos\phi_G + v_L^r \cos\phi_L - (\vec{v}_L \cdot \hat{r}_{LG} - \vec{v}_G \cdot \hat{r}_{LG})]. \quad (2.10)$$

Thus a relationship constraining the angles  $\phi_G$  and  $\phi_L$  have been obtained. From geometrical considerations the angles  $\phi_G$  and  $\phi_L$  can be seen to be related to the bending angle  $\alpha$  by

$$\alpha = \theta + \phi_G + \phi_L - \pi \quad (2.11)$$

and the impact parameter is related to the same angles by

$$a = r_G \sin\phi_G = r_L \sin\phi_L. \quad (2.12)$$

Using the equations (2.10), (2.11), and (2.12) the bending angle  $\alpha$  and the impact parameter  $a$  can be derived through an iterative procedure. For each sample in the occultation measurement, connected values of  $\alpha$  and  $a$  are obtained in this way resulting in a bending angle profile  $\alpha(a)$ .

The derived bending angle profile  $\alpha(a)$  is to be used to calculate the refractive index from the Abel transform (2.7). As it is assumed that both the GPS and the LEO satellite are orbiting outside the atmosphere of the Earth, there will be no contributions to the Abel transform integral (2.7) outside the occultation measurement area, and the integration can be cut off at the maximum measured impact parameter.

The Earth is slightly ellipsoidal. Thus, a better approximation of the atmosphere of the Earth - although still neglecting horizontal variations - is an ellipsoidal model. It has been shown [Syndergaard, 1998] that in the inversion, it is sufficient to approximate the ellipsoid by a sphere tangential to the ellipsoid at the occultation location. Then the satellite positions are referred to the center of this sphere instead of the center of the Earth and the spherically symmetric derivation still applies.

## 2.2 Resolution and Error Aspects

The spherically symmetric assumption used for deriving the GO inversion necessarily implies that the horizontal resolution along the propagation path be poor, as no horizontal variations in the local area intersected during an occultation is taken into account. On the other hand, the resolution in the radial direction, i.e., the vertical resolution will be good, as this will mainly be limited by the GO approximation. However, large derivations from spherical symmetry will impose limitations on the vertical resolution. Both the vertical and the horizontal resolution will of course also be degraded in the presence of noise.

The horizontal resolution  $\Delta L$  in an occultation measurement is normally defined as [Kursinski *et al.*, 1997]

$$\Delta L = 2\sqrt{2r\Delta r} \quad (2.13)$$

where  $\Delta r$  is the vertical resolution and  $r$  is the tangent radius. Thus, the horizontal resolution is defined by the distance traversed by the signal as it enters and exits a spherical layer of thickness  $\Delta r$ , at the distance  $r$  from the center of the Earth. As the density of the atmosphere of the Earth increases exponentially as  $r$  decreases, the gradient of the refractive index, and thereby the bending angle, will increase in a similar way. Thus, the contributions to the bending of a ray path is highly peaked at the tangent radius  $r$  [Kursinski *et al.*, 1997] and therefore, the thickness  $\Delta r$  is a good measure to define the horizontal resolution.

With regards to the vertical resolution, the measurements in the geometrical optics approximation are treated as if the contributions to the measured signal originates from just the stationary phase path. In reality there will be contributions that originates from all over the first Fresnel zone in every phase and amplitude measurement. Therefore the vertical resolution of the GO inversion method is limited, and the first Fresnel zone is a measure of the vertical resolution. The diameter of the first Fresnel zone  $\Delta r$  is given by [Melbourne *et al.*, 1994]

$$\Delta r = 2\sqrt{\lambda D \zeta(r)} \quad (2.14)$$

where  $\lambda$  is the wavelength of the signal,  $D$  is the distance of the LEO from the tangent point, and

$$\zeta^{-1} = 1 - D \frac{d\alpha}{dr}. \quad (2.15)$$

A LEO satellite will often be orbiting at a height of approximately 800 km above the surface of the Earth. For instance, the Microlab 1 satellite carrying the GPS/MET experiment has this height. This means that for the GPS-LEO occultation geometry  $D \approx 3000$  km. By using typical values of the variations of the refractive index to calculate  $\alpha(r)$ , it can be seen that the vertical resolution  $\Delta r$  will vary from approximately 0.4 km near the surface of the Earth (the lower troposphere) to approximately 1.5 km in the upper part of the atmosphere (the stratosphere). On the topside of large refractive index gradients the resolution can improve beyond these numbers. Large refractive index gradients often occurs in the lower troposphere. The corresponding horizontal resolution can from these measures and (2.13) be estimated to vary from approximately 150 km in the lower troposphere to approximately 280 km in the stratosphere.

In the third direction, i.e., the horizontal direction perpendicular to the ray path, the same finite width of the ray as in the vertical direction applies. Thus, the resolution can be said to be  $\approx 1.5$  km. However, seen from a point on the surface of the Earth the plane defined by the ray paths in an occultation measurement in a spherically symmetric atmosphere will not be vertical if the orbital planes of the satellites are at an angle. Normally, occultations are only measured if the angle between the anti-velocity direction of the LEO satellite and the GPS-LEO line is small, such as less than  $45^\circ$ . In this case, the horizontal movement perpendicular to the ray path, which may also be used as the measure of the resolution, is around 100 km.

Both the measure for the vertical and the measure for the horizontal resolutions have been derived under the assumption of spherical symmetry. The real atmosphere of the Earth is a three dimensional (3-D) varying medium, although the dominating variations in the refractive

index are radial. The relationship between the horizontal and vertical resolution derived under the assumption of spherical symmetry is such that it complies reasonably well with the scale sizes in the real atmosphere [McIlveen, 1986]. On the other hand, small-scale and large-scale phenomenon deviating from spherical symmetry will act as error sources in the inversion. Small-scale variations of sizes much less than the resolution can often be treated as being random while larger-scale variations will act as a bias sources in the inversion.

As just mentioned, the GPS and the LEO satellites do not generally orbit in the same plane and therefore, rays corresponding to lower radius will have passed through a different part of the upper atmosphere than those measured in the upper part. A horizontal gradient perpendicular to the ray paths will thus introduce an error in the GO inversion method. However, as the gradient of the refractive index decreases exponentially with height, these errors will have limited influence on the inversion. Worse is that horizontal gradients perpendicular to the ray path can change the ray path direction so that the ray path will not lie in a plane. This will introduce errors in the inversion. Horizontal gradients along the ray paths will also map into errors in the inversion. The errors will limit both the vertical resolution and the accuracy of the retrieved profiles, as the horizontal gradients will be mapped into vertical gradients. An assessment of some of the problems encountered can be found in [e.g., Ahmad, 1998]. The errors that can possible be encountered have been estimated to at least 1-2% of the refractive index close to the surface of the Earth [Ahmad and Tyler, 1998a].

### 2.2.1 Multipath

Small-scale structures in the atmosphere of sufficient amplitude can cause the GO inversion to give unreliable results. Small scale structures of large amplitude implies large gradients. In the presence of large vertical gradients there can be more than one ray path fulfilling Fermat's principle (2.8). This situation is called multipath. In the derivation of the bending angle profile from an occultation measurement, described in Section 2.1.2, a single ray path was assumed. Therefore, this approach will lead to erroneous calculations of the bending angle, if the phase measurement in reality must be approximated as the sum of several rays. When the bending angle as a function of the impact parameter is calculated, oscillations in the profile will appear such that several bending angles corresponds to the same impact parameter [Gorbunov *et al.*, 1996]. Thereby, the value to be used in the Abel transform (2.7) is ambiguous and an inversion, even if based on smoothing, will not necessarily give reasonable results.

As the different ray paths in the case of multipath propagation correspond to different incident angles and different Doppler residuals an advanced tracking algorithm in the LEO receiver and several channels could make it possible to track each ray path and thereby avoid the ambiguity problems [Kursinski *et al.*, 1997]. At present this has not been implemented in the receiver, and the multiple ray tracking method may cause problems in practise due to the influence from noise and the diffraction pattern on the tracking stability [Karayel and Hinson, 1997]. This is because even if multiple ray paths are taken into account, the geometrical optics approximation

is still an approximation of the real propagation of the electromagnetic signal.

In the real atmosphere the existence of layers with large refractive index gradients causing multipath propagation is common in the lower part of the atmosphere. Particularly, water vapor is known to cause gradients at the order of critical refraction, i.e., gradients that causes a signal to become trapped in a horizontal layer [Skolnik, 1980, sec. 12.5].

### 2.2.2 Other Errors

So far only errors originating from the deviation of the atmosphere from spherical symmetry and from the violation of the GO approximation have been discussed. This is because these errors are specific for the inversion method. There are numerous other error sources, however, in an occultation measurement. These must be taken into account if the overall inversion error for the derivation of the refractive index is to be estimated.

A general error source is measurement errors. The positions of the satellites are only known with a finite accuracy and thus, the phase measurement can only be performed with a finite accuracy. The measurement method in it self also introduces thermal noise on the phase. Furthermore, the LEO satellite is not necessarily orbiting outside the atmosphere of the Earth, which introduces initialization errors in the inversion process.

As already mentioned, small scale variations of sizes much less than the resolution in the atmosphere will act as noise on the measurement. This noise together with the thermal noise will cause inversion problems, particularly for large tangent heights (the tangent radius subtracted by the radius of curvature of the Earth) where the atmosphere is thin. As the noise is random, smoothing the data can limit the inversion errors. It is common to use a simple smoothing window with the width of the estimated vertical resolution [Rocken *et al.*, 1997]. At tangent heights above 60-80 km the atmosphere is so thin that a model atmosphere is often used in combination with the measured results to limit the inversion error, as the noise is large compared to the obtained refractive index [Hocke, 1997; Sokolovskiy and Hunt, 1996; Gorbunov and Gurvich, 1998b]. Error sources that are not of random nature but rather systematic will cause biases in the inversion results.

Measurement error sources and their influence on the GO inversion method have been extensively treated by others. Detailed descriptions of the error sources with estimates of their sizes can be found in [Kursinski *et al.*, 1997; Syndergaard, 1999b] and [Steiner, 1998]. The total error estimates for the refractive index is height dependent and varies between 0.1% at  $\approx 35$  km and 1% at  $\approx 0$  km [Kursinski, 1997]. This does not account for multipath problems or large-scale horizontal variations where some of the basic assumptions of the inversion method are violated.

### 2.3 Derivation of Atmospheric Parameters

The refractive index in the atmosphere depends on the dry neutral atmosphere, water vapor, free electrons in the ionosphere, and particulates. In this thesis, only the neutral atmosphere is considered, and the aim has been to derive temperature profiles for meteorological usage. According to the assumption of spherical symmetry, the refractive index is dependent on the radius. When deriving profiles in the atmosphere the height  $h$  compared to the surface of the Earth is a more common term to use than the radius. The relation between  $h$  and  $r$  is given by

$$h = r - R_e \quad (2.16)$$

where  $R_e$  denotes the the local radius of curvature of the Earth. The refractive index in the atmosphere is very close to unity, so instead the refractivity defined by

$$N(h) = (n(h) - 1) \cdot 10^6 \quad (2.17)$$

is used. To first order the refractivity in the atmosphere of the Earth is given by [Bevis *et al.*, 1994]

$$N = 77.6 \frac{P}{T} + 3.73 \cdot 10^5 \frac{P_W}{T^2} + 70.4 \frac{P_W}{T} - 4.03 \cdot 10^7 \frac{n_e}{f_T^2}. \quad (2.18)$$

In this,  $P$  denotes the atmospheric pressure in mbar,  $T$  is the atmospheric temperature in kelvin,  $P_W$  is the water vapor partial pressure in mbar,  $n_e$  is the electron number density per cubic meter, and  $f_T$  is the signal frequency in hertz. The dependence of the parameters on height has been omitted. The influence of particulates can be ignored in a first order approximation [Kursinski, 1997]. This expression has been derived for microwave signal frequencies, e.g., it is valid for the GPS signals. The refractivity dependence on the neutral atmosphere has been found experimentally [Bevis *et al.*, 1994]. In this reference, the constants and their uncertainties are discussed. Ordinarily, the uncertainties are ignored in the processing of occultation data although a more thorough investigation of the relationship and the error introduced by it may be desirable [Kursinski *et al.*, 1997]. The ionosphere term, which in (2.18) is the term depending on  $n_e$ , is found from a first order expansion of the Appleton-Hartree formula for the refractive index in the ionosphere [e.g., Høeg *et al.*, 1995]. The higher order terms are not always negligible, i.e., by using (2.18) residual ionospheric errors may be introduced [Melbourne *et al.*, 1994].

To derive the neutral atmosphere parameters from the refractivity it is necessary to correct for the ionospheric contribution. In (2.18) the only frequency dependent term is the ionospheric term. Thus by combination of the two signals from the GPS with frequencies  $f_1$  and  $f_2$ , it is possible to correct for the ionospheric term. If the first order expansion of the ionosphere term in (2.18) is assumed to be correct, a correction method can be inferred from (2.8) using height  $h$  instead of the radius  $r$ :

$$\Delta\phi_{f_T} = \frac{2\pi f_T}{c} \left( \int_T \left[ n_{neu}(h) - 40.3 \frac{n_e(h)}{f_T^2} \right] d\tau - r_{LG} \right) \quad (2.19)$$

where  $f_T$  is either  $f_1$  or  $f_2$  and  $n_{neu}$  denotes the first 3 terms of (2.18). If it is assumed that the propagation paths for the two signals are the same, an expression for the neutral atmospheric excess phase is

$$\Delta\phi_{L_c} = \frac{c}{2\pi} \frac{f_1\Delta\phi_{f_1} - f_2\Delta\phi_{f_2}}{f_1^2 - f_2^2} = \int_T n_{neu}(h) d\tau - r_{LG}. \quad (2.20)$$

Thus, if normalized by the wave number  $k_T$ , the expressions for the Doppler residual (2.9)-(2.10) in Section 2.1.2 can be used to calculate the neutral atmosphere bending angle if the neutral atmospheric excess phase  $\Delta\phi_{L_c}$  is used in the expressions instead of  $\Delta\phi$ .

The assumption that the two signals follow the same path in the ionosphere is only approximately fulfilled [Melbourne *et al.*, 1994], and use of this assumption introduces an error in the correction method. To avoid this problem, and also the problem with the higher order ionosphere terms contributing to the refractivity, other ionospheric correction methods have been and are being developed [Vorob'ev and Krasi'nikova, 1994; Hocke, 1997; Syndergaard, 1999a]. The main influence on the retrieved neutral atmospheric parameters from errors in the ionosphere correction is at large heights, i.e., above  $\approx 40$  km.

Now only three terms remains in the expression (2.18) for the refractivity dependence on atmospheric parameters. Two of them dependent on  $P_W$  and thus they are water vapor terms. For heights larger than  $\approx 8$  km the water vapor contribution to the refractivity is negligible [Kursinski, 1997]. For lower heights the water vapor must generally be taken into account but in many cases - away from the tropic regions - the atmosphere will be dry so that the water vapor terms can be ignored. Therefore, the so called dry temperature, assuming no water vapor, is derived from the refractivity expression. If there is a significant amount of water vapor in the atmosphere, the dry temperature will be of the order of  $\approx 2 - 5$  K in error close to the Earth compared to the actual temperature [Rocken *et al.*, 1997]. In an atmosphere with a significant amount of water vapor, which is spatially highly variable, multipath propagation is often seen [Gorbunov and Gurvich, 1998a]. As previously mentioned this can cause the GO inversion method to give unreliable results.

Now, only the first term of the refractivity expression (2.18) is left. This term depends on the relation between the pressure and the temperature. Using the equation of state this can be translated to density. So in case of negligible water vapor content, the density  $\rho(h)$  can be found from the refractivity as

$$\rho(h) = \frac{1}{77.6R} N(h) \quad (2.21)$$

where  $R = 287.09 \text{ JK}^{-1} \text{ kg}^{-1}$  is the gas constant normalized with the mean molar mass of dry air. The pressure  $P(h)$  can then be derived from the density using the assumption of hydrostatic equilibrium, i.e.,

$$\frac{dP(h)}{dh} = -g(h)\rho(h) \quad (2.22)$$

where  $g(h)$  is the height dependent acceleration of gravity. To obtain the total pressure, the hydrostatic equilibrium equation (2.22) need to be integrated giving

$$P(h) = \int_h^{\infty} dP = - \int_h^{h_{max}} \rho(h)g(h) dh + P(h_{max}) \quad (2.23)$$

where  $h_{max}$  denotes the maximum height used in the inversion and  $P(h_{max})$  denotes the pressure at this height. Finally, reusing the equation of state the temperature is given by

$$T(h) = \frac{P(h)}{R\rho(h)}. \quad (2.24)$$

The derivation of neutral atmospheric parameters are usually initiated at a height of 60-80 km. Above this, the measurement errors and the residual errors from the ionosphere correction will be dominating and thus make the inversion to neutral atmospheric parameters difficult. The pressure profile can be initialized at  $h_{max}$  with a climatologic atmosphere model. As the pressure decreases exponentially with height, the error introduced from using a climatological model for initialization of the pressure calculation (2.23) will be  $\ll 1$  K below  $\approx 40$  km [Kursinski *et al.*, 1997].

When taking all error sources into account, the average expected accuracy in the temperature inversion amounts to  $\approx 1$  K below 40 km height for dry atmosphere conditions [Steiner, 1998; Kursinski *et al.*, 1997]. As already mentioned, this expectation can however be violated by multipath propagation and large-scale horizontal variations. These theoretical results have been confirmed by statistical analysis of occultation data from the GPS/MET experiment [Rocken *et al.*, 1997; Kursinski *et al.*, 1996; Steiner *et al.*, 1999].

## 2.4 Summary

In this chapter it has been shown how the geometrical optics approximation for the signal propagation in an occultation measurement results in an inversion method for a spherically symmetric atmosphere. From the measured Doppler residual of the GPS signal and the geometry, the bending angle profile can be derived. This can be inverted to a refractive index profile by use of the Abel transform. From the refractive index, density, pressure and temperature profiles can be derived for the neutral atmosphere by assuming negligible water vapor content. The resolution limits and error sources arising from using the geometrical optics approximation on a real 3-D atmosphere have been discussed. Large vertical gradients and horizontal variations in the atmosphere are the dominating error sources connected to the geometrical optics inversion method in the troposphere.

## Chapter 3

# Inversion Using the Fresnel Transform

Even though the vertical resolution of the geometrical optics (GO) inversion method, described in the previous chapter, is good, inversion methods that can improve it have been developed. For example it is of interest to have the best possible vertical resolution in the region around the tropopause where very sharp changes in the temperature profile occurs, see [e.g., *Høeg and Jensen, 1998*]. Furthermore, it is of interest to overcome the multipath problem in the GO inversion method. In connection with the planetary mission experiments, the method of enhancing the vertical resolution of the recovered refractive index profiles by using the theory of Fresnel diffraction was developed and extensively used [e.g., *Hubbard et al., 1978; Hinson and Magalhaes, 1991; Marouf et al., 1986*]. Use of the same method to enhance the resolution of the recovered refractive index profiles for Earth measurements was proposed by *Melbourne et al. [1994]*. The method has been further developed and tested showing promising results [*Mortensen and Høeg, 1998a*].

The idea in using the theory of Fresnel diffraction in the inversion of atmosphere profiles from radio occultation measurements is schematically illustrated in Figure 3.1. The first Fresnel zone define the vertical resolution and is, as described in Chapter 2, the area from which contributions

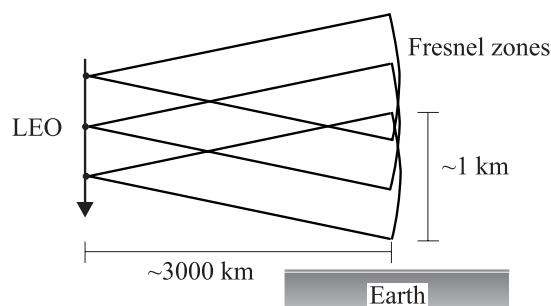


Figure 3.1: *Schematic illustration of the overlapping first Fresnel zones at the Earth's limb contributing to the LEO measurement.*

to the electromagnetic signal measured in one point originates. The figure illustrates that when a sufficiently high sampling rate is used by the receiver onboard the LEO satellite, the first Fresnel zones from different samples will overlap. The theory of Fresnel diffraction is a way to deconvolve the information contained in the overlapping first Fresnel zones from different samples, to obtain a better vertical resolution in the inversion to refractive index.

In Section 3.1 the theory of Fresnel diffraction for radio occultation measurements of the atmosphere of the Earth is described. In Section 3.2 an inversion method based on Fresnel diffraction theory will be derived, and in Section 3.3 the resolution and the limitations of the method are described.

### 3.1 The Thin Screen Approximation

The basis of the Fresnel diffraction theory used here is the thin screen model. In this model it is assumed, that the propagation distance of the GPS signal through the atmosphere of the Earth is so short, compared to the distances to the satellites, that the atmosphere of the Earth can be approximated as a infinitesimal thin screen. Outside the thin screen the signal is assumed to propagate in free space. For the thin screen approximation to be valid it is necessary that the atmosphere is thin. The validity of the approximations for the atmosphere of the Earth can be expressed in terms of the geometrical optics parameters used in Chapter 2. Thus, the atmosphere and the occultation geometry must fulfill [Melbourne *et al.*, 1994]:

$$\alpha/\sqrt{H/a} \ll 1 \quad (3.1)$$

The atmospheric scale height is denoted by  $H$ , and  $\alpha$  and  $a$  is the bending angle and the impact parameter, respectively. For the Earth,  $\alpha/\sqrt{H/a} \approx 0.5$  near the surface [Melbourne *et al.*, 1994]. Thus it should be noted, that the condition for validity of the thin screen approximation is not very well fulfilled, and particularly not so close to the surface of the Earth.

The thin screen model is illustrated in Figure 3.2. The thin screen is placed in the  $xy$ -plane at  $z = 0$ , where the  $z$ -axis is placed along the straight line between the GPS and the LEO satellite. In the figure,  $d_L$  and  $d_G$  denote distances from the GPS and the LEO satellite, respectively, to an area element  $d\vec{S}$  in the thin screen. The area element  $d\vec{S}$  is directed towards the GPS

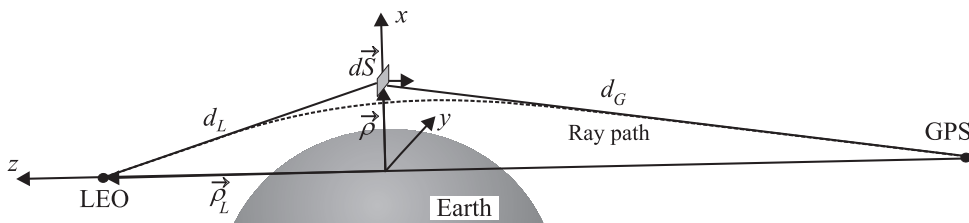


Figure 3.2: *Geometry of the thin screen model.*

satellite. Furthermore,  $\vec{\rho}$  is the vector going from the center of the coordinate system to  $d\vec{S}$ , and  $\vec{\rho}_L$  is the vector from the center of the coordinate system to the LEO satellite.

The basic equation used in the model is the Helmholtz-Kirchhoff integral theorem for the thin screen [Born and Wolf, 1993, sec. 8.3], [Goodman, 1986], which is a solution to the free space wave equation

$$\mathcal{E}(\vec{\rho}_L, t) = \frac{1}{2\pi c} \iint_S \frac{\partial \mathcal{E}(\vec{\rho}, t_\rho)}{\partial t_\rho} \frac{(\vec{\rho} - \vec{\rho}_L) \cdot d\vec{S}}{|\vec{\rho} - \vec{\rho}_L|^2}. \quad (3.2)$$

The theorem is a general expression giving the scalar electric field  $\mathcal{E}$  at  $(\vec{\rho}_L, t)$  if the field is known all over a distant, plane surface  $S$  at a time  $t_\rho$ . In (3.2)  $c$  is the velocity of light. The time  $t_\rho$  must fulfill

$$t_\rho = t - \frac{|\vec{\rho} - \vec{\rho}_L|}{c} = t - \frac{d_L}{c}, \quad (3.3)$$

thus allowing the signal to propagate from the point  $\vec{\rho}$  in the thin screen  $S$  to the point  $\vec{\rho}_L$ . The integral theorem (3.2) is valid for  $k_T |\vec{\rho} - \vec{\rho}_L| \gg 1$ ,  $k_T$  being the wave number corresponding to the signal frequency, which is  $f_1$  or  $f_2$  for the GPS signal.

In the case of radio occultation measurements at the Earth, the field described by the integral theorem (3.2) is the field at the LEO. The field arriving at the thin screen is the signal from the GPS. It is assumed that the GPS signal propagates in free space. Because of the long distance from the GPS satellite to the thin screen, the field will be a spherical wave, attenuated with the reciprocal of the distance to the GPS, and with the phase equally delayed by the distance the spherical wave has propagated. Thus, the field from the GPS at the thin screen will be the real part of the expression

$$\mathcal{E}(\vec{\rho}, t) = \frac{\tilde{A}}{d_G} \exp \left[ -i\omega_T \left( t_\rho - \frac{d_G}{c} \right) \right]. \quad (3.4)$$

Here  $\tilde{A}$  is the amplitude of the signal emitted by the GPS satellite and  $\omega_T = 2\pi f_T$  is the angular frequency.

The propagation of the field through the atmosphere is modulated by adding a phase modulation, in the form  $\exp(i\Psi(x, y))$ , to the field from the GPS at the thin screen. The phase modulation  $\Psi(x, y)$  due to the atmosphere is found from a geometrical optics (GO) approximation of the signal propagation through the atmosphere

$$\Psi(x, y) = k_T \int_T (n(r) - 1) d\tau, \quad (3.5)$$

where  $n(r)$  is the refractive index as a function of the radial distance from the Earth, and the integration is performed along the actual ray path  $T$  through the Earth's atmosphere. The refractive index dependency of radius indicate that spherical symmetry is assumed. This is a

natural assumption on the basis of the thin screen approximation which cannot account for variations perpendicular to the thin screen. The geometrical optics approximation is known to be good for the atmosphere, if the propagation distance is short, see Section 2.2. The propagation distance through the atmosphere is a short distance relative to the distances from the atmosphere to the satellites. Thus as the phase modulation only accounts for the phase propagation through the atmosphere, the GO approximation can be used without imposing limitations on the inversion results. This is true both with respect to the vertical resolution and with respect to multipath problems.

If the complex version of the measured field  $\mathcal{E}(\vec{\rho}_L, t)$  at the LEO is expressed as  $E(\vec{\rho}_L, t) \cdot \exp(i\phi(\vec{\rho}_L, t) - i\omega_T t)$ , then the Helmholtz-Kirchoff integral theorem (3.2) can be rewritten as

$$E(\vec{\rho}_L) \exp(i\phi(\vec{\rho}_L)) = \frac{k_T}{2\pi i} \iint_S \frac{\hat{A}(x, y)}{d_L d_G} \exp[ik_T (d_L + d_G)] \exp[i\Psi(x, y)] dx dy, \quad (3.6)$$

giving a measure of the amplitude and total phase at the LEO-satellite. The real part of the expression will be equal to the actual measured field. The harmonic time-dependence has been suppressed by use of (3.3). The attenuation and absorption by the atmosphere is added into the amplitude factor  $\hat{A}$ , giving a modified amplitude factor  $\hat{A}$ , which also accounts for the obliquity factor  $(\vec{\rho} - \vec{\rho}_L) \cdot d\vec{S} / |\vec{\rho} - \vec{\rho}_L| dS$  of the ray incident at the screen. The receiving antennas gain function should be taken into account in order to modulate the field received by the LEO, but it will be assumed to equal 1 here, or already taken into account in the measured signal.

It is possible to introduce further simplifications in the expression (3.6). First of all, the Fresnel approximation can be used. The Fresnel approximation consists of using the second order Taylor expansion of a distance  $d$  [Collin, 1985, sec. 2.6], i.e.,

$$d \simeq z + \frac{x^2 + y^2}{2z} \approx z \quad (3.7)$$

which is valid for  $z_L, z_G \gg x, y$ . In (3.7)  $x, y$  are coordinates in the thin screen, and  $z_L, z_G$  are the perpendicular distances from the satellites to the thin screen. The second order development of the distance is used for phase expressions. To approximate the amplitude, it is sufficient to use the perpendicular distances  $z_L$  and  $z_G$ . The Fresnel approximation can be used, because the small size of the first Fresnel zone at the screen compared to the distances to the satellites implies that the condition for validity of (3.7) is fulfilled. The first Fresnel zone is a good measure of the area that will give important contributions to the integral (3.2). The size of the first Fresnel zone is approximately 1.5 km for the atmosphere of the Earth, as seen in Section 2.2, while the distance to the LEO satellite is approximately 3000 km and the distance to the GPS satellite is more than 20.000 km. In the horizontal direction perpendicular to the propagation path of the field (the  $y$ -axis), it is furthermore assumed that the Earth is flat, and that the amplitude and the phase modulation does not change. This is reasonable assumptions because of the small size of the Fresnel zone at the screen.

By use of these approximations a very much simplified result can be achieved for the total

amplitude and phase [Melbourne et al., 1994]

$$E(h_L) \exp[i\phi(h_L)] = K \int_{-\infty}^{\infty} A(h) \exp \left[ i \left( k_T \frac{(h - h_L)^2}{2D} + \Psi(h) \right) \right] dh. \quad (3.8)$$

In this, height relative to the Earth's limb is used instead of the  $x$ -dependence. The height  $h$  is the altitude of the local point in the thin screen, and  $h_L$  is the altitude with respect to the limb of the Earth of the LEO-GPS line at the point of intersection with the thin screen. The height  $h_L$  can be found from the geometrical optics formulation of the occultation measurement, which was described in Section 2.1.2:

$$h_L = h - z_L \gamma \quad (3.9)$$

The angle  $\gamma$  is the angle between the ray path direction at the LEO and the direct line between the LEO and the GPS. The height  $h$  can be found as the tangent height connected with the impact parameter  $a$  with the relation  $a = n(h)(h + R_e)$ ,  $R_e$  being the radius from the center of refraction for the occultation (the center of refraction must be used to account for the ellipsoidal shape of the Earth [Syndergaard, 1998]). As can be seen, exact calculation of  $h$  requires knowledge of  $n$  but as  $n - 1 \ll 1$  the approximation  $h \approx a - R_e$  can be used.

The distance  $D$  is the reduced distance from the thin screen to the LEO

$$\frac{1}{D} = \frac{1}{z_L} + \frac{1}{|z_G|}. \quad (3.10)$$

The amplitude  $A(h)$  is a modified version of  $\hat{A}$ . The new  $A(h)$  only accounts for the relative attenuation and absorption in the atmosphere, together with the obliquity factor. The quantity  $K$  is a complex normalization constant given by

$$K = \frac{E_0}{\sqrt{\lambda D}} \exp \left[ i \left( \phi_0 - \frac{\pi}{4} \right) \right] \quad (3.11)$$

where the constants  $E_0, \phi_0$  are the amplitude and phase that would be observed in the case of no atmosphere and no Earth in the path, i.e., free space conditions. Thus,  $K$  is found from (3.8) using  $\Psi(h) = 0$  and  $A(h) = 1$ . In (3.8) the  $z$ -dependence, originating from  $\vec{\rho}_L$  being dependent on  $z$ , has been removed from the measured signal  $E, \phi$ . The measurement dependence on  $z$  is instead assumed to be contained in the normalization factors  $E_0, \phi_0$ .

The approximate situation characterized by (3.8) is illustrated in Figure 3.3 for the case of infinite distance to the GPS satellite. In the figure the signal propagation is illustrated as a ray path, i.e., the signal propagation is shown as in the geometrical optics approximation. If there is no multipath propagation, the ray path shows the propagation direction of the center of the Fresnel zones. As mentioned in the introduction, the Fresnel diffraction theory compare to a deconvolution of the measured field and as the distortion of the field in the atmosphere is small, the ray optics geometry still characterizes the occultation.

In (3.8) the parameter  $\Psi(h)$  is the phase modulation due to the atmosphere, while  $A(h)$  approximates the attenuation and the absorption of the signal by the atmosphere of the Earth.

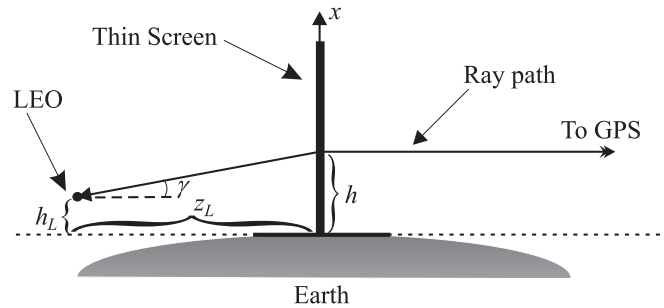


Figure 3.3: One-dimensional thin screen showing the propagation path for the case of infinite distance to the GPS.

The expression (3.8) can be used to derive an inversion scheme that derives the atmospheric parameters  $A$ ,  $\Psi$  from the measured amplitude and phase  $E$ ,  $\phi$ .

### 3.2 The Fresnel Transform

The inversion to atmospheric parameters is performed through the so called Fresnel transform [Melbourne *et al.*, 1994]. The expression (3.8) for the measured amplitude and phase is a modified form of a Fourier transform. Thus an inverse transform must exist. Rewriting the previously written result (3.8) for the measured signal at the LEO to a form where it is easy to find an inverse transform, the two equations for forward and inverse transform becomes

$$\overline{E}(u_L) \exp[i\Delta\phi(u_L)] = \frac{1}{1+i} \int_{-\infty}^{\infty} A(v) \exp[i\Psi(v)] \exp\left[\frac{i\pi}{2}(u_L - v)^2\right] dv \quad (3.12)$$

and

$$A(v) \exp[i\Psi(v)] = \frac{1}{1-i} \int_{-\infty}^{\infty} \overline{E}(u_L) \exp[i\Delta\phi(u_L)] \exp\left[-\frac{i\pi}{2}(u_L - v)^2\right] du_L \quad (3.13)$$

where  $u_L = h_L \sqrt{2/\lambda D}$  and  $v = h \sqrt{2/\lambda D}$  [Melbourne *et al.*, 1994]. In (3.12) and (3.13) the normalized fields are used. These are given by

$$\overline{E} \exp[i\Delta\phi(u_L)] = E \exp[i\phi] / E_0 \exp[i\phi_0], \quad (3.14)$$

i.e., the measured field divided by the field that would be measured without the Earth and the atmosphere of the Earth.

The inverse transform (3.13) shows that it is possible to calculate the attenuation and absorption factor and the atmospheric induced phase modulation from the measured fields. Considering the infinite integration limits it should be noted that  $A(v) = 0$  for  $v < 0$  as the field is cut-off at the limb of the Earth, and  $\Psi(v) = 0$ ,  $A(v) = 1$  for  $v > v_{max}$  where  $v_{max}$  is the chosen cut-off in

altitude, where the atmosphere has no noticeable influence. Also  $\overline{E}(u_L) \exp[i\Delta\phi(u_L)] = 1$  for  $u_L > u_{max}$  where  $u_{max}$  corresponds to  $v_{max}$ .

The direct calculation of  $\Psi(v)$  in (3.13) will give the phase as varying between  $0 - 2\pi$ . This must be unwrapped to avoid the  $2\pi$  ambiguities to give the total phase modulation  $\Psi$ , as it is the total phase modulation that corresponds to the refractive index through (3.5). The unwrapping is performed by adding  $2\pi$  to the phase modulation each time zero has been passed between two samples in the anti-clockwise direction. To do this, a high sampling rate in  $v$  is necessary.

### 3.2.1 Determining the Distance to the Thin Screen

The primary problem in performing the Fresnel transform is to choose a suitable placement of the thin screen relative to the LEO, i.e., the distance  $D$  (3.10). The theory of the Fresnel transform assumes that the distance  $D$  is constant during an occultation. This assumption is necessary to perform the inversion (3.13). A natural choice is to use the distances between the LEO and the tangent point, and between the GPS and the tangent point to define  $D$ , even though the tangent point is defined from the geometrical optics approximation. The problem in this is, that both the tangent point and the position of the LEO changes during an occultation and thereby introduces variations in  $D$ . The distance from the tangent point to the GPS can be approximated as a constant without problems. The tangent point shift and the LEO movement during an occultation is illustrated in figure 3.4, where the propagation of the field is again illustrated as rays to simplify the illustration.

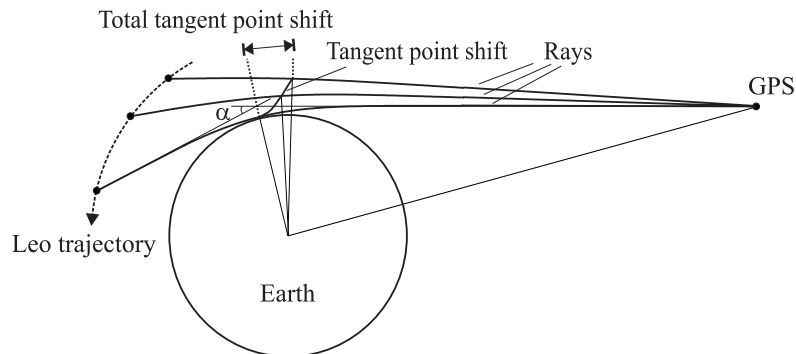


Figure 3.4: *The tangent point shift and the LEO position movement during an occultation.*

If  $D$  is calculated as following the tangent point and the satellite movement, the variation in  $D$  during an occultation is significant - more than 200 km, while  $D$  is of the order of 3000 km. Therefore, the variation in  $D$  cannot be ignored without introducing a significant error in the inversion result. A modified version of the Fresnel transform uses as  $D$  a varying distance from the LEO to the thin screen during the occultation, modified with the distance to the GPS. This is not an option according to the theory of the Fresnel transform as it is but as long as the variation in  $D$  is slowly varying the theory will still be approximately fulfilled [Mortensen and

Høeg, 1998a]. The Fresnel transform using a varying  $D$  has the form of (3.13) but with the height dependencies given as  $u_L = h_L \sqrt{2/\lambda D(h)}$  and  $v = h \sqrt{2/\lambda D(h)}$ .

In Figure 3.5 the dashed line shows a typical example of the actual variation of  $D_a(h)$  during an occultation. The actual reduced distance  $D_a(h)$  is calculated as the distance from the tangent

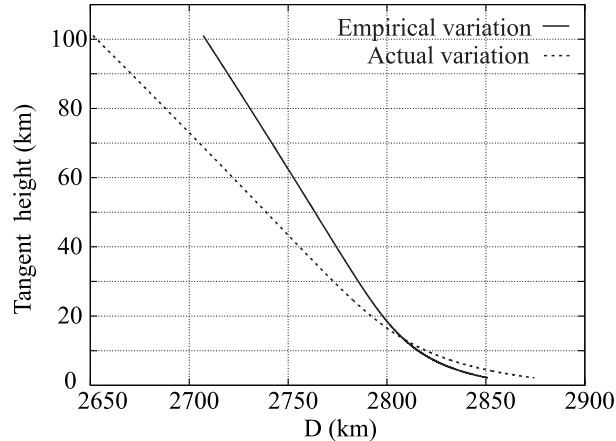


Figure 3.5: *The empirically chosen variation in  $D(h)$  compared to the actual variation. For model data based on the GPS/MET occultation no. 39 the 5th of May 1995.*

point to the LEO, reduced with the distance from the tangent point to the GPS, according to (3.10) for all samples. In the figure, the tangent height is shown on the vertical axis and  $D$  is shown on the horizontal axis. Figure 3.5 also shows the empirical variation in  $D(h)$  which is used in the Fresnel transform (solid line). This is a slower variation than the actual variation, as the slow variation complies best with the modified Fresnel transform.

The method for determining the empirical variation in  $D(h)$  was found experimentally from simulated occultation data sets by looking at the obtained accuracy of the inversion results. The upper limit  $D_u$  and the lower limit  $D_l$  of the empirical variation in  $D(h)$  are obtained as the average value of the actual  $D_a(h)$  for tangent heights between 40-100 km and 0-7.5 km, respectively. Values of  $D(h)$  in between the upper and lower limit are then found by interpolation of  $D_a(h)$  onto the interval determined by  $D_u$  and  $D_l$  as

$$D(h) = D_l + \frac{D_a(h) - D_a(h_{min})}{D_a(h_{max}) - D_a(h_{min})} (D_u - D_l) \quad (3.15)$$

where  $h_{max}$  and  $h_{min}$  denotes the maximum tangent and the minimum tangent height of the occultation, respectively. This method was found to give good results in general.

### 3.2.2 Noise filtering

The integral for performing the Fresnel transform (3.13) has infinite integration limits. In reality these limits will be finite, as the integral depend on measured amplitude and phase results. Use

of the finite integration limits will be equal to a kind of filtering. It can be shown that the smaller the integration limits are chosen, the better noise filtering is achieved through the Fresnel transform integral. On the other hand, narrow integration limits can limit the accuracy of the results. This is a problem which has been addressed earlier by *Marouf et al.* [1986] when the Fresnel diffraction theory was used for profiling of Saturn's rings. In [Marouf et al., 1986] it was described, how introducing a weighting function in the Fresnel transform integral can improve the results by reducing the amount of both numerical and random noise without degrading the accuracy and the resolution. Random noise originates from small scale atmospheric variations, and from the thermal noise introduced by the measurement itself.

The Fresnel transform using a weighting function has the form

$$A(v) \exp[i\Psi(v)] = \frac{1}{1-i} \int_{-\infty}^{\infty} \overline{E}(u_L) \exp[i\Delta\phi(u_L)] w(u_L - v) \exp\left[-\frac{i\pi}{2}(u_L - v)^2\right] du_L \quad (3.16)$$

where  $u_L = h_L \sqrt{2/\lambda D(h)}$  and  $v = h \sqrt{2/\lambda D(h)}$  as previously, and the weighting function is given by

$$w(u_L - v) = \begin{cases} \cos^2[\pi(u_L - v)/W] & \text{for } |u_L - v| \leq W/2 \\ 0 & \text{otherwise.} \end{cases} \quad (3.17)$$

Other weighting functions can be used, but the  $\cos^2$ -function has been chosen on the basis of its good frequency characteristic combined with its simplicity. The  $\cos^2$ -function represents a significant improvement from the simple cut-off of integration limits [Harris, 1978].

The numerical problems, that can occur when using just finite integration limits without a proper weighting function, are due to the sharp cut-off giving a frequency characteristic with very high side lobes. High side lobes in the frequency characteristic of the weighting function are known to introduce numerical noise in the results as unwanted frequencies are folded into the result of the integral. The weighting function will suppress high frequency noise, as the frequency characteristic of the filter has low side lobes.

The parameter  $W$ , which sets the integration width, has been chosen variable as a function of height. The phase of the measurements grows exponentially with decreasing height. Thus, the phase variations of the Fresnel transform integral become faster and faster varying with decreasing height. As long as the phase is slowly varying the integration width can be small, but the width has to grow as the phase variations become faster. The reason for not choosing a constant width, that can be used for all heights, is that it will be a lot wider than necessary for a large range of heights, and thus more noise will be folded into the integral than necessary. The variable integration width has been determined experimentally [Mortensen and Høeg, 1998b], and is given by

$$W = \begin{cases} 3 & \text{for } h \geq 45 \text{ km,} \\ 6 & \text{for } 30 \text{ km} \leq h < 45 \text{ km,} \\ 600 \exp(-0.15h) & \text{for } h < 30 \text{ km.} \end{cases} \quad (3.18)$$

### 3.2.3 Calculation of the Refractive Index

The phase  $\Psi(h)$  derived from the Fresnel transform is a measure of the phase modulation in the atmosphere. Therefore, from the knowledge of  $\Psi(h)$  it is possible to recover the refractive index.

In order to invert to refractive index profiles  $n(h)$  for the neutral atmosphere, it is necessary to perform a correction for the delay caused by the ionosphere. As  $\Psi(h)$  is defined as (3.5):

$$\Psi(h) = k_T \int_T (n(h) - 1) d\tau \quad (3.19)$$

the same principle for derivation of the ionosphere correction method can be used as in the geometrical optics (GO) inversion method in Section 2.3. Thus, the Fresnel transform is performed for both GPS signals giving the results  $\Psi_1$  and  $\Psi_2$  corresponding to the two frequencies  $f_1$  and  $f_2$ . With  $\Psi_1$  and  $\Psi_2$  the ionosphere corrected expression for the phase modulation  $\varphi$  will be given as

$$\varphi(h) = \frac{c}{2\pi} \frac{f_2 \Psi_2(h) - f_1 \Psi_1(h)}{f_2^2 - f_1^2} = \int_T (n_{neu}(h) - 1) d\tau. \quad (3.20)$$

This expression corrects for the first order ionospheric contribution. The primary problem with this correction method is due to a residual term which is dependent on the LEO position. However, the accuracy of this ionosphere correction method is as good as the accuracy of the simple ionosphere correction method, described in Section 2.3, for the GO inversion method. For a thorough discussion of the limitations of the correction method see [Melbourne *et al.*, 1994].

It can be shown [Melbourne *et al.*, 1994] that the relationship (3.20) between  $\varphi(h)$  and  $n_{neu}$  is equal to a correspondence given by

$$\varphi(h) \leftrightarrow -2 \int_r^\infty \frac{n'}{n} \sqrt{n^2 r'^2 - a^2} dr' \quad (3.21)$$

with  $r$  being the closest distance of the ray to the center of refraction (the tangent radius),  $n$  being a function of  $r'$  and  $n'(r')$  the derivative of  $n(r')$ . The neutral atmosphere indication of the refractive index term has been dropped for convenience. The correspondence is valid for a thin atmosphere. It then follows from the Abel transform [Melbourne *et al.*, 1994] that

$$n(a) \cong \exp \left( -\frac{1}{\pi} \frac{d}{da} \left[ \int_a^\infty \frac{a\varphi(a' - R_e)}{a' \sqrt{a'^2 - a^2}} da' \right] \right). \quad (3.22)$$

It is noted, that the Abel transform assumes spherical symmetry, and that the relation  $h \approx a - R_e$  has been used for the dependence on height in the phase modulation  $\varphi$ . Knowing  $n(a)$ , the exact height  $h$  can be calculated as

$$h = \frac{a}{n(a)} - R_e. \quad (3.23)$$

The equal signs in the expression (3.22) applies under the assumption that  $n(a) - 1 \ll 1$ ,

which is a reasonable, but not very accurate assumption for the atmosphere of the Earth where  $n(a) \approx 1.0003$  at maximum at the surface of the Earth. Once the neutral atmosphere refractive index has been determined, the density, pressure, and temperature profiles can be derived as described in Section 2.3.

### 3.3 Resolution and Approximations

The Fresnel transform (3.16) contains no direct constraints on the resolution, so this result is in principle achievable at any height, giving a vertical resolution limited only by the wavelength, in the ideal case with no noise and with a spherically symmetric atmosphere. As already mentioned in Section 3.1, the calculation of  $n$  from  $\varphi$  by use of a geometrical optics (GO) approximation does not impose a significant limitation on the results. However, there are uncertainties that makes the wavelength limited resolution of the Fresnel transform impossible. Use of the Fresnel approximation and the thin screen approximation introduces errors and thereby uncertainties in the knowledge of  $h$ . Also, there are not an infinite number of samples for each occultation, so the integration accuracy will be limited.

An uncertainty in the knowledge of  $h$  transfers directly to a limit in the resolution. One of the biggest contributions to the uncertainty in  $h$  is uncertainty in the determination of  $D$  [Melbourne *et al.*, 1994]. The reduced distance  $D$ , which is approximately equal to the distance from the LEO to the thin screen, will not be known exactly as an exact placement of the thin screen is not possible. This will be the case even when using the modified Fresnel transform. It can be shown [Melbourne *et al.*, 1994] that an uncertainty  $\delta D$  in  $D$  gives the uncertainty  $\Delta h_{\delta D}$ :

$$\Delta h_{\delta D} \geq 1.25 \sqrt{\frac{\lambda \delta D}{2}}. \quad (3.24)$$

A reasonable estimate of the uncertainty in  $D$  is 75 km, giving an uncertainty in  $h$  of  $\Delta h_{\delta D} = 110$  m.

The expression (3.24) is only the minimum limit of the error in  $h$ . This is because the integration limits must be chosen with care not to increase the error introduced by  $\delta D$ . It can be shown that an estimate of the uncertainty in  $h$ , arising from the finite integration limits, is given as

$$\Delta h_W = \frac{2}{W} \sqrt{\frac{\lambda D}{2}} \quad (3.25)$$

[Marouf *et al.*, 1986]. This expression is derived for a rectangular filter function, but the  $\cos^2$ -filter-function (3.17) will not alter this result significantly for a first order estimate of the resolution limitation.

For the filter widths used here (3.18), it will be the filter width that limits the resolution above  $\approx 25$  km, while it will be the uncertainty in  $D$  that will limit the resolution for lower altitudes. Thus, by use of (3.24) it can be seen that compared to the resolution of the GO inversion method, the Fresnel transform should be able to enhance the resolution in  $h$  by a factor of 2-5 in the

troposphere. As mentioned in the introduction of this chapter, the troposphere is the area of primary interest for high vertical resolution inversion results. This vertical resolution can only be achieved if the horizontal variations are small.

Even though the estimates of the vertical resolution of the Fresnel transform method show a very good resolution there are problems with the method. As described, there are numerous approximations in the method, and therefore the recovery of refractive index profiles can only be promised to be qualitatively close to the surface of the Earth. This means that even though the resolution is promised to be very good, the average accuracy of the refractive index profiles obtained by the inversion will be relatively low. Thus the method cannot be expected to meet the demands of recovering temperature profiles with an average accuracy better than 1K, which is the obtainable accuracy for the geometrical optics inversion method [Rocken *et al.*, 1997]. Apart from the errors originating from the approximations in the method, systematic and random measurement errors limit the accuracy. This is the same limitations as applies to the GO inversion method, see Section 2.3.

The two large approximations in the Fresnel transform inversion method are: the thin screen approximation, and the thin atmosphere approximation in the refractive index calculation from the phase modulation. With the thin screen approximation, the propagation is approximated with a straight line from the GPS to the thin screen, and another straight line from the thin screen to the LEO. The atmospheric bending of the signal will be approximated as a change of direction at the thin screen. Close to the surface of the Earth, the total bending of the GPS signal amount to  $\approx 1^\circ$ , i.e., the field will propagate along a curved path. This problem is illustrated in Figure 3.6. The approximation of the propagation of the field with two straight lines will

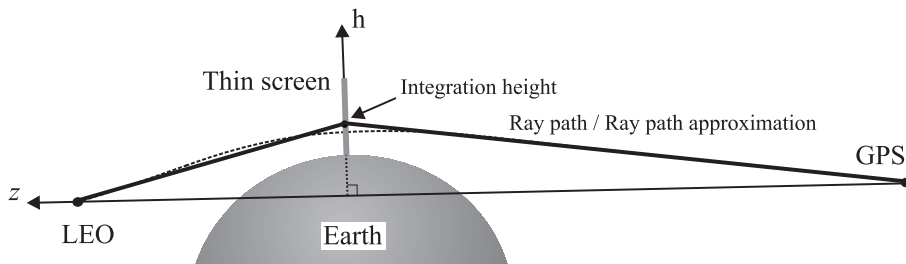


Figure 3.6: *Illustration of the thin screen approximation showing the ray path and the approximation used in the Fresnel transform.*

introduce an error in the propagation path length of the signal. This error will increase as the bending of the ray path increases. Therefore, the Fresnel transform using a single thin screen will have an error in the average inversion result. The size of the error and the sign of it will be dependent on the position of the thin screen and on the integration height. The integration height is the height of the point in the thin screen, where the two lines used for approximating the propagation path of the field meet. The position of the thin screen has been chosen to be approximately equal to the tangent point, while the integration height has been chosen to be slightly above the tangent height. This has the effect of  $\Psi$  becoming slightly overestimated close

to the Earth. The calculation of the refractive index  $n$  from  $\Psi$  through (3.22) also introduces an error in the result, as this calculation is based on a thin atmosphere approximation. A study of the approximate refractive index calculation (3.22) shows that for a given  $\Psi(a - R_e)$ , the refractive index profile  $n(h)$  will be underestimated. This should be compared with the fact, that  $\Psi(a - R_e)$  calculated from the Fresnel transform becomes overestimated close to the Earth. Thus, close to the Earth, where the errors will be largest, the errors from the two approximations work in opposite directions making the overall error less than it would be from either of the approximations seen individually.

As just mentioned, the integration height is chosen to be slightly above the tangent height. This choice of the integration height is determined by the use of the approximation  $h \approx a - R_e$  in the inversions. This approximation is used both when calculating the Fresnel integral and when the refractive index is calculated from the phase modulation. In this way the approximations should cancel, but a study of the Fresnel transform integral will show that the approximations will not be carried directly through the transform, and thus a small bias will appear. This bias is the difference between the integration height and the tangent height. The bias will be carried into the height calculation of the refractive index. Thus apart from the average error in the inversion result there will also be a spatial displacement. This effect will be of importance in areas with large vertical gradients.

The Fresnel transform is a wave solution which takes multipath into account. That the refractive index is found from the phase modulation due to the atmosphere through a GO approximation does not alter this conclusion. This has been confirmed by numerical tests [Mortensen and Høeg, 1998a]. The reason why the GO approximation does not generate multipath propagation is that the propagation distance in the GO calculation of the phase modulation is short, and multipath problems does not normally occur for short propagation distances in the atmosphere.

As the method is based on a single screen, and the inversion from the phase modulation due to the atmosphere to the refractive index profile is based on a geometrical optics approximation assuming a spherically symmetric atmosphere, the inversion as such is implicitly based on an assumption of spherical symmetry. The horizontal resolution will thus be determined as it was determined for the geometrical optics approximation described in Section 2.2. According to this, the horizontal resolution in the direction of the propagation will be of the order of 200 – 300 km. In the direction perpendicular to the ray path the resolution will be of the order of 1.5 km.

### 3.3.1 Occultation Sampling Rate

A parameter, which is strictly determined by the occultation measurement, and which is of importance for the quality of the inversion results obtained using the Fresnel diffraction theory, is the sampling rate of the occultation data. Figure 3.7 shows an example of the distance between samples at the thin screen as a function of tangent height for different sample rates for an occultation. As the Fresnel diffraction theory enhances the resolution of the inverted occultation data by devolving the information in samples with overlapping Fresnel zones, it is

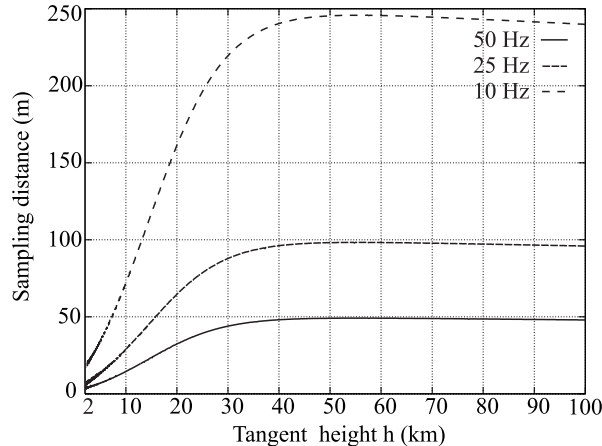


Figure 3.7: *Sampling distance in meters as a function of the tangent point height for different sampling rates.*

obvious that the resolution of the method will be limited by the distance between to samples. Furthermore, the Fresnel transform assumes continuous samples so the finite sampling rate will also cause an error in the inverted results. This implies use of as high a sampling rate as possible to obtain the best results from the method.

According to Shannon's sampling theorem the sampling distance in a measurement must at least be less than half the size of the smallest object to be resolved. In Figure 3.7 this implies that with 50 Hz sampling rate the resolution limit due to sampling is less than 100 m for all heights, and improving significantly below 30 km. Thus, 50 Hz sampling rate is sufficient for the Fresnel transform as the resolution will be limited by the uncertainty in  $D$  and the filter width. If on the other hand the sampling rate is lowered to 10 Hz the resolution limit due to the sampling at 20 km will be  $\approx 300$  m, and at 10 km it will be  $\approx 150$  m. With a sampling rate of 10 Hz the resolution will be limited by the sampling rate, and use of the Fresnel transform will only make real sense for altitudes less than  $\approx 10$  km.

### 3.4 Summary

The Fresnel diffraction theory for inversion of radio occultation measurements is a promising new method giving high vertical resolution. The method is based on a thin screen approximation of the atmosphere of the Earth. This approximation limits the accuracy of the method. Introduction of an empirical modification of the theory, where the thin screen is moved during the occultation, improves the accuracy of the inversion results. But still, the temperature error of the obtained profiles must be expected to exceed 1 K close to the surface of the Earth. The lower limit of the vertical resolution of this method is caused by uncertainties in the parameters of the methods and is of the order of approximately 100 m. If the thermal and the atmospheric noise is large the vertical resolution can be lowered. The method cannot take horizontal variations into account.

## Chapter 4

# Inversion Using the Back-Propagation Inversion Method

The back-propagation inversion method is another inversion method that has been developed for overcoming multipath problems and for enhancing the vertical resolution. The method has been developed specifically for inversion of radio occultation data for dense atmospheres [*Gorbunov et al.*, 1996; *Karayel and Hinson*, 1997].

The method is as the Fresnel transform based on the methods developed for enhancing the resolution for the planetary missions [e.g., *Hubbard et al.*, 1978]. Also the idea in using the information in the occultation measurement from samples with overlapping first Fresnel zones is the same. The main difference to the Fresnel transform is that the theory is formulated such that use of the thin screen for approximation of the atmosphere of the Earth is avoided. In the back-propagation inversion method the electromagnetic field is back-propagated using the solution to the wave equation in free space. When the field is back-propagated to a position much closer to the atmosphere, the geometrical optics approach can be used in this position, but giving an enhanced resolution and less multipath problems. The principle is equivalent to solving a lens focusing problem.

Very good results are obtained with the method, [*Karayel and Hinson*, 1997; *Mortensen et al.*, 1999; *Gorbunov and Gurvich*, 1998a]. The accuracy is as good as the results of the geometrical optics inversion method but the vertical resolution is improved with a factor of 2-5, and most cases of multipath propagation can be resolved. The method is already used as standard in the University Cooperation for Atmospheric Research (UCAR) data inversion program [*Rocken et al.*, 1997].

In Section 4.1 the model for the wave propagation of the GPS signal, which is the basis for the back-propagation inversion method, is described. In Section 4.2 the inversion method is described, and in Section 4.3 the resolution of the method and the errors are discussed.

## 4.1 2-D Wave Propagation

For means of simplicity the back-propagation inversion method is based on a two dimensional (2-D) approximation. A schematic illustration of the 2-D back-propagation occultation geometry is shown in Figure 4.1. In Figure 4.1 a ray path is illustrated. In the geometrical optics

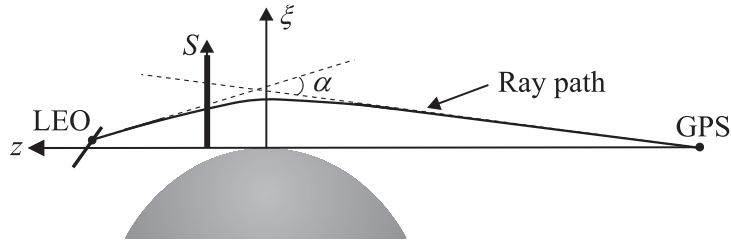


Figure 4.1: *The geometry of the occultation and the coordinate system used for the back-propagation.*

approximation the signal from the GPS to the LEO satellite will follow this ray path as was described in Chapter 2. The total bending of the ray path is given by the angle  $\alpha$ . When there is no multipath propagation the ray paths will show the propagation of the center of the first Fresnel zones for the signal. As described in Section 2.2, the first Fresnel zones for the occultation measurements of the atmosphere of the Earth has a very limited extent, i.e., less than 1.5 km. In comparison, the typical horizontal scale sizes in the atmosphere is of the order of 100 km [McIlveen, 1986]. The 2-D approximation is thus justified by the limited extent of the GPS signal in the horizontal direction perpendicular to the propagation direction. The width of the GPS signal in this direction can be approximated by the first Fresnel zone.

Figure 4.1 also illustrates the coordinate system used for the 2-D approximation. The coordinate system lies in the plane given by the GPS position, the LEO position, and the center of the Earth. The  $z$ -axis is the vector from the GPS satellite tangential to the Earth in the direction of the LEO satellite. The center  $z = 0$  is where the  $z$ -axis is tangential to the Earth. The  $\xi$ -axis is perpendicular to the Earth's surface at  $z = 0$  and directed outwards [Gorbunov *et al.*, 1996]. The path of the LEO satellite during the occultation is approximated by the line drawn. A single sample is indicated by the dot. In this  $(\xi, z)$ -coordinate system,  $S$  denotes a line parallel to the  $\xi$ -axis.

As the occultation measurement in general will be three dimensional it is necessary to perform a transformation to the 2-D geometry first. The occultation measurements give positions in a Cartesian coordinate system  $(x, y, z)$  with center at the center of the Earth. For each sample in the occultation measurement, coordinates  $(\xi, z)$  in the 2-D coordinate system can be calculated from the definition above. The transformation from Cartesian coordinates to the new coordinates  $(\xi, z)$  is relatively simple. A description can be found in [Mortensen, 1998]. The GPS and the LEO satellite move during the occultation, so the samples in an occultation measurement will

not lie in the same plane during the occultation. The new coordinate system  $(\xi, z)$  is thus slowly rotating and translating with respect to the coordinate system  $(x, y, z)$ .

The back-propagation inversion method is based on using a solution to the wave equation just as the Fresnel transform. To obtain the back-propagation solution the propagation of the electromagnetic signal must be described. The complex amplitude  $E$  of the scalar electric field in vacuum satisfies the Helmholtz equation

$$\Delta E + k_T^2 E = 0 \quad (4.1)$$

where  $k_T$  is the free space wave number. The harmonic time dependence of the signal has been suppressed. The atmosphere is sufficiently tenuous to justify the use of the scalar version of the wave equation [Tatarski, 1967]. Because the scalar version of the wave equation applies, the same equation applies to the magnetic field, and thus it is only necessary to consider the electric field in the following.

If the electric field  $E_0$  is known all over a distant line  $S$ , a boundary solution  $E(\vec{x})$  to the Helmholtz equation can be found in a given point  $\vec{x}$ . This is the two dimensional solution for the external boundary problem for the Helmholtz equation [Chew, 1995, sec. 8.1]

$$E(\vec{x}) = \frac{i}{2} \int_S E_0(\vec{y}) \frac{\partial}{\partial n_y} H_0^{(1)}(k_T |\vec{x} - \vec{y}|) dS_y \quad (4.2)$$

where  $n_y$  is the normal to  $S$ , directed toward  $\vec{x}$ , and  $H_0^{(1)}$  is the Hankel function of first kind of zero order. The solution (4.2) is the free space solution for a straight line  $S$ .

The large argument expansion  $k_T |\vec{x} - \vec{y}| \rightarrow \infty$  of  $H_0^{(1)}$  in the expression for the electric field (4.2) is given by

$$H_0^{(1)}(k_T |\vec{x} - \vec{y}|) \simeq \sqrt{\frac{2}{\pi k_T |\vec{x} - \vec{y}|}} \exp\left(ik_T |\vec{x} - \vec{y}| - i\frac{\pi}{4}\right). \quad (4.3)$$

This approximation can be used under the assumption that the line  $S$  is distant from the measurement point, i.e., points  $y$  on  $S$  must fulfill  $k_T |\vec{x} - \vec{y}| \gg 1$ .

When using the high frequency approximation the expression for the electric field becomes

$$E(\vec{x}) = \left(\frac{k_T}{2\pi}\right)^{1/2} \int_S E_0(\vec{y}) \cos \varphi_{xy} \frac{\exp(ik_T |\vec{x} - \vec{y}| - i\pi/4)}{|\vec{x} - \vec{y}|^{1/2}} dS_y \quad (4.4)$$

where  $\varphi_{xy}$  is the angle between the normal  $\vec{n}_y$  to  $S$  and the vector  $\vec{x} - \vec{y}$ . This solution can be used to describe the field measured at the LEO if the field is known on the line  $S$  indicated in Figure 4.1.

## 4.2 Back-Propagation

The boundary problem of the wave equation, which leads to the solution (4.4) for the measured electric field, in general has two solutions. The solution, which describes the propagation of the electric field (4.4), propagates outwards from the line  $S$ . The other solution propagates inwards, and can be considered to be the inverse solution to the boundary problem of the Helmholtz equation. This inverse solution is given by

$$E_0(\vec{y}) = \left(\frac{k_T}{2\pi}\right)^{1/2} \int_{S_L} E(\vec{x}) \cos \varphi_{xy} \frac{\exp(-ik_T|\vec{x} - \vec{y}| + i\pi/4)}{|\vec{x} - \vec{y}|^{1/2}} dS_x. \quad (4.5)$$

Due to the similarity with the solution that describes the propagation of the signal, the inverse solution is termed the back-propagation solution. This solution can be used to derive the field  $E_0$  at the line  $S$  if the field  $E$  at the LEO is known.

In (4.5),  $S_L$  is the curve formed by the movement of the LEO satellite during the occultation, and  $E(\vec{x})$  is the measured complex signal. The expression (4.5) is the solution derived for a straight line  $S_L$ . This solution can be used – with the actual curved  $S_L$  – due to the large radius of the LEO satellite orbit and the short duration of the occultation measurement. The vector  $\vec{y}$  indicates a point on the back-propagation line  $S$ . The field  $E_0(\vec{y})$  is thus the complex electric back-propagated field.

The parameters in the expression (4.5) for the back-propagated electric field can be formulated in accordance with the occultation geometry. Using the  $(\xi, z)$ -coordinate system, the  $\vec{y}$ -vector at the back-propagation line  $S$  is given by  $(\xi, z_0)$ . That is,  $z_0$  determines the position of the line  $S$ . The measurement vector  $\vec{x}$  can be described by the parametric equation

$$\vec{x}(\xi) = (\xi, p\xi + q) \quad (4.6)$$

where  $p$  and  $q$  are local constants known from the position of the LEO satellite. This is a straight line approximation of the LEO path, and in order to keep the error from this approximation small, the parameters  $p$  and  $q$  has been made local. This means that the most suitable value of  $p$  and  $q$  is chosen for each point  $\vec{y}$  in the back-propagated electric field calculation. The angle  $\varphi_{xy}$  is defined as the angle between the normal  $\vec{n}_x$  to  $S_L$ , directed toward  $\vec{y}$ , and the vector  $\vec{y} - \vec{x}$ . Using the local slope  $p$  of the LEO path, the normal vector  $\vec{n}_x$  will be given by

$$\vec{n}_x = \left(-1, \frac{1}{p}\right) \quad (4.7)$$

so the angle  $\varphi_{xy}$  can be found from

$$\cos \varphi_{xy} = \frac{\vec{n}_x \cdot (\vec{y} - \vec{x})}{|\vec{n}_x| |\vec{y} - \vec{x}|}. \quad (4.8)$$

Finally, the integration can be transformed from the curve  $S_L$  to the variable  $\xi$ , whereby the back-propagation integral becomes

$$E_0(\vec{y}) = \left(\frac{k_T}{2\pi}\right)^{1/2} \int_{-\infty}^{\infty} E(\vec{x}) \cos \varphi_{xy} \frac{\exp(-ik_T|\vec{x} - \vec{y}| + i\pi/4)}{|\vec{x} - \vec{y}|^{1/2}} \sqrt{1+p^2} d\xi. \quad (4.9)$$

As the back-propagation solution (4.5) is based on free space conditions, the field  $E_0$  will be the field measured at the back-propagation line  $S$ , if  $S$  is placed outside the atmosphere of the Earth. Thus, when  $E_0$  has been found from the measured field  $E$  through (4.5), the geometrical optics (GO) approximation can be applied at the line  $S$  to derive the refractive index. This will be similar to the GO inversion method described in Chapter 2. The line  $S$  is closer to the atmosphere of the Earth than the original LEO path. Therefore, the distance  $D$  from the atmosphere to the measurement line will be smaller. As the resolution in the GO approach is proportional to  $\sqrt{D}$ , the resolution of the derived refractive index will be improved when using the back-propagation method. How significant the improvement will be depends on how far back the back-propagation line is placed. Just as importantly however, multipath problems can be resolved by the back-propagation method [Gorbunov and Gurvich, 1998b]. This is because the occurrence of multipath problems is dependent on the distance from the atmosphere to the measurement line. The larger the distance, the larger is the risk for multipath propagation.

In Figure 4.2 the back-propagation occultation geometry is shown together with the parameters needed for performing the inversion from measured electric field  $E_0$  to refractive index. The coordinate system was defined in Figure 4.1. In Figure 4.2,  $r_G$  is the length of the vector  $\vec{r}_G$

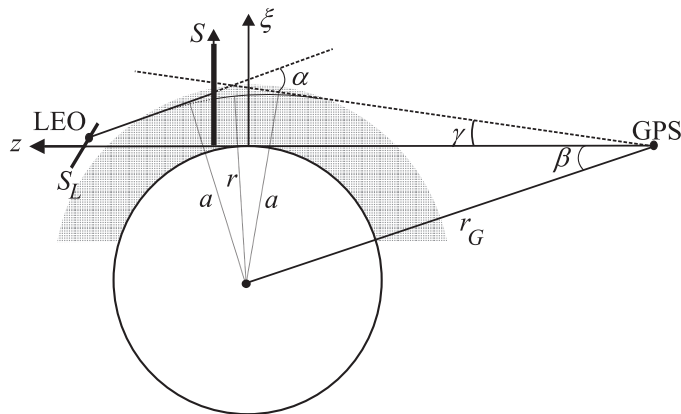


Figure 4.2: *The geometry of the back-propagation occultation.*

from the center of the Earth to the GPS satellite. The angle  $\beta$  is the angle between the vector  $-\vec{r}_G$  and the  $z$ -axis. Figure 4.2 also illustrates a ray path. The ray path has been shown as dashed behind the back-propagation line. This is to indicate that it is the field back-propagated to the line  $S$  that will be used to derive the refractive index. The thick solid line from the LEO to the back-propagation line is a straight line following the ray path asymptote at the LEO. This is a consequence of (4.4) being the solution to the free space propagation problem. When

using the back-propagation method free space propagation is assumed, and thus the field will be back-propagated along the ray path asymptote. The field can be back-propagated into the atmosphere of the Earth along the ray path asymptote. Only, if the back-propagation line is placed inside the atmosphere of the Earth, the field obtained is not equal to the physical field that would be measured at this point, but equal to a virtual measured field. This will not introduce errors or approximations in the derivation of the refractive index, if it is taken into account when deriving the refractive index from the back-propagated field. The angle between the ray path and the  $z$ -axis at the GPS satellite is denoted by  $\gamma$ . The closest distance to the Earth is given by the tangent radius  $r$  and the right-angled distance to the straight line asymptote of the ray path is  $a$  (the impact parameter). The angle between the two asymptotes is the bending angle  $\alpha$ .

The occultation samples used to calculate the back-propagated field are in reality a time series. Thus, the back-propagation solution must assume stationarity in time. This is a good approximation for the atmosphere, as the occultation measurement in the neutral atmosphere typically only will take about a minute (the GPS/MET experiment), during which time interval the atmosphere does not change significantly. On the other hand, the back-propagation solution is only valid under the assumption that the GPS does not move during the occultation, as the measurements must be assumed to originate from the same point in order to derive the back-propagation solution. This is not entirely true but the distance from the atmosphere to the GPS satellite is very large compared to the distance from the atmosphere to the LEO, and relative to this the GPS moves very little. Only, when calculating the back-propagation integral, the measured field  $E(\vec{x})$  must be normalized with the phase due to the distance change to account for the dependence on the varying distance to the GPS satellite.

#### 4.2.1 Geometrical Optics Inversion

The back-propagated field  $E_0(\xi)$  at the line  $S$  can be split into amplitude and phase  $\phi_E$ . The phase  $\phi_E(\xi)$  must be unwrapped to avoid  $2\pi$  ambiguities as it is the total phase  $\phi(\xi)$  that is of interest. The total phase  $\phi$  will be given as  $\phi(\xi) = \phi_E(\xi) + N(\xi) \cdot 2\pi$  where  $N$  is an integer. The sampling density in the back-propagation integral must be chosen sufficiently dense to avoid cycle slips when  $N$  is determined.

The field calculated from the back-propagation approach has lost the time dependence as the samples are combined to form the back-propagated field. Thus the GO approach for finding the bending angle and the impact parameter from the phase  $\phi$  will be different from the approach described in Chapter 2. From geometrical considerations the dependence of the bending angle and the impact parameter on  $\phi$  can be derived [Karayel and Hinson, 1997]. The necessary parameters are all illustrated in Figure 4.2. The bending angle  $\alpha$  is given by

$$\alpha - \gamma = \arcsin \left( \frac{-\lambda d\phi}{2\pi d\xi} \right) \quad (4.10)$$

and the impact parameter  $a$  is given by

$$a = (z_S - z_R) \sin(\alpha - \gamma) + (\xi - \xi_R) \cos(\alpha - \gamma) \quad (4.11)$$

where  $(\xi_R, z_R) = (-R_e, 0)$  are the coordinates for the center of the Earth and  $(\xi, z_S)$  are the coordinates of a point on the line  $S$ . The angle  $\gamma$  can be determined from  $\gamma = \arcsin(\frac{a}{r_G}) - \beta$  and  $\beta = \arcsin(\frac{-\xi_R}{r_G})$ . The distance from the GPS satellite to the center of the Earth is denoted by  $r_G$  and  $R_e$  is the Earth radius.

The derivation of the expression for the bending angle uses the ray path asymptotes. Thus the derivation is based on the back-propagation integral being derived under free space conditions. The derivation will therefore also account for the situation where the back-propagation line is placed inside the atmosphere of the Earth. No errors or approximations of the bending angle are introduced by this. When approximating the wave propagation by a ray path, the bending angle derived at the back-propagation line will in principle be the same as the one, that can be derived at the LEO. This is if there is no multipath. The ray path situation is illustrated in Figure 4.2. In reality the measured field will be dependent on contributions from a finite area in space, rather than have the ray structure illustrated in Figure 4.2. The effect of the back-propagation is to focus the electric field such that a better resolution in the bending angle is achieved. In the presence of multipath propagation the focusing will have the effect of resolving the multipath propagation into single rays if the back-propagation line is placed suitably [Gorbunov and Gurvich, 1998b].

The expressions (4.10) and (4.11) for the bending angle and the impact parameter is derived for a spherical Earth. Taking the ellipsoidal shape of the Earth into account can be done in a manner similar to what has been derived for the geometrical optics inversion method [Syndergaard, 1998]. The coordinate system used for the back-propagation method is based on using the center of the Earth, so a slight change in the expressions (4.10) and (4.11) must be introduced. When calculating the impact parameter, the center of refraction, where the occultation takes place  $(\xi_R, z_R, y_{1,R})$ , must be used instead of the center of the Earth in (4.11). In this case  $(\xi_R, z_R)$  denotes the coordinates of the center of refraction in the 2-D coordinate system. The contribution  $y_{1,R}$  must be added into the expression because the center of refraction is not necessarily in the  $(\xi, z)$ -plane. Thus, the impact parameter (4.11) must be corrected to

$$a_E = \sqrt{a^2 + y_{1,R}^2}. \quad (4.12)$$

Furthermore, when the angles  $\gamma$  and  $\beta$  are derived, the distance from the center of refraction in the plane  $(\xi_R, z_R)$  to the GPS satellite must be used instead of  $r_G$ .

When the bending angle and the corresponding impact parameters have been derived, the inversion to refractive index can be performed as in the geometrical optics inversion method described in Chapter 2. Under the assumption of spherical symmetry in the atmosphere, the conversion from bending angles  $\alpha$  as a function of impact parameter  $a$  to refractive index  $n$  is performed

through the Abel transform [Fjeldbo *et al.*, 1971]

$$n(r) = \exp \left[ \frac{1}{\pi} \int_a^\infty \frac{\alpha(a')}{\sqrt{a'^2 - a^2}} da' \right] \quad (4.13)$$

where  $a = nr$  is the impact parameter for the ray whose tangent radius is  $r$ . The subscript  $E$  to  $a$  has been dropped for convenience.

In order to derive the neutral atmosphere refractive index, a correction for the ionospheric influence must be performed before the refractive index is calculated from the Abel transform (4.13). The back-propagation is performed for both the signal with the  $f_1$  frequency and for the signal with the  $f_2$  frequency. The two phases  $\phi_1$  and  $\phi_2$  can be used to derive an ionosphere corrected phase, in a similar manner as was described in Chapter 2, for the use of the geometrical optics inversion method. The other ionosphere correction methods that has been derived for the geometrical optics inversion method can also be used due to the similarity between the methods [Gorbunov *et al.*, 1996].

Once  $n$  has been found, the temperature, pressure, and density can be derived as described in Section 2.3.

#### 4.2.2 Parameter Choices

Two parameters are important when calculating the back-propagation integral: the position of the back-propagation line  $S$  and the integration limits of the integral.

In Figure 4.2,  $S$  is placed inside the atmosphere. This cannot be avoided if the resolution is to be enhanced significantly. In most cases the back-propagation line will actually be placed far into the atmosphere of the Earth. As already described this is not a problem for the method. The optimal position of  $S$  will in general depend on the data. The main aim will be to place the line such that multipath propagation is avoided. As mentioned previously in Section 2.2.1 multipath propagation can for instance be seen as an ambiguity in the bending angle determination. In [Karayel and Hinson, 1997] a heuristic formula for positioning of the line  $S$  is described. The position of the back-propagation line must be seen relative to the tangent point of the occultation as the tangent point will be the approximate focus point of the back-propagation. During an occultation, the tangent point moves, and particularly close to the Earth this movement will be fast (see Section 3.2.1). This means that there is not a well defined focus-point of the back-propagation, and therefore there is a limitation on the obtainable resolution of the signal. At the focus-point, the resolution would equal the wavelength of the signal. In most cases placing the line  $S$  at 25 – 50 km from the tangent point gives good results. That is, most multipath propagation is resolved and the resolution is optimal [Mortensen *et al.*, 1999]. Moving the line further back does not improve the results significantly.

As there is a finite limit for the focusing of the signal there is also a lower limit for the resolution

of multipath propagation. Multipath propagation will arise from sharp vertical refractive index gradients. Thus, gradients can occur which cannot be resolved by the back-propagation inversion method. However, the limit is very close to the limit where the LEO receiver will lose track of the GPS signal due to super refractive propagation [Karayel and Hinson, 1997; Mortensen *et al.*, 1999].

It is not quite so obvious that the integration limits are parameters. In the back-propagation integral (4.5) the integration limits are infinite. To evaluate this integral as fast as possible the stationary phase points must be found, i.e., the extrema points of the function  $\varphi = \arg(E(x)) - k_T|\vec{x} - \vec{y}|$ . It has then been determined that using integration limits equivalent to phase variations  $\varphi \pm 10\pi$  the most important contributions to the integral will be included [Gorbunov, 1988]. A small contribution to the integral value is furthermore found at the lower limit of the integral interval, i.e., at the surface of the Earth. If there is no multipath propagation there is only one stationary point of the phase variations. Choosing a narrow integration interval will also have the effect of decreasing the influence from noise on the back-propagation inversion results [Marouf *et al.*, 1986]. In a general approach a weighting function could be introduced to improve the filtering. This will be similar to what was described in Section 3.2.2. Here, the simple cut-off without weighting has been used. The vertical resolution limit imposed by the width of the integration area is  $\approx 60$  m (calculated as given in [Marouf *et al.*, 1986]) which is sufficient in all realistic cases.

The reason, why introducing a weighting function has not been seen as necessary in the back-propagation inversion method, is that the method is often only used in the lower part of the atmosphere. As the back-propagation solution is a rather slow method compared to using the geometrical optics inversion method directly at the measured data, the two methods are normally combined [Gorbunov *et al.*, 1996]. Multipath propagation in the neutral atmosphere is normally only seen for low heights so the back-propagation inversion method is used in the lower part of the measurement while the geometrical optics inversion method is used in the upper part. The two solutions can easily be combined, as both calculate bending angles as a function of impact parameter, and in areas where the atmosphere is smooth the two solutions will be equal. The tropopause or a little above can be used as the upper limit for use of the back-propagation inversion method. So, the method is only used below approximately 15 – 17 km.

### 4.3 Resolution and Approximations

The inversion to refractive index in the back-propagation inversion method is based on the geometrical optics approximation. Only, the distance to the atmosphere is less than when the GO inversion method is applied directly at the receiver. Also, the method is based on an assumption of spherical symmetry. The vertical resolution  $\Delta r$  in the GO approximation for a

spherically symmetric atmosphere will be given by

$$\Delta r = 2\sqrt{\lambda D \zeta(r)} \quad (4.14)$$

as described in Section 2.2. In (4.14),  $\lambda$  denotes the wavelength,  $D$  denotes the distance from the atmosphere to the back-propagation line, and  $\zeta(r)$  is a factor which corrects for the bending of the atmosphere. When the back-propagation inversion method is applied on a spherically symmetric atmosphere a resolution of about 100 m can be reached [Mortensen *et al.*, 1999]. The limitation is due to the smearing of the focus-point. This limit is the lower limit of the vertical resolution of method. The high resolution is gained while keeping the high accuracy of the geometrical optics inversion method.

With regards to the horizontal resolution the back-propagation inversion method assumes horizontal homogeneity in the entire area covered by the occultation. This area includes the horizontal area perpendicular to the signal propagation direction which is created by the satellite movement in this direction. The reason is that the coordinate transformation from the 3-D measurement geometry to the 2-D back-propagation geometry is performed under the assumption of spherical symmetry in the atmosphere. But often, the width of the first Fresnel zone of the signal which is  $\approx 1.5$  km is used as the measure of the resolution [Gorbunov and Gurvich, 1998b]. This measure is justified by the exponential decrease of the gradient of the refractive index with height, as this decrease causes the contributions to the signal bending to be highly peaked in height range when performing the Abel transform.

In the direction of the signal propagation, the horizontal resolution, and thereby the area where homogeneity must be assumed, is estimated to be equal to the ray path propagation length inside one vertical resolution cell. As the back-propagation inversion method gives a very good vertical resolution, the measure for the horizontal resolution in the direction of the signal propagation will also be improved. However, when considering the area in which the horizontal structure should be homogeneous the movement of the tangent point should be taken into account. Also, it should be noted that the coordinate transformation from the 3-D measurement geometry to the 2-D back-propagation geometry is performed under the assumption of spherical symmetry in the atmosphere. This causes a smearing effect along the ray path as the 2-D coordinate system will move some in the direction along the ray due to the movement of the GPS satellite. Altogether this implies, that it should not be expected that the horizontal resolution will improve beyond that of the GO inversion method (Section 2.2).

More importantly however, horizontal inhomogeneities in the atmosphere will degrade the vertical resolution. Small scale horizontal inhomogeneities can be considered as random noise and will, together with small scale vertical variations and thermal noise on the measurement, degrade the accuracy and the resolution. The noise will have impact on the resolution because of the integration performed to back-propagate the signal [Marouf *et al.*, 1986]. Larger scale horizontal inhomogeneities can cause bigger problems. This is because horizontal inhomogeneities with scale sizes less than or comparable to the horizontal resolution will be mapped into vertical gradients, as the back-propagation inversion method cannot distinguish the horizontal variations

from vertical gradients. Thus, giving rise to an error in the obtained vertical profiles of refractive index [e.g., *Ahmad*, 1998].

Finally, it should be remembered that the back-propagation inversion method similarly to the Fresnel transform requires a high sampling rate for the method to work. This is because both methods are based on improving the resolution by integration over measured data. Thus, 50 Hz sampling rate seems to be necessary but also sufficient for most problems (see Section 3.3.1).

When sampling rates are sufficiently high, the back-propagation inversion method produces results of the same accuracy as the geometrical optics inversion method but with an improved vertical resolution. Systematic measurement errors and random errors will effect the accuracy of the results in a manner similar to the effect seen on the geometrical optics inversion results – see Section 2.2.2. That is, on the average 1 K accuracy on real data can be achieved [*Rocken et al.*, 1997; *Gorbunov and Gurvich*, 1998a].

## 4.4 Summary

The back-propagation inversion method for inversion of radio occultation measurements has been described. The method is based on a solution to the 2-D Helmholtz equation. This solution is used to back-propagate the measured field to a line much nearer to the atmosphere. At the new virtual measurement line the geometrical optics approximation is applied to invert to refractive index profiles. The back-propagation inversion method has very good vertical resolution and can overcome most multipath problems. The accuracy in smooth areas is as good as the accuracy of the geometrical optics inversion method and furthermore, large vertical refractive index gradients are resolved with high accuracy. The method is, as the geometrical optics inversion method, based on an assumption of spherical symmetry, and deviations from spherical symmetry can seriously degrade the vertical resolution.



## Chapter 5

# Validation and Comparisons: Simulated Data

In this chapter the Fresnel transform inversion method described in Chapter 3 and the back-propagation inversion method described in Chapter 4 will be evaluated based on inversions of simulated occultation data sets. The results will be compared to the results obtained with the geometrical optics inversion method described in Chapter 2.

Model atmospheres containing large vertical refractive index gradients have been used in the simulation of occultations. Through inversion of the obtained simulated occultation data sets the resolution and accuracy of all three inversion methods will be assessed. This will take place in Section 5.1. With respect to the back-propagation inversion method and the geometrical optics inversion method the issues of accuracy and resolution have been addressed previously in [Karayel and Hinson, 1997] and [Mortensen *et al.*, 1999]. Tests of the inversion results when noise has been superimposed on the simulated occultation data sets will be shown in Section 5.2. Finally, in Section 5.3 the importance of the sampling rate of the occultation data set will be discussed through showing an example of the inversion results obtainable with a low sampling rate, and comparing it to the results obtained with a high sampling rate.

The differences between the three inversion methods are in the way the inversion to refractive index is performed. However, in all the examples the obtained temperature profiles will be shown instead of the refractive index profile. This is because the temperature profiles are a more familiar representation of the results, and furthermore the variations in the profiles are more easily seen in the temperature profiles.

### 5.1 Inversion Tests using Simulated Data

#### 5.1.1 Example 1: A Smooth Atmosphere

The first example that will be shown is inversions of a simulated occultation which takes place in a smooth model atmosphere. This example is included to test the average accuracy of the

inversion methods. The simulation has been performed using a ray tracing technique. The method is described in [e.g., *Høeg et al., 1995*]. The ray tracing method originates from a geometrical optics approximation of the signal propagation. For a smooth atmosphere this method gives an accurate simulation of the occultation data.

The atmosphere model used is the MSIS90 model which is an empirical model describing the climatological features of the atmosphere [*Hedin, 1991*]. The model contains slow horizontal variations. No water vapor is included. In the lower part of the atmosphere there is therefore a direct correspondence between temperature and refractive index (see Section 2.3). A simple Chapman layer ionosphere model has been used in the simulation. Finally, in the simulation the Earth has been modeled as ellipsoidal.

The lowest 30 km of the model atmosphere temperature profile used in the simulation is shown in the top panel in Figure 5.1. The temperature profile is the model profile at the position  $76.8^\circ\text{N}$ ,  $126.8^\circ\text{E}$ . This position corresponds to the tangent point of the simulated occultation in the

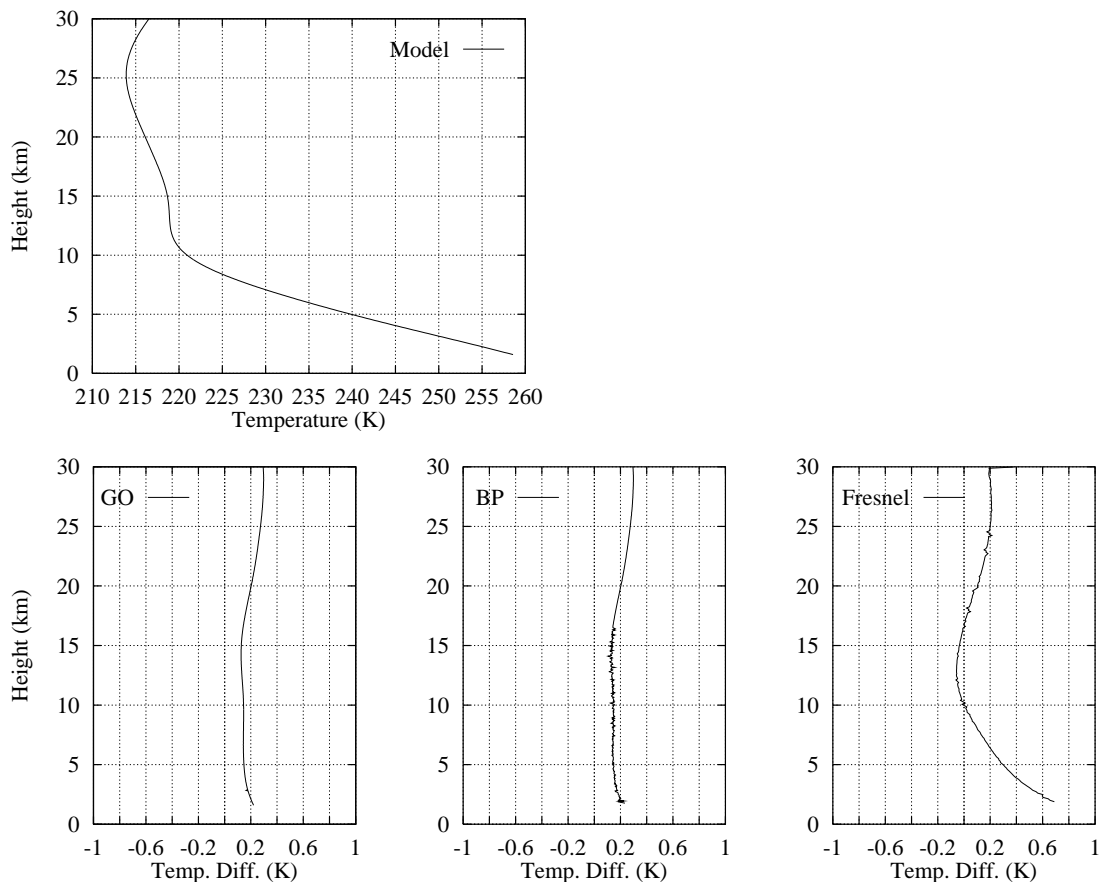


Figure 5.1: *Simulated occultation data based on ephemerides from GPS/MET occultation no. 1, October 14, 1995. Top panel: The atmospheric temperature profile used in the simulation. Bottom panels: Difference between the model atmosphere temperature profile and the derived profiles from inversion of the simulated occultation data set.*

lowest part of the occultation. The ephemerides of the occultation is taken from a GPS/MET occultation. In the first example the simulation is based on the ephemerides of GPS/MET occultation no. 1, October 14, 1995.

The bottom panels in Figure 5.1 show the error of the inversion methods. The error is defined as the model temperature at the position  $76.8^{\circ}\text{N}$ ,  $126.8^{\circ}\text{E}$  subtracted by the temperatures obtained by the inversions. On the left, the error of the geometrical optics (GO) inversion method is shown. In the middle panel, the error of the back-propagation (BP) inversion method is shown. And on the right, the error of the Fresnel transform (Fresnel) inversion method is shown. The simulated occultation data set stops at the same height as the GPS/MET occultation it is based on. In this case it is at a height of 2 km.

As would be expected, because the atmosphere is smooth, all three inversion methods give good results. Both the GO method and the BP method gives errors less than 0.4 K in the height range from 30 km to 2 km. The errors are largest at the top of the profile. This is due to residual errors from the ionosphere correction which can bias the results far down in the neutral atmosphere [Kursinski *et al.*, 1997]. Also, the GO result and the BP result are similar. The BP result shows a little bit of noise, which is numerical noise from the computation of the back-propagation integral. This noise is however of insignificant size. The BP result should be similar to the GO result in a case like this where the atmosphere is smooth without large gradients. The Fresnel method also gives good results. As expected due to the thin screen approximation in the method there is an increasing bias in the inversion result close to the Earth. In this case the bias is less than 0.8 K at the height 2 km. The Fresnel result has the same type of residual error from the ionosphere correction as the GO and the BP method.

The small bias, seen in the GO and the BP results all the way down to the surface, is the result of the influence of horizontal inhomogeneities in the model atmosphere on the simulated occultation data set. The horizontal variations in the climatological MSIS90 model are small and spatially slowly varying. Therefore, the bias would be expected to be small and this is also what is seen. Normal daily large scale variations particularly due to water vapor in the lower part of the troposphere must be expected to be able to introduce significantly larger errors in the inversions [Ahmad and Tyler, 1998a]. The bias in the Fresnel result is mostly caused by the approximations in the Fresnel method.

### 5.1.2 Example 2: The Effect of a Large Vertical Gradient Simulated with the Ray-tracer

The second example is inversion results of a simulated occultation, which takes place in an atmosphere with a large disturbance around the tropopause in an otherwise smooth profile. Thus, this example contains large gradients in the refractive index. As in the previous example a ray-tracing technique was used to perform this simulation. In the area around the disturbance multiple rays have been tracked and added to simulate the effect of multipath. This method

cannot simulate the correct diffraction pattern that will occur in the case of large vertical gradients, but the method gives a sufficient accuracy for the purpose of testing the effect of multipath on the inversions [Gorbunov *et al.*, 1996].

The smooth background atmosphere is again based on the MSIS90 model. In this case the position of the profile is  $51.3^\circ\text{N}$ ,  $123^\circ\text{E}$  which denotes the tangent point of the last sample of the simulated occultation. The top panel in Figure 5.2 shows the lowest 30 km of the temperature profile of the model atmosphere. As in Example 1 it should be noted, that the MSIS90 model contains slow horizontal variations. The added disturbance is spherically symmetric. A simple Chapman layer ionosphere model has been used in the simulation, and the Earth has been assumed to be a sphere.

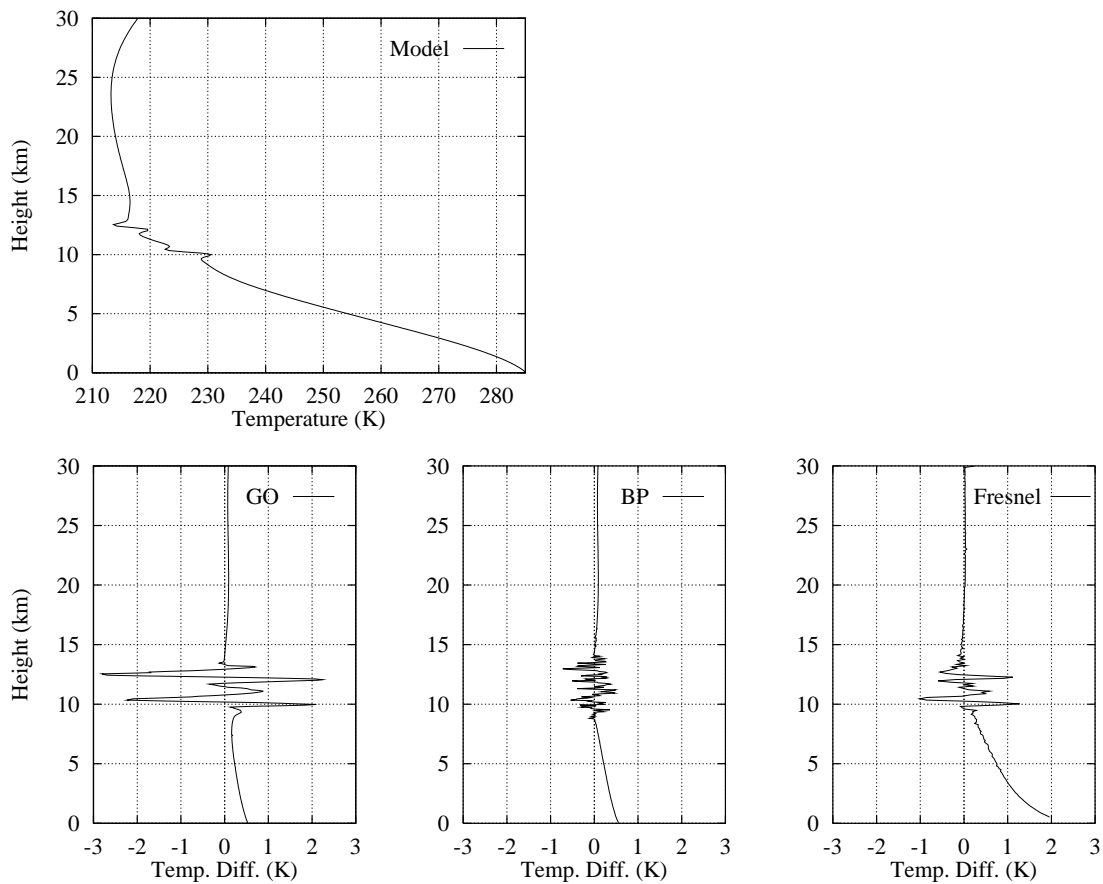


Figure 5.2: *Simulated occultation data based on ephemerides from GPS/MET occultation no. 43, October 22, 1995. Top panel: The atmospheric temperature profile used in the simulation. Bottom panels: The difference between the model atmosphere temperature profile and the derived profiles from inversion of the simulated occultation data set.*

The bottom panels in Figure 5.2 shows the errors of the inversion results. The figure is organized as Figure 5.1 and the error computed in the same manner. In this case, the most interesting part of the results is in the area between 9 km and 14 km, which is the area where the disturbance is placed. The simulated occultation data set in this case goes down below the surface of the

Earth, but the results are only shown down to the height 0 km. The reason why the data set can go below the surface of the Earth is that the simulation is based on ephemerides from a real occultation while the Earth in the simulation has been assumed to be a sphere.

As the gradients of the disturbance are large enough to cause multipath propagation, the GO method is not expected to give very good results. And as can be seen in the bottom, left panel in Figure 5.2 the result of the GO method is indeed not very good in the area around the tropopause. The maximum error that is seen is 2.8 K. The errors are a result of both the multipath propagation and the insufficient resolution of the GO method. The GO method simply smoothes out the variations in the disturbance and calculates a profile through the middle of the disturbance. Hence, the large errors. The BP result, which is shown in the middle, bottom panel in Figure 5.2, gives significantly better results. The maximum error of the method is  $\approx 0.7$  K, and in most parts of the disturbance the error is less than 0.5 K. The BP result looks a little noisy in the area of the disturbance. This is because the BP method expects a diffraction pattern in the occultation data set in an area around the disturbance. As this pattern is wrongly not generated by the ray-tracing forward simulator, the BP method generates the pattern in the inversion result. The effect can be inferred from the similarity to the Fourier transform pair [Goodman, 1986, ch. 3]. A similar effect is seen in the Fresnel result, which is shown in the bottom, right panel. The error of the Fresnel method is a little larger than the error of the BP method. The maximum error is 1.3 K. The error of the Fresnel transform is increased by a slight height-bias. This means that the disturbance is nicely retrieved but slightly displaced in height (less than 100 m). This slight height bias is an artifact of the approximations used in the Fresnel transform, see Section 3.3.

Above 14 km the errors of the GO method and the BP method are less than 0.1 K. The error of the Fresnel method is less than 0.05 K. The very small errors even though there is an ionosphere included in the simulation are a coincidence, i.e., not a generally valid result, as can be seen from the previous example.

Below the disturbance all three inversion methods gives an increasing bias. For the GO method and the BP method it increases to 0.6 K at the surface. This bias must be referred to influence from horizontal variations in the model atmosphere on the simulated occultation data set, which cannot be taken into account by any of the inversion methods. For the Fresnel transform the bias increases to 2 K at the surface, which is a combined effect of the bias arising due to the thin screen approximation and the rather significant effect of horizontal variations on the simulation.

### 5.1.3 Example 3: The Effect of a Small Vertical Gradient Simulated with a Wave Optics Method

The third example is inversion results of a simulated occultation, which takes place in an atmosphere with a moderate disturbance at a height of 8 km in an otherwise smooth profile. The difference to the previous examples is that the simulation in this case is performed with a wave

optics forward simulator. Wave optics in this case implies, that a combination of ray tracing and diffraction theory was used in the forward simulation, such that the diffraction effects around a vertical gradient in the model atmosphere could be correctly simulated. The method is described in more detail in [Kursinski, 1997].

The lowest 30 km of the temperature profile of the model atmosphere used for the simulation is shown in the top panel in Figure 5.3. It should be noted that the occultation simulation stops at a height of 4 km. The atmosphere model is spherically symmetric with no ionosphere model and no water vapor. Thus, the temperature profile determines the refractive index profile uniquely. The temperature profile is piecewise linear as can be seen in the figure. The disturbance in the atmosphere model consists of a change in the temperature profile between 8.5 km and 8 km. The gradient change equals a jump of 3 K in the back-ground temperature profile. This disturbance resembles an inversion layer in the atmosphere.

In the simulation, the Earth has been assumed to be spherical and the LEO and GPS orbits have been assumed to be circular symmetric, and in plane, with radius 7,163.136 km and 26,609 km, respectively.

In the middle panels of Figure 5.3 the errors of the inversion methods are shown. All three methods show good results for this simulation example. The effect of a spherically symmetric atmosphere is seen in the GO and the BP result, as the average errors of the inversion results are 0 K in areas away from gradient changes. The effect of changes in the temperature gradient is most visible in the GO result. In this, the four changes in the temperature gradient, which equals disturbances in the refractive index profile, show up as oscillations in the inversion results. This is the effect of the diffraction pattern on the GO inversion. Still, the error of the GO method is less than 0.35 K in the entire height range shown. Even though the GO method gives good results for this relatively smooth example, the improvement obtained using the BP method shows up very clearly. This improvement is illustrated in the middle central panel of Figure 5.3. It should be noted that the GO method is used in the BP method above 17 km. Thus, the top one of the four disturbances still shows up in the inversion result. However, the other three disturbances are removed completely by the inversion, and the residual error is negligible. Below 5 km the BP method shows oscillations in the result. The BP method expects a diffraction pattern from the edge of the Earth in the lowest part of the occultation data set. Thus, the oscillations in the inversion result are artifacts of the simulation occultation data set ending abruptly at 4 km. The effect has not been seen in the previous examples because the inversions have been terminated a little before the end of the occultation data sets. The right, middle panel in Figure 5.3 shows the error of the Fresnel result. As expected due to the approximations in the method the error seen for the Fresnel result is larger than what is seen for the two other methods. The maximum inversion error is almost 0.6 K and occurs in the area of the disturbance at 8 km. The Fresnel method has the same tendency as the BP method to introduce oscillations in the lowest part of the inversion. The reason why the effect is not obvious in the example here is due to differences in the integration method between the Fresnel and the BP method, which causes the effect to start at slightly different heights. The steps seen in the error result of the Fresnel method occur

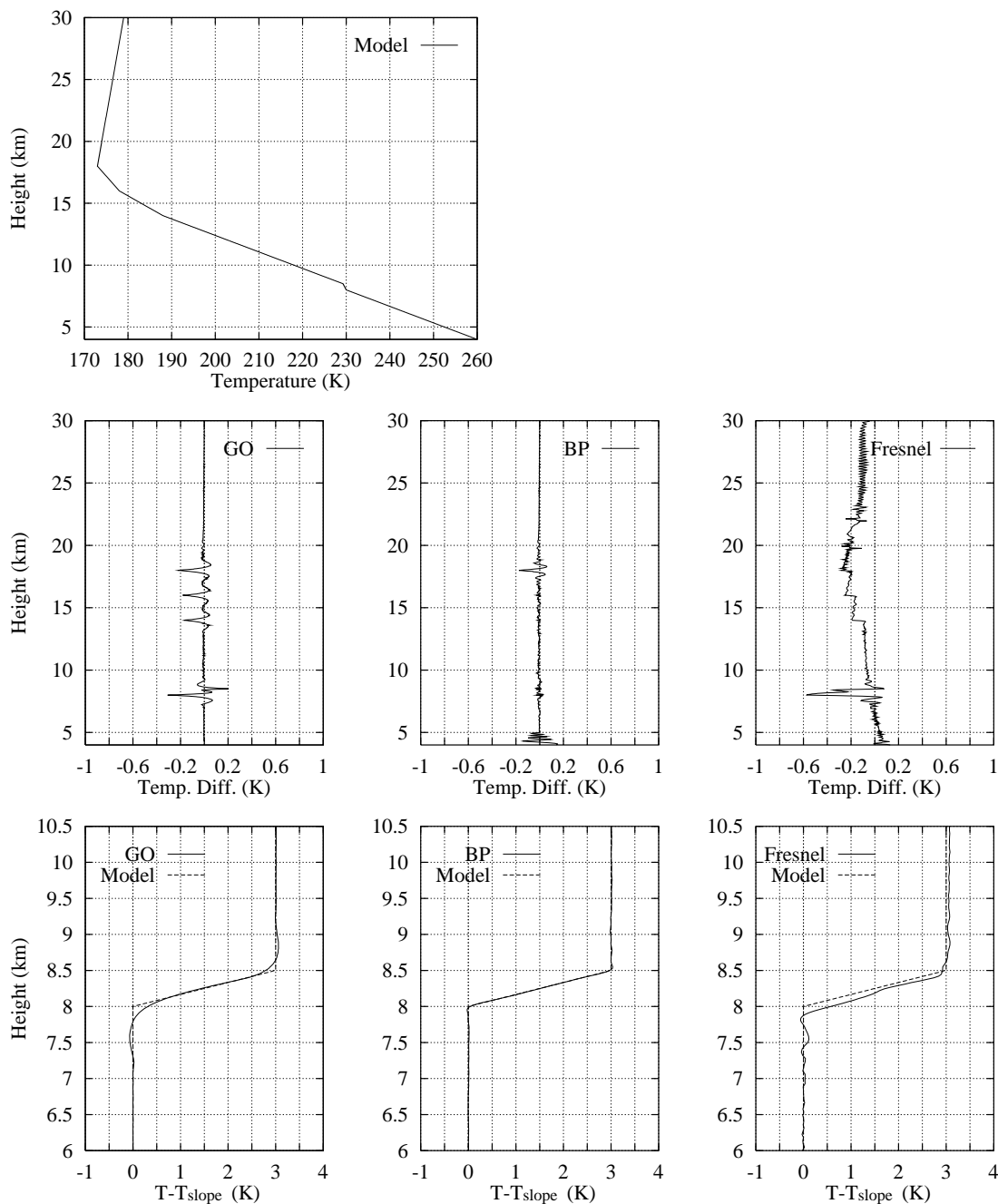


Figure 5.3: *Simulated occultation data, wave optics model. Model atmosphere with a small gradient. Top panel: The atmospheric temperature profile used in the simulation. Middle panels: The difference between the model atmosphere temperature profile and the derived profiles from inversion of the simulated occultation data set. Bottom panels: The inverted temperature profiles together with the model profile where the back-ground temperature slope has been subtracted.*

where there is a change in the temperature gradient. The steps are caused by a small height bias of the change in the gradient in the inversion result.

The bottom panels in Figure 5.3 show a limited area of the temperature profile around the disturbance at 8 km. The temperature profiles have been plotted with the linear back-ground temperature slope subtracted, such that the temperature gradient in areas away from the disturbance is zero. The dashed line in the plots is the model atmosphere temperature profile. These plots illustrate how the inversion errors are connected with the resolution. In the GO result, which is shown on the left, it can be seen that the error of the inversion is due to the GO method smoothing the edges of the disturbance due to the limited resolution of the method. The BP method can be seen to retrieve the disturbance almost perfectly in compliance with the error result. Finally, on the right it can be seen why the Fresnel result shows a bigger error than the other two methods. The disturbance is actually resolved well, but it is spatially biased which leads to large errors when the difference to the model profile is calculated. The spatial bias can be estimated to  $\approx 100$  m. Also it can be seen, that the Fresnel result is not quite as smooth as the two other profiles. This is an effect of numerical noise that could be reduced by improving the filtering (see Section 3.2.2).

#### 5.1.4 Example 4: The Effect of a Large Vertical Gradient Simulated with a Wave Optics Method

The fourth example is inversion of an occultation, which has been simulated with the wave optics method in the same manner as described for Example 3. The lowest 30 km of the temperature profile of this example is shown in the top panel of Figure 5.4.

The only difference to the previous example is that the disturbance at 8 km is significantly larger. The disturbance in the atmosphere model consists of a change in the temperature profile between 8.5 km and 8 km. The gradient change equals a jump of 10 K in the back-ground temperature profile. As in Example 3, the disturbance resembles an inversion layer in the atmosphere. The refractive index gradient corresponding to this temperature gradient is likely to occur often in a real atmosphere. However, in general this kind of refractive index gradient will be caused by a combined effect of water vapor and a large temperature gradient. This is not important for the tests, as the inversion methods invert to refractive index profiles, and the conversion to temperature is only a convenient way of presenting the results.

The disturbance in this case is so large that multipath propagation becomes significant. The effect of this shows up in the errors, which are shown in the middle panels in Figure 5.4. Note the scale difference in comparison with the previous figures. The GO result in this case shows a large error at the disturbance ( $\approx 3.5$  K). Furthermore, a bias in the inversion result appears which is significant even 1 km below the end of the disturbance. Neither the BP result nor the Fresnel result has the same kind of problems with resolving the multipath propagation.

In the bottom panels, the temperature profiles obtained in the area around the disturbance are shown. The profiles have been displayed with the back-ground temperature slope subtracted. As expected from the error profile, the GO result has significant resolution problems. Due to

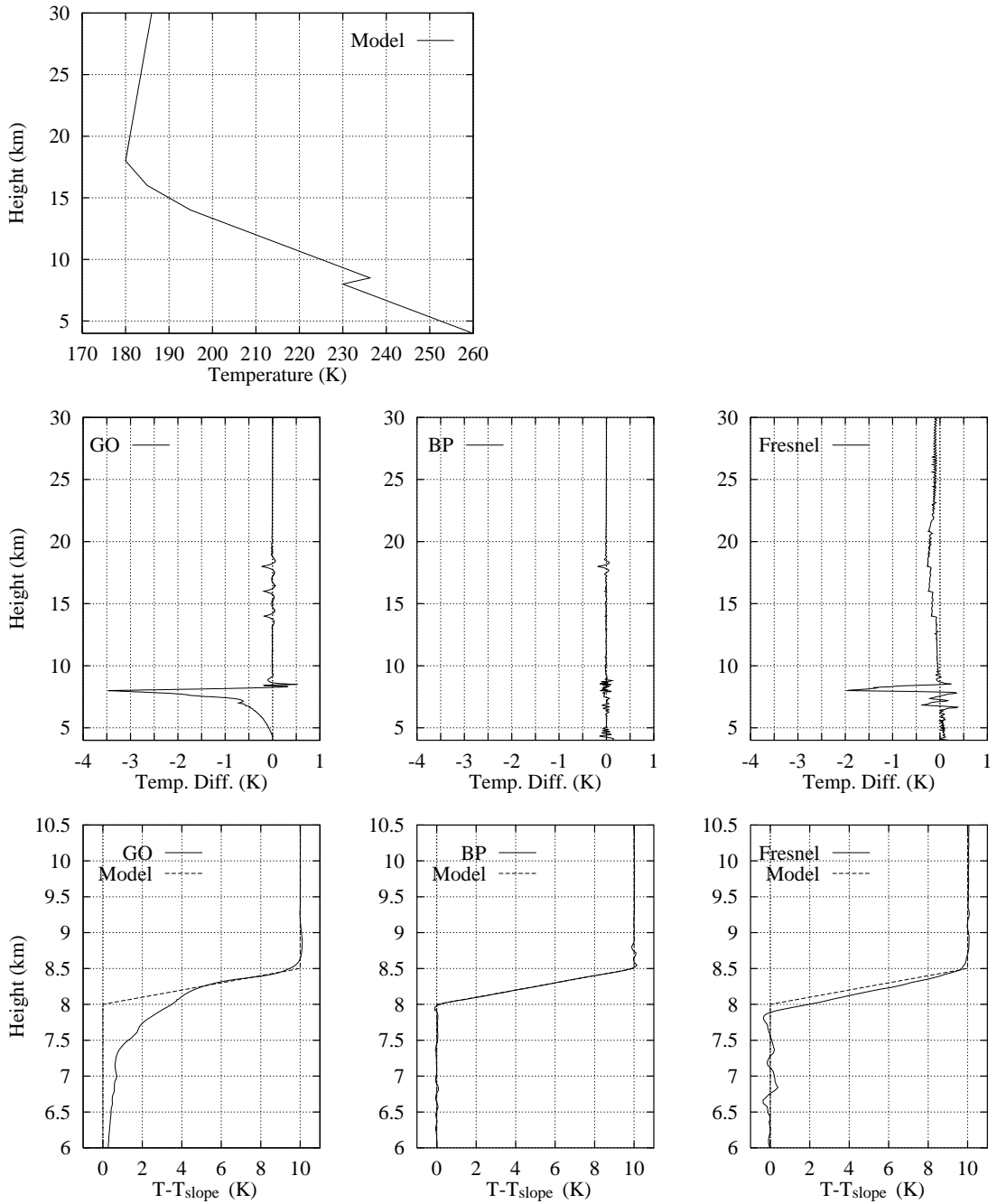


Figure 5.4: *Simulated occultation data, wave optics model. Model atmosphere with a large gradient. Top panel: The atmospheric temperature profile used in the simulation. Middle panels: The difference between the model atmosphere temperature profile and the derived profiles from inversion of the simulated occultation data set. Bottom panels: The inverted temperature profiles together with the model profile where the back-ground temperature slope has been subtracted.*

the large bias it would be difficult to define a resolution of the disturbance for the GO method. The main problem for the GO method in this case is the multipath propagation which disturbs

the inversion. The BP result and the Fresnel result, on the other hand, are very similar to the results seen in Example 3. These methods have no problems with the multipath propagation in this simulation. As in Example 3, the larger inversion error of the Fresnel transform can be attributed to a height bias. It should be noted, that both in this example and in Example 3 the height bias in the Fresnel result is a more significant error than the error in the average result of the Fresnel method. This is partly because the simulations stop at a height of 4 km, which is before the worst bias of the Fresnel method will appear.

### 5.1.5 General Remarks on the Results

The examples show that both the back-propagation inversion method and the Fresnel transform inversion method is superior to the geometrical optics inversion with regards to vertical resolution and handling of multipath propagation. Due to the approximations in the Fresnel method, which limits the accuracy of the results, the vertical resolution of this method has not been studied in further detail. Detailed studies of the lower limits of the vertical resolution of the BP method can be found in [Karayel and Hinson, 1997] and [Mortensen et al., 1999].

The conclusion of the studies of the BP method is, that the lower theoretical vertical resolution limit of the method is of the order of 100 m. The lower limit is a result of the focus point of the signal in the occultation geometry being smeared, due to the satellite movements, such that a well defined focus point cannot be found [Mortensen et al., 1999]. This vertical resolution cannot always be expected to be achievable in practice due to the influence from horizontal variations on the occultation data [Karayel and Hinson, 1997; Gorbunov and Gurvich, 1998a].

The maximum vertical gradient of the refractive index that was retrieved in the experiments in [Karayel and Hinson, 1997] and [Mortensen et al., 1999] was  $8.5 \cdot 10^{-8} \text{ m}^{-1}$ . The disturbance in Example 4 shown here has a gradient of  $2.09 \cdot 10^{-8} \text{ m}^{-1}$ . For comparison critical refraction - which is the case where the signal is bend so much that it will be trapped in the vertical layer - occurs at a gradient of  $\approx 16.0 \cdot 10^{-8} \text{ m}^{-1}$ . If critical refraction occurs, the signal will be lost by the LEO satellite receiver. For larger gradients than  $\approx 8.5 \cdot 10^{-8} \text{ m}^{-1}$  the BP method cannot resolve the multipath propagation. This is because there can be found no position of the back-propagation line (see Section 4.2.2) where the multipath propagation is not present.

## 5.2 Inversion Tests using Simulated Data with Noise

In the examples shown so far, the back-propagation inversion method in particular, and to some extent also the Fresnel inversion methods, show very good inversion results with high vertical resolution. An important concern however, is how the inversion methods will perform when the occultation data sets contain measurement noise.

To illustrate the effect of random measurement noise on the BP results and the Fresnel results,

Example 4 will be reused. The simulated occultation data set used in Example 4 has been modified such that 10 mm (sample to sample) random noise is added to the phase of the data set. This noise level is a realistic guess of the noise level in an occultation measurement in moderate cases, where the random atmospheric noise is not too large. This can be inferred from a study of the GPS/MET data [Kursinski *et al.*, 1997].

In the top panel in Figure 5.5 the temperature profile of Example 4 is shown again. The inversion results shown in the middle and the bottom panels are Fresnel results.

On the left, in the middle panel in Figure 5.5, the error of the Fresnel method in the case where there is no noise on the occultation data is shown. This equals the result shown in Figure 5.4. In the right, middle panel in Figure 5.5, the error of the Fresnel method is shown for the case where noise has been added to the occultation data set. As can be seen, the disturbance at 8 km is retrieved just as well as in the no noise case. On the other hand, there is a significant amount of noise in the inverted result particularly above  $\approx 17$  km. The noise in the inversion could probably be limited if a better filtering technique was used when the Fresnel transform integral is calculated (see Section 3.2.2).

The bottom panels in Figure 5.5 show the inverted temperature in an area around the large disturbance. As could already be inferred from the inversion errors, the disturbance is well retrieved despite the noise. Furthermore, it can be seen that the noise has no significant impact on the inversion at this height.

In the top panel in Figure 5.6 the temperature profile of Example 4 is shown again. The inversion results shown in the middle and the bottom panels are BP results.

On the left, in the middle panel in Figure 5.6, the error of the BP method in the case where there is no noise on the occultation data is shown. This equals the result shown in Figure 5.4. In the right, middle panel in Figure 5.6, the error of the BP method is shown for the case where noise has been added to the occultation data set. As in the Fresnel case the disturbance at 8 km is retrieved just as well as in the no noise case. The amount of noise in the results increases with height, but the noise in the inversion result does not get larger than 1 K before  $\approx 24$  km. That the noise level for larger heights is low for the BP method is mainly because the method is merged into the GO result above 17 km. As can be seen in Figure 5.6, the noise in the BP method is larger in the area from 12 – 17 km than from 17 – 23 km. This indicates that it might be a good idea to improve the simple filtering technique used in the back-propagation integral (see Section 4.2.2). The reason for doing this would be that the noise level, used in the simulation shown here, is lower than what can be seen in a real measurement.

The bottom panels in Figure 5.6 show the inverted temperature in an area around the large disturbance. As could already be inferred from the inversion errors, the disturbance is well retrieved despite the noise. Furthermore, it can be seen that the noise has no significant impact on the inversion at this height.

Figure 5.5 and Figure 5.6 illustrate that the Fresnel transform inversion method and the back-propagation inversion method have very similar behavior toward noise. This is due to the

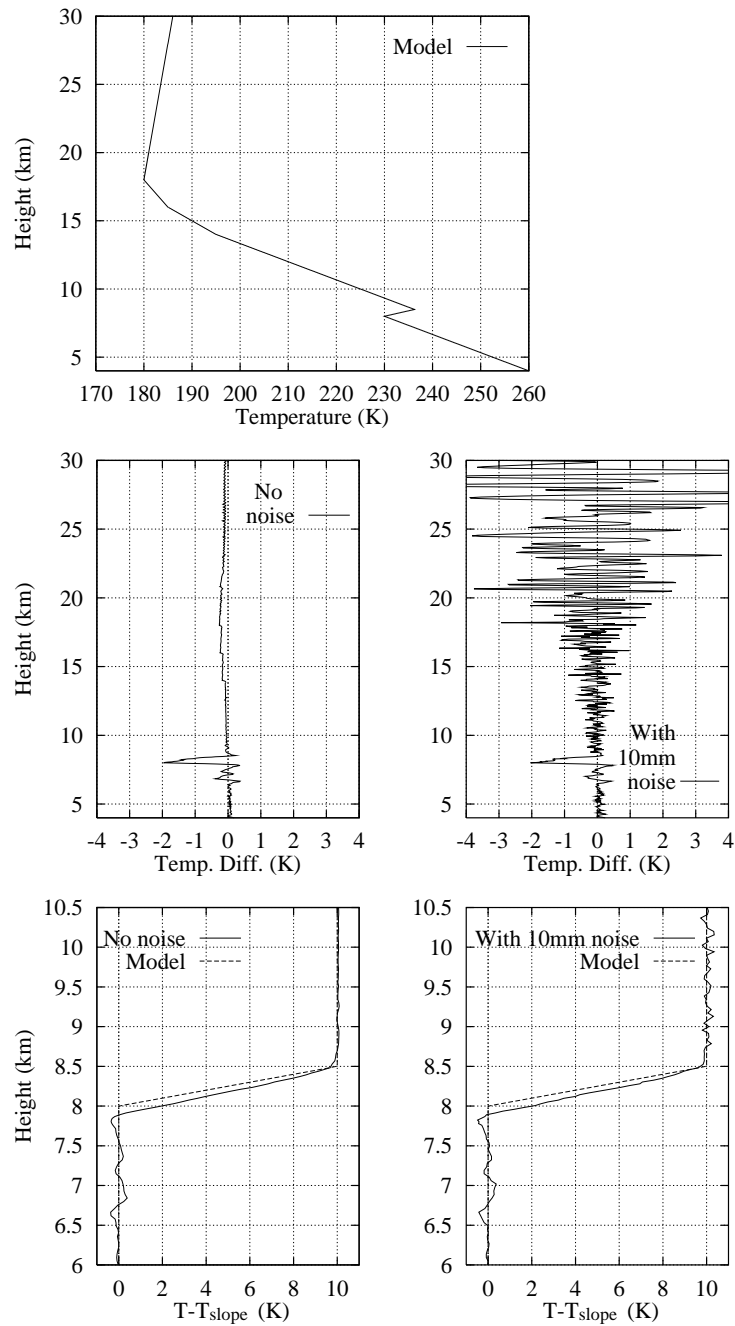


Figure 5.5: *Simulated occultation data, wave optics model. Comparisons of Fresnel inversion results with and without noise. Top panel: The atmospheric temperature profile used in the simulation. Middle panels: The difference between the model atmosphere temperature profile and the derived profiles from inversion of the simulated occultation data set. Bottom panels: The inverted temperature profiles together with the model profile where the back-ground temperature slope has been subtracted.*

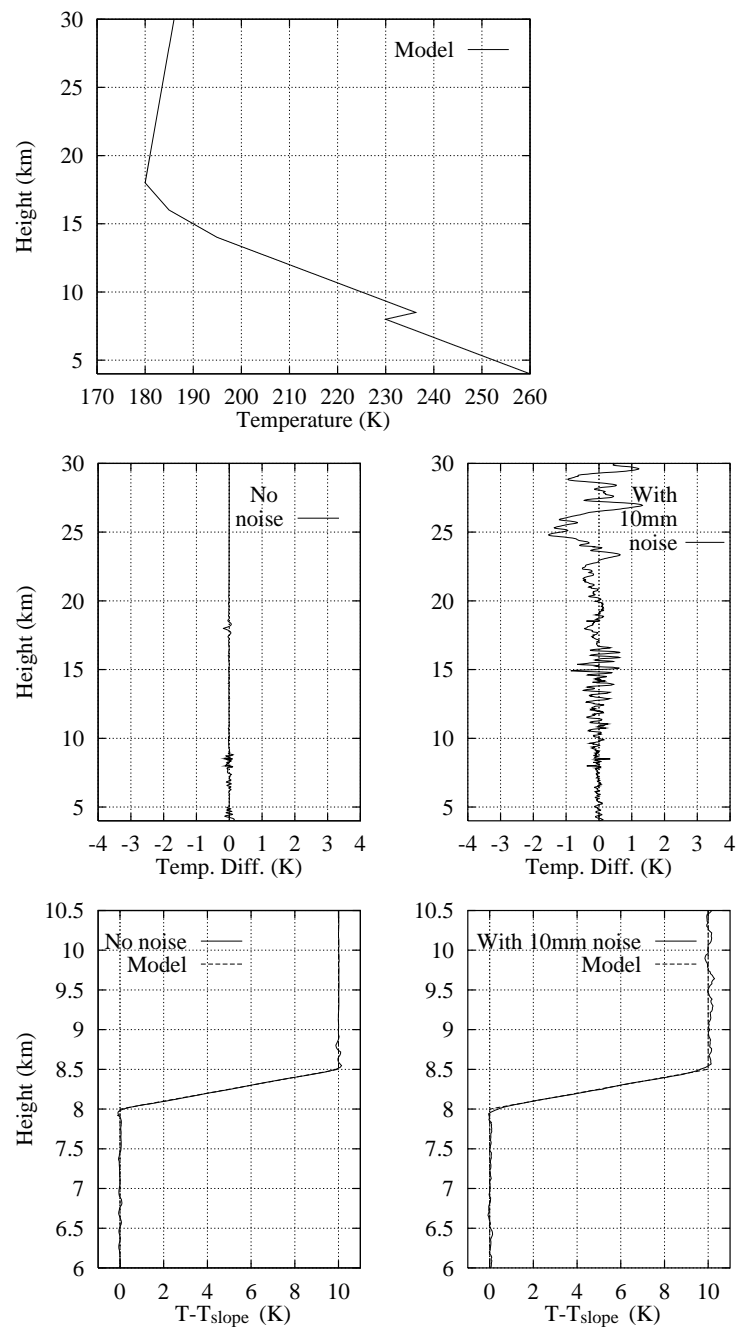


Figure 5.6: *Simulated occultation data, wave optics model. Comparisons of back-propagation inversion results with and without noise. Top panel: The atmospheric temperature profile used in the simulation. Middle panels: The difference between the model atmosphere temperature profile and the derived profiles from inversion of the simulated occultation data set. Bottom panels: The inverted temperature profiles together with the model profile where the back-ground temperature slope has been subtracted.*

similarity in the principle of how the improved vertical resolution and the removing of multipath propagation is achieved. That is, both methods are based on an integral transform of the measured signal, which is based on the solution to the wave equation. The test shows no degradation of the resolution due to the noise. In practice however, it is not yet certain that the atmospheric noise in the lower troposphere is not larger than the estimate used here, and thus a degradation of the resolution might be the result in practice [Gorbunov and Gurvich, 1998a].

### 5.3 Inversion Tests of the Importance of the Sampling Rate

As mentioned in Section 3.3.1 and Section 4.3 the sampling rate of the occultation is important when the Fresnel transform inversion method and the back-propagation inversion method is to be used. The sampling rate is mainly of importance when the atmosphere contains large gradients, because these will generate a diffraction pattern in the received signal which must be sufficiently densely sampled to be retrieved.

To illustrate the impact of reducing the sampling rate a simulated occultation data set similar to the one used in Example 3 has been used. The difference to Example 3 is, that the disturbance in the atmosphere model consists of a change in the temperature profile between 8.0625 km and 8 km. The change equals a temperature jump of 3 K. Thus, the gradient in this case is large over a short range.

Figure 5.7 illustrates the impact of changing the sampling rate. The top panel in Figure 5.7 shows the model temperature profile. The middle panels show the results obtained with the Fresnel method, compared to the model data in the area around the disturbance. The middle panel on the left shows the result obtained with the full sampling rate (50 Hz), i.e., the sampling rate that was used in the simulation examples shown previously. On the middle, right is shown the result when the sampling rate of the occultation data set is reduced by a factor of five (10 Hz).

The results shown in the middle panels in Figure 5.7 show only a very slight degradation of the vertical resolution when using the 10 Hz occultation data compared to the 50 Hz data. The reason, why the difference is small, is that the spatial sampling density at 8 km is high, even for 10 Hz data (see Figure 3.7). At larger heights bigger problems must be expected, while the sampling density increases even more when the height decreases further. Thus, at low heights the sampling rate of 50 Hz does not seem to be a critical issue with regards to achieving good inversion results. The gradients in the atmosphere can easily become larger than the one used in this example - the gradient in the example is only about  $\frac{1}{6}$  of the gradient causing critical refraction. The requirements on the sampling density will be larger when the gradients are larger, but tests have not been performed.

The test indicates that for most purposes a sampling rate of 10 Hz is sufficient to achieve good inversion results in the troposphere and around the tropopause, where high vertical resolution

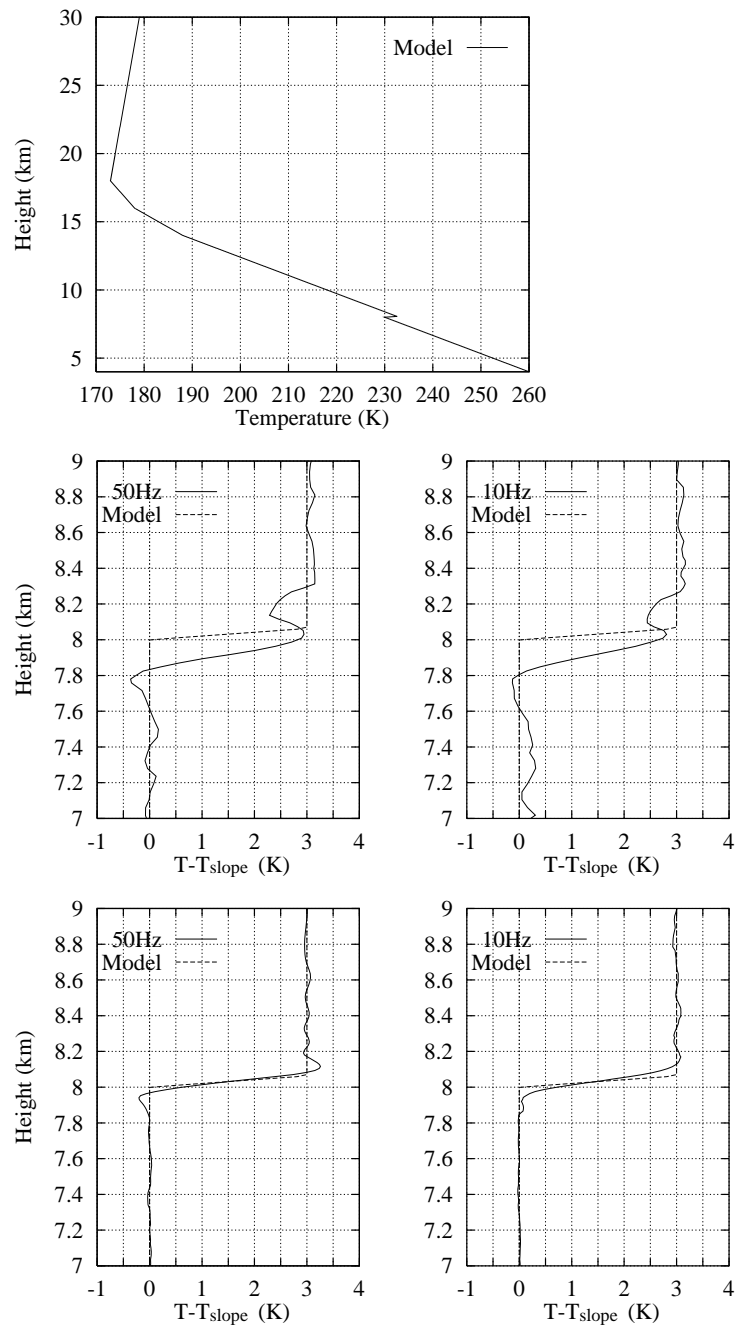


Figure 5.7: *Simulated occultation data, wave optics model. Comparisons of Fresnel and BP results for different sampling rates. Top panel: The atmospheric temperature profile used in the simulation. Middle panels: The temperature profiles inverted with the Fresnel method together with the model profile where the back-ground temperature slope has been subtracted. Bottom panels: The temperature profiles inverted with the BP method together with the model profile where the back-ground temperature slope has been subtracted.*

inversion results are of main interest. However, the test has been performed without noise and a high sampling rate offers the possibility to smooth the data without losing resolution. Also, the high sampling rate ( $\geq 50$  Hz) seems necessary for the measurement anyway to avoid cycle slips when the signal is received, due to the very fast varying phase in the troposphere [Gorbunov and Gurvich, 1998a].

The bottom panels in Figure 5.7 shows the same test of the importance of the sampling rate performed for the back-propagation inversion method. The bottom panels in Figure 5.7 show the inverted results compared to the model data in the area around the disturbance. The bottom panel on the left shows the result obtained with the full sampling rate. On the bottom, right is shown the result when the sampling rate of the occultation data set is reduced by a factor of five.

As expected due to the similarities between the BP method and the Fresnel method, the result for the BP method is similar to the result achieved for the Fresnel method. Only a slight degradation of the vertical resolution is seen in the inversion of the 10 Hz data in comparison with the result obtained by inversion of the 50 Hz data. Thus, the same comments to the result, as was given to the result of the test of the Fresnel method, applies.

## 5.4 Summary

The simulations in this chapter illustrates the main differences between the occultation inversion methods. The back-propagation inversion method is seen to manage the inversion at least as good as the geometrical optics inversion method. In areas with large gradient, where good resolution is needed, the back-propagation inversion method is clearly superior. Thus, this indicates that the back-propagation inversion method is to be preferred under all circumstances. The Fresnel transform inversion method has good vertical resolution, but there is a significant bias ( $> 1$  K) in the average result below  $\approx 4$  km. Both the back-propagation inversion method and the Fresnel transform inversion method can resolve multipath problems to a large extent. All three methods have similar problems with horizontal variations, as the methods are all based on an assumption of spherical symmetry.

## Chapter 6

# Validation and Comparisons: GPS/MET Data

The Microlab-1 satellite carrying the GPS/MET experiment was the proof-of-concept mission for GPS radio occultation measurements of the atmosphere of the Earth. For the validation and comparison tests in this chapter two GPS/MET occultations have been selected. Both are from periods where the GPS anti-spoofing system was turned off. This gives the highest accuracy of the data [*Hofmann-Wellenhof et al.*, 1993].

The two examples will be used to illustrate the results that can be obtained with the back-propagation inversion method and the Fresnel transform inversion method. In Section 6.1 the results obtained will be compared with the results obtained with the geometrical optics inversion method. Furthermore, in Section 6.2 the results will be compared to an independent data set. A more general statistical analysis of the obtainable inversion results with the back-propagation inversion method can be found in [*Rocken et al.*, 1997] where a mean accuracy of approximately 1 K is reported.

As in the previous chapter, the inversion results shown are temperature profiles. In the case of real measurements, the atmosphere will generally contain water vapor in the lower troposphere. Water vapor cannot be distinguished from the temperature in the conversion from refractive index to temperature without inclusion of prior information from another source. The results shown here will be the dry temperature results. That is, results derived as if there was no water vapor in the atmosphere.

### 6.1 Comparing the Results from the Inversion Methods

The first example is inversion results of GPS/MET occultation no. 174, February 4, 1997. This occultation took place at 51.7°N, 139.0°E. The obtained temperature profiles are shown in

Figure 6.1. The temperature profiles are shown from 30 km to the surface or as far down as the occultation has measured the profile. In this case the occultation stops at a height of 3 km. The top panels show the back-propagation (BP) inversion result compared with the geometrical

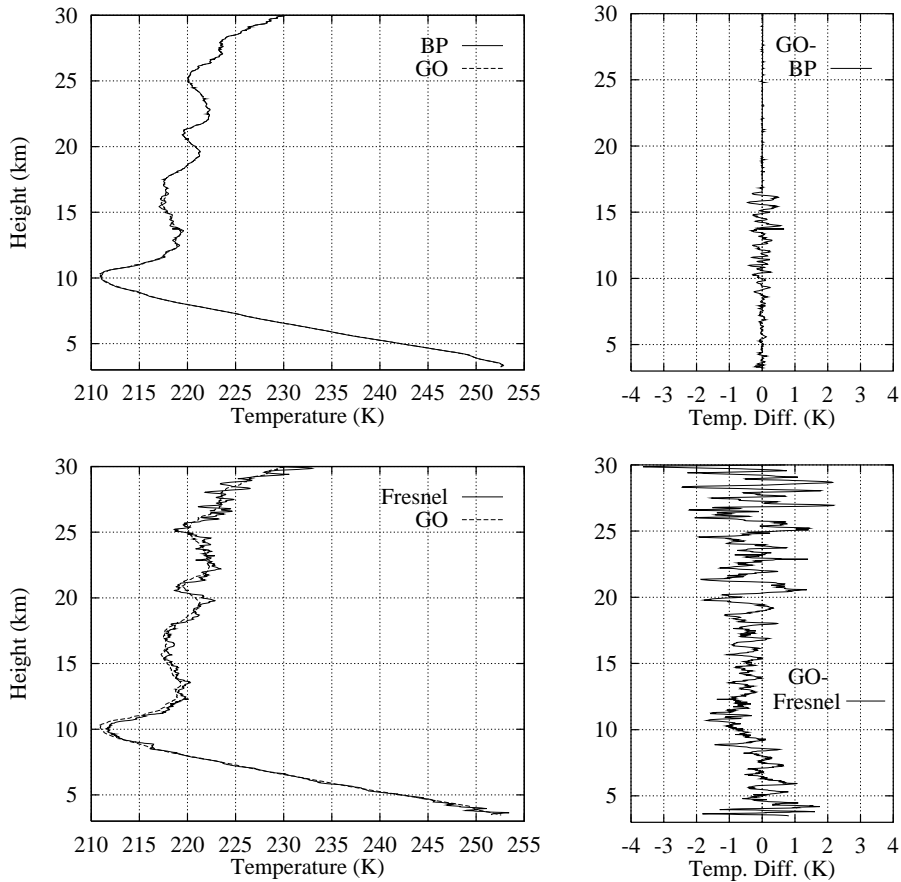


Figure 6.1: Inversion of GPS/MET occultation no. 174, Feb. 4 1997. Position:  $51.7^\circ N$ ,  $139.0^\circ E$ . Top, left: BP result (solid line) and GO result (dashed line). Top, right: Difference between GO and BP result. Bottom, left: Fresnel result (solid line) and GO result (dashed line). Bottom, right: Difference between GO and Fresnel result.

optics (GO) inversion result. In the top, left panel the BP result is shown as the solid line, and the GO result as the dashed line. In the top, right panel the temperature difference  $T_{GO} - T_{BP}$  is shown. Similarly, in the bottom panels the Fresnel transform (Fresnel) inversion result is compared with the GO inversion result. In the bottom, left panel the Fresnel result is shown as the solid line, and the GO result is again shown as the dashed line. In the bottom, right panel the temperature difference  $T_{GO} - T_{Fresnel}$  is shown.

The obtained temperature profiles shown in Figure 6.1 are relatively smooth. Thus, as would be expected, the differences between the BP and the GO result are small. Above 17 km the GO method is used in both cases. The slight difference between the results is noise, and is caused by the smoothing algorithm for the data set being initialized at slightly different altitudes for the two inversions. Below 17 km the difference between the BP result and the GO result is less than

0.7 K. From 17 km down to the tropopause at  $\approx 10$  km there is a little more structure in the BP result than in the GO result. When comparing to the noise test results shown in Section 5.2, it seems most reasonable to attribute most of this difference to noise in the BP result. In the troposphere there is hardly any difference between the results.

The difference between the Fresnel result and the GO result is somewhat larger. Two of the problems which were also seen in the inversion of simulated occultation data sets (see Chapter 5) appear in this result: there is noise in the Fresnel result because the filtering technique used in the Fresnel method is not good enough, and there is a small bias in the average result. However, the average error when compared to the GO result is less than 1 K and the noise is also less than  $\pm 1$  K from 20 km down to  $\approx 4$  km. From  $\approx 4$  km down to 3 km the noise is larger. This can be due to the combination of the problem with reducing the noise in the Fresnel result and the abrupt ending of the data set at 3 km. As the effect is not pronounced in the BP inversion, the main problem must be noise in the Fresnel inversion result. The structure of the bias in the average result seen in Figure 6.1 very much resembles the bias seen in Example 1 in the previous chapter, which was the inversion result of a simulated occultation in a smooth atmosphere.

The second example is inversion results of GPS/MET occultation no. 52, February 4, 1997. This occultation took place at  $32.3^\circ\text{S}$ ,  $10.2^\circ\text{E}$ . The obtained temperature profiles are shown in Figure 6.2. This is an example of inversion of an occultation which has taken place in a not so smooth atmosphere. The occultation in this case stops at a height of 1.8 km. Figure 6.2 is organized as the previous figure. In the top, left panel in Figure 6.2 the BP result is shown as the solid line and the GO result as the dashed line. In the top, right panel the temperature difference  $T_{\text{GO}} - T_{\text{BP}}$  is shown. Similarly, in the bottom, left panel the Fresnel result is shown as the solid line and the GO result is again shown as the dashed line. In the bottom, right panel the temperature difference  $T_{\text{GO}} - T_{\text{Fresnel}}$  is shown.

Some of the general features of this example are the same as the ones seen in the first example. That is, both the BP result and in particular the Fresnel result contain noise in the inversion result. Furthermore, the Fresnel result is slightly biased in the average result. The bias seen for large heights in the Fresnel result is due to a combination of two effects. First of all, a difference in the ionosphere correction method (see Section 3.2.3 and Section 4.2.1) causes the residual error due to the ionosphere correction to be different in the Fresnel result than in the other methods. Secondly, the larger noise level in the Fresnel results for large heights makes a good initialization of the temperature calculation (see Section 2.3) difficult.

The tropopause is in this example at a height of  $\approx 16$  km. Both the BP result and the Fresnel result show a better resolution of the tropopause than the GO result. A disturbance is seen clearly in the BP result and can also be seen in the Fresnel result, although it is partly hidden by the noise. The level of this disturbance is bigger than what can be explained by noise, and besides a random noise disturbance would not show up similarly in the Fresnel and the BP result. At low heights; below  $\approx 8$  km, the differences to the GO result are more significant. There is a pronounced difference in the temperature gradient of both the Fresnel result and the BP result to the GO result around 8 km. This causes a difference of approximately 2 K to the GO result.

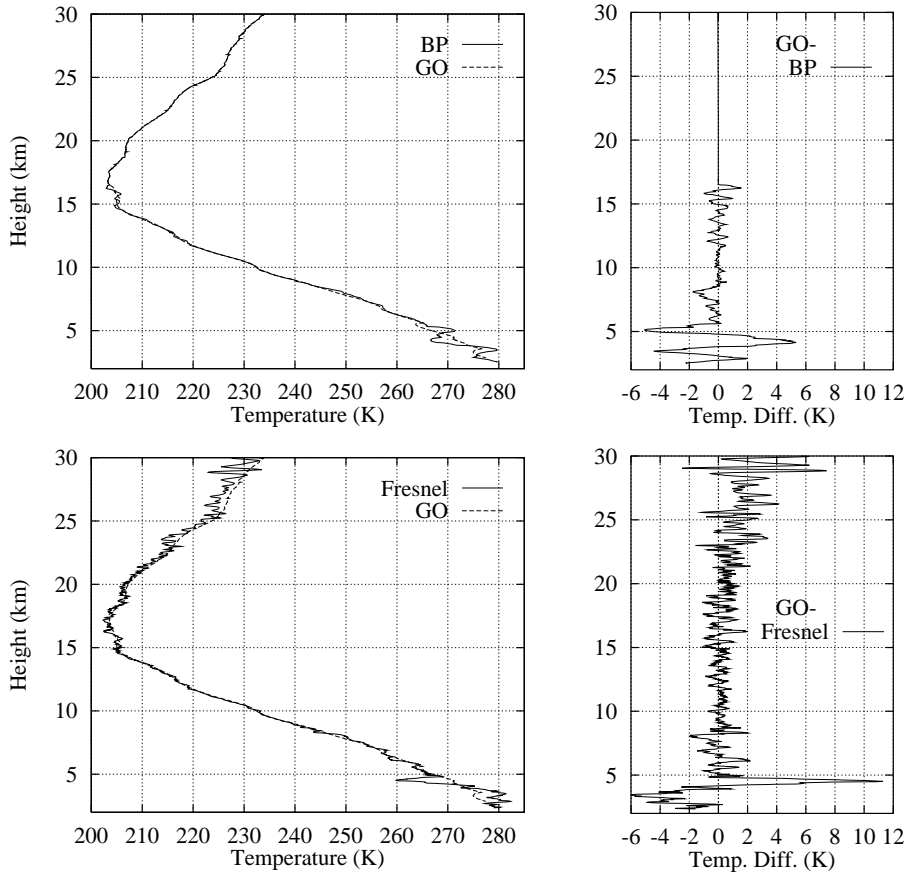


Figure 6.2: *Inversion of GPS/MET occultation no. 52, Feb. 4 1997. Position:  $32.3^{\circ}$  S,  $10.2^{\circ}$  E. Top, left: BP result (solid line) and GO result (dashed line). Top, right: Difference between GO and BP result. Bottom, left: Fresnel result (solid line) and GO result (dashed line). Bottom, right: Difference between GO and Fresnel result.*

This difference is of the same level as the difference seen around the tropopause. Around 4 km a larger disturbance is detected by the BP method and the Fresnel method. The Fresnel method is height biased as was also seen with large gradients in the inversion of simulated occultation data sets. Apart from this bias, the results of the Fresnel method and the BP method have similar structure. The Fresnel method shows a larger disturbance than the BP method. This could be an effect of noise in the inversion as has been seen previously. However, compared to the BP and the Fresnel result, the GO result seems to be significantly oversmoothed. The cause of this discrepancy will be further discussed when the results are compared to an independent data set in the next section.

## 6.2 Comparisons with Independent Data

The two examples of inversion of GPS/MET occultation data sets have also been compared to ECMWF reanalysis model data. The ECMWF model data denotes data from the European

Centre for Medium-Range Weather Forecasts [Shaw *et al.*, 1987]. These data are numerical weather prediction data based on primarily radiosonde data as input. This means that if there is a radiosonde station close by, then the ECMWF data will generally resemble this measurement.

In Figure 6.3, the results of inversion of GPS/MET occultation no. 174, February 4, 1997 are shown together with the ECMWF data. The ECMWF data consist of 14 levels between the surface and  $\approx 24$  km. Thus, these data have low vertical resolution and the comparisons to the occultation inversion results stops at the height  $\approx 24$  km. The top panels in Figure 6.3 show the

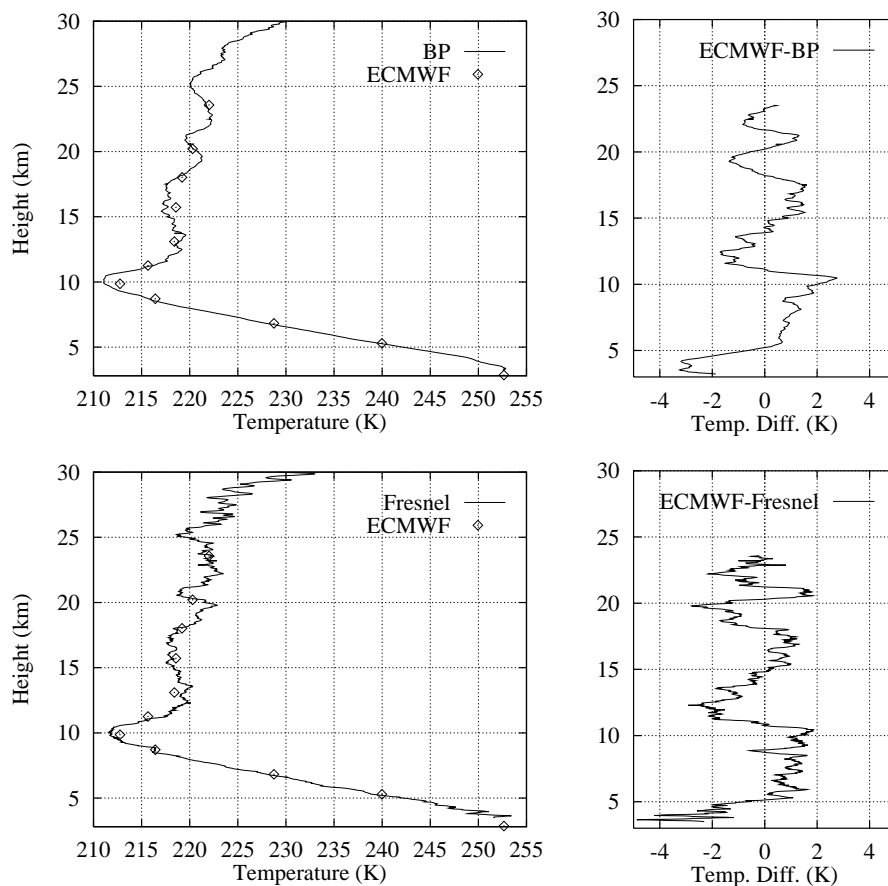


Figure 6.3: *Inversion of GPS/MET occultation no. 174, Feb. 4 1997. Position: 51.7° N, 139.0° E. Top, left: BP result (solid line) and ECMWF model result (diamonds). Top, right: Difference between ECMWF and BP result. Bottom, left: Fresnel result (solid line) and ECMWF model result (diamonds). Bottom, right: Difference between ECMWF and Fresnel result.*

BP result compared with the ECMWF model data. In the top, left panel the BP result is shown as the solid line and the ECMWF model data are shown as diamonds. In the top, right panel the temperature difference  $T_{\text{ECMWF}} - T_{\text{BP}}$  is shown. Similarly, in the bottom panels the Fresnel result is compared with the ECMWF data set. In the bottom, left panel the Fresnel result is shown as the solid line and the ECMWF data set is again shown as diamonds. In the bottom, right panel the temperature difference  $T_{\text{ECMWF}} - T_{\text{Fresnel}}$  is shown. To calculate the temperature difference linear interpolation has been used between the samples in the ECMWF data set.

As can be seen from Figure 6.3 there is a fairly good agreement between the inversion results and the ECMWF data set. Generally, the difference is less than  $\pm 2.5$  K except between 3 km and  $\approx 4$  km where the difference is larger. This accounts for both the Fresnel and the BP method. The major part of the differences between the inversion results and the ECMWF data, seen in the difference plots in the right side of the figure, are due to the sparseness of the ECMWF data. If the individual points of the ECMWF data set are compared with the BP and the Fresnel result very good agreement is seen in most areas. Both for the BP result and for the Fresnel result there is a deviation to the ECMWF data at the tropopause. This is a typical result of the low sampling density in the ECMWF data set. Furthermore, there is a difference around the end of the occultation at the height  $\approx 3$  km. The reason for this difference can be a large gradient in the refractive index. A large gradient will give rise to diffraction effects which will significantly lower the signal to noise ratio. As the signal to noise ratio is already low in the lower part of the tropopause a large gradient poses a problem for the occultation measurement which may cause the signal to be lost [Kursinski, 1997]. As the signal is lost at a height of  $\approx 3$  km where also the large difference to the ECMWF data set occurs, it seems reasonable to attribute the difference to the occurrence of a large gradient, which is not correctly included in the occultation inversions because the data set stops at this height.

In Figure 6.4 the results of inversion of GPS/MET occultation no. 52, February 4, 1997 are shown together with the corresponding ECMWF data. As in the previous figure, the top, left panel shows the BP result as the solid line and the ECMWF model data as diamonds. In the top, right panel the temperature difference  $T_{\text{ECMWF}} - T_{\text{BP}}$  is shown. Similarly, in the bottom, left panel the Fresnel result is shown as the solid line and the ECMWF data set is again shown as diamonds. In the bottom, right panel the temperature difference  $T_{\text{ECMWF}} - T_{\text{Fresnel}}$  is shown. To calculate the temperature difference linear interpolation has been used between the samples in the ECMWF data set.

As in the first example, the agreement to the ECMWF data is generally good. In most areas the difference to the ECMWF data for both the Fresnel result and the BP result is less than  $\pm 2$  K. The major disagreements occur due to the very low vertical sampling density of the ECMWF data set. Thus, the large gradient seen in both the BP and the Fresnel result around 5 km, and the smaller disturbance at the tropopause can neither be confirmed nor put into doubt by the ECMWF data set. A collocated high resolution radiosonde would probably be the only way to get an independent data set to compare with the vertical resolution of the occultation results, and such a measurement has unfortunately not been available for this study.

The two ECMWF samples at  $\approx 14$  km and  $\approx 17$  km are the ECMWF samples nearest to the tropopause and thereby nearest to the tropopause disturbance. These samples are in very good agreement with the inversion results in Figure 6.4. Furthermore, the disturbance found from inversion of the occultation data set has a very reasonable size - about  $\pm 3$  K - when compared to the examples shown in Section 5.1. Together these two observations about the disturbance indicate that the tropopause disturbance is likely to be correctly retrieved by the Fresnel and the BP method.

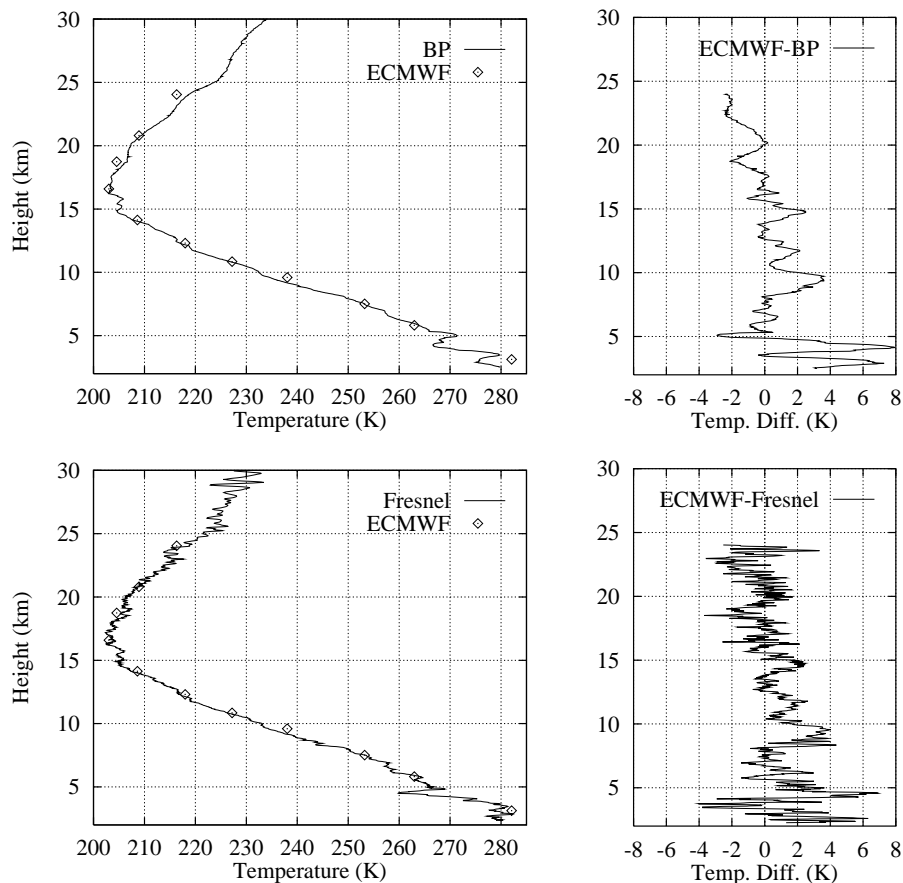


Figure 6.4: Inversion of GPS/MET occultation no. 52, Feb. 4 1997. Position:  $32.3^{\circ}$  S,  $10.2^{\circ}$  E. Top, left: BP result (solid line) and ECMWF model result (diamonds). Top, right: Difference between ECMWF and BP result. Bottom, left: Fresnel result (solid line) and ECMWF model result (diamonds). Bottom, right: Difference between ECMWF and Fresnel result.

The large gradient causing a large disturbance around 4 km in the temperature profiles shown in Figure 6.4 is more difficult to judge. The two nearby samples of the ECMWF data at  $\approx 6$  km and  $\approx 3$  km are in reasonably good agreement with the occultation inversion results, but they are both placed away from the very large disturbance. It is very possible, that the disturbance is a combination of a temperature inversion and a significant water vapor content, which is mapped into the temperature inversion result. However, it has been suggested by *Gorbunov and Gurvich* [1998a] that the GPS/MET receiver, which is tracking the total phase by means of a phase lock loop, in many cases has problems with correctly updating the  $2\pi$  phase ambiguities in the lower troposphere, where the phase is varying very fast. That is, cycle slips in the phase are introduced by the instrument. An instrument error in the determination of the  $2\pi$  phase ambiguity in connection with a large gradient will cause the size of the gradient to be wrongly determined by both the Fresnel and the BP inversion method.

There seems also to be a tendency of a discrepancy between the occultation inversion results and the ECMWF data set for large heights, i.e., above  $\approx 17$  km. It is a relatively small bias

that is primarily seen in the BP result. In the Fresnel result it is more or less masked by the higher noise level in this inversion result. This bias can be due to different things. First of all, a residual error from the ionosphere correction can bias the occultation inversion far down in the neutral atmosphere [Kursinski *et al.*, 1997]. Also, high altitude noise can be a difficulty in the initialization of the temperature calculation from the refractive index (see Section 2.3). Finally, the drift in the occultation location with height (see Section 3.2.1) means that the comparison with the ECMWF data set can only be expected to fit for low heights if there are horizontal variations at large heights.

It should be noted in both examples, that although the Fresnel method is known from the simulation results to give less accurate results than the BP method, this difference is too small to be visible when comparing to the ECMWF data. The agreement between the ECMWF data and the Fresnel result is just as good and in some areas better than the agreement between the ECMWF data and the BP result.

### 6.3 Summary

The inversion tests of GPS/MET occultation data in this chapter show results that agree well with the results obtained from inversion of simulated occultation data sets. Both the back-propagation inversion method and the Fresnel transform inversion method show high vertical resolution inversion results that cannot be obtained by use of the geometrical optics inversion method. The results of both the back-propagation inversion method and the Fresnel transform inversion method compare well with ECMWF data. Independent data sets with high vertical resolution have not been available for the comparisons. It cannot be determined whether some of the variations in the inversion results are due to horizontal variations that have been mapped into the vertical profiles. Nevertheless, the results in general are in accordance with the expectations with an average difference to the ECMWF data less than  $\pm 2$  K in most areas.

## Chapter 7

# The Fresnel Transform using Two Thin Screens

The inversion methods which have been described in the previous parts of this thesis are all based on an assumption of local spherical symmetry. Use of this assumption limits the horizontal resolution of the radio occultation method to approximately 250 km [*Mortensen and Høeg, 1998b; Gorbunov, 1988*]. So, while the back-propagation inversion method gives highly accurate results with respect to vertical resolution, the horizontal resolution is limited. This property is inherent to the methods described previously.

The prospective for occultation measurements on Earth is that the data should be used for weather prediction and climate monitoring purposes. Thus, with time the density of occultation data is expected to be high. Therefore, it is of interest to develop advanced inversion methods which can give high horizontal resolution as well as high vertical resolution even though a single occultation measurement does not contain enough information for this purpose.

The thin screen model used in the Fresnel transform in Chapter 3 has high vertical resolution but is not a very good approximation for the atmosphere of the Earth. This is because the atmosphere of the Earth close to the surface is too dense for this model. On the other hand, the thin screen model contains an obvious possibility for improvement, which will also open up the possibility for improving the horizontal resolution: Use of more than one thin screen for modeling the atmosphere. As more screens are introduced, the accuracy will improve in the dense part of the atmosphere. The vertical resolution will be unchanged compared to the single screen case, i.e., it will be high. The multiple thin screen model is a well known model for accurate simulation of forward propagation through the atmosphere [*Karayel and Hinson, 1997; Grimault, 1998; Gorbunov and Gurvich, 1998a*]. However, when the purpose of the multiple thin screen model is to perform an inversion, the model must be kept as simple as possible to avoid unnecessary complexity of the inversion.

In this chapter a two thin screen model for inversion of occultation data will be described. Use of two thin screens is the simplest possible extension of the Fresnel transform described in Chapter 3. In Section 7.1 the possible achievements of the two thin screen model compared to the one thin screen model are discussed. The wave propagation in the two thin screen model is described in Section 7.2. The inversion of this model is described in Section 7.3. In Section 7.4 the inversion process is illustrated through an example and the obtained result is discussed. Finally, in Section 7.5 the perspective of the method is discussed.

## 7.1 Two Thin Screens versus one Thin Screen

In Figure 7.1 the thin screen approximation of an occultation is illustrated. In the figure the dashed line illustrates the ray path which characterizes the signal propagation in the geometrical optics (GO) approximation. The solid line in the figure illustrates the signal propagation as it will be approximated using the thin screen model. At the thin screen a phase modulation due to the atmosphere is added. This leads to a change of direction of the signal propagation. To and from the screen the signal is assumed to propagate in free space. The thin screen is shown parallel to the  $\xi$ -axis in Figure 7.1 but in the optimal solution it has a slope with respect to the  $\xi$ -axis and it is bend. This was described more carefully in Chapter 3. The figure

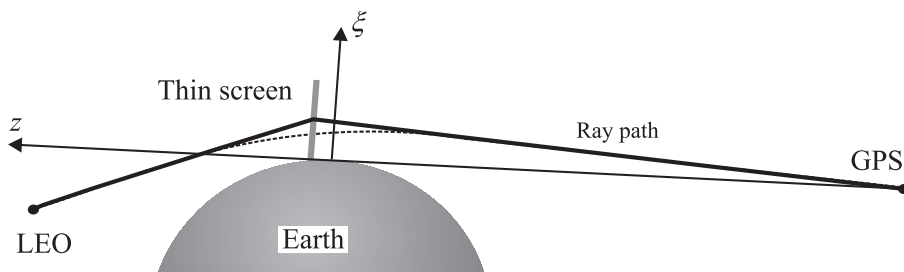


Figure 7.1: *The thin screen approximation of an occultation.*

illustrates the problem with the single thin screen model: As the atmosphere is an extended medium the signal will be bend over a large area, while the single thin screen model tries to approximate the signal propagation by two straight lines. This will introduce an error in the average accuracy of the inversion result. In [Mortensen and Høeg, 1998a] and in Chapter 5 and Chapter 6 of this thesis, it was shown that this very rough approximation gives surprisingly accurate results. This is because the distances to the satellites are large compared to the extent of the atmosphere, and because the atmosphere is relatively thin. The distance from the thin screen to the GPS satellite is approximately 26000 km and the distance from the thin screen to the LEO satellite is approximately 3000 km, while the signal propagates approximately 300 km through the atmosphere of the Earth. Also, the signal which passes closest to the surface of the Earth has a total bending angle of approximately  $1^\circ$ . Thus, the total path length deviation from a straight line propagation between the two satellites is 300-400 m.

Because of the relatively small error that can be obtained using a single thin screen for modeling the atmosphere of the Earth, there is good reason for extending the model with only one extra screen as an initial try. A schematic illustration of the model of the occultation geometry using two thin screens is shown in Figure 7.2. The screens are shown parallel to the  $\xi$ -axis in the figure,

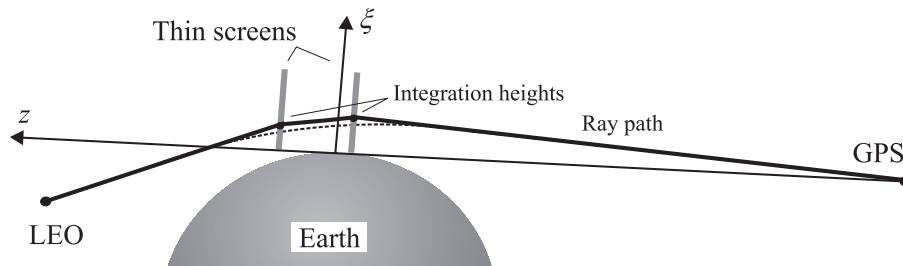


Figure 7.2: *The two screen approximation of an occultation.*

but in general they may be bend and/or have a slope seen relatively to the  $\xi$ -axis. Again the dashed line illustrates the actual ray path, which approximates the propagation of the signal, and the solid line shows the signal propagation as it will be approximated using two thin screens. At each thin screen a phase modulation due to the atmosphere is added. In between the screens and to and from the screens, the signal is assumed to propagate in free space. As can be seen from Figure 7.2 this will still be an approximation of the length of the signal propagation path, and this will introduce an error in the average accuracy of the inversion result.

When few screens are used in the approximation of the occultation measurement, the quality of the inversion result will be very dependent on choosing the right parameters for the inversion. As can be seen from Figure 7.1 and Figure 7.2 the accuracy of the length of the signal propagation path will depend very much on the positions of the screens and also on the integration heights. In Figure 7.2 the integration heights in the atmosphere are the points where the solid line crosses the thin screens. The positions of the thin screens and the integration heights are parameters in the inversion. The parameter choices giving the optimal results for the length of the signal propagation path will not necessarily comply with the actual signal propagation path.

If the model is accurate, the integration height will equal the actual height of the signal propagation path in the atmosphere. Otherwise, a bias in the height will appear in the inversion result. Furthermore, the positions of the screens should be centered around the tangent point of the occultation in order to control the horizontal resolution. With two thin screens it should be possible to improve the approximation of the signal propagation path length. At the same time it should be possible to choose the integration heights and the positions of the thin screens to comply better with the actual signal propagation path than is the case for the one thin screen model. Whether the expected improvement is sufficient, considering the very high accuracy demands for atmospheric measurements, can only be determined through tests of the method. Conceptually the model can easily be extended to include more screens once the improvement of introducing the extra thin screen has been determined.

## 7.2 Wave Propagation with two Thin Screens

In this section the signal propagation in the two thin screen model will be described. It has been chosen to use a formulation which is very close to the one used in the back-propagation method described in Chapter 4. The only difference to the Fresnel transform formulation in Chapter 3 is that a two dimensional model is introduced from the very beginning, while in the Fresnel transform the transformation to two dimensions is introduced rather late in the formulation. The two methods are equivalent but use of the two dimensional model from the beginning simplifies the derivations.

The transformation from the three dimensional occultation measurement geometry to the two dimensional model is performed as in Chapter 4 ([see also *Mortensen, 1998*]). For each sample in the occultation measurement, a coordinate system  $(z, \xi)$  is defined in the plane given by the position of the GPS, the LEO satellite, and the center of the Earth. In this plane, the  $z$ -axis is the vector from the GPS satellite tangential to the Earth in the direction of the LEO satellite. The  $\xi$ -axis is perpendicular to the Earth's surface at the point where the  $z$ -axis is tangential to the Earth and directed outwards. As described in Chapter 4, this two dimensional approximation can be used under the assumption that the horizontal structures in the atmosphere are large compared to the lateral dimensions of the first Fresnel zone. As the first Fresnel zone size is less than 1.5 km the two dimensional approximation is normally good.

In Figure 7.3 the parameters of the two thin screen approximation are shown. The thin screens

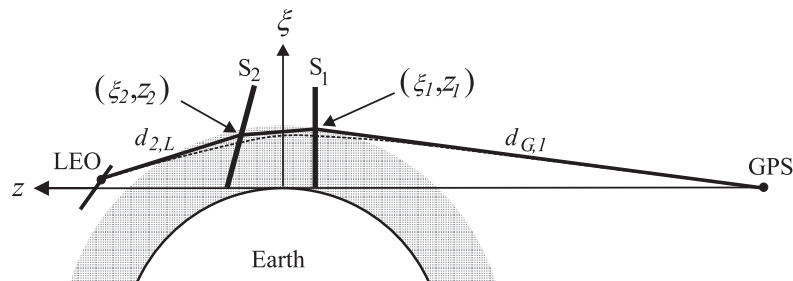


Figure 7.3: *The parameters of the two screen approximation.*

are denoted by  $S_1$  and  $S_2$ . It has been chosen to keep  $S_1$  parallel to  $\xi$ , while  $S_2$  has a slope seen relatively to the  $\xi$ -axis. The LEO trajectory during an occultation is illustrated by a solid line, and the approximated signal propagation path is illustrated by a thicker solid line. As before the signal ray path is indicated by a dashed line. The distance from the GPS satellite to the first thin screen is denoted by  $d_{G,1}$ , and the point where the signal passes  $S_1$  is  $(\xi_1, z_1)$ . Similarly, the point where the signal passes  $S_2$  is denoted by  $(\xi_2, z_2)$  and the distance from  $S_2$  to the LEO satellite is  $d_{2,L}$ .

The propagation of the electro-magnetic field in the two dimensional thin screen model is determined by the two dimensional solution to the external boundary problem for the Helmholtz

equation [Chew, 1995, sec. 8.1]. Thus, the complex amplitude  $E$  of the scalar electric field at the point  $\vec{x}$ , due to the field  $E_0$  at either  $S_1$  or  $S_2$ , is given as

$$E(\vec{x}) = \left(\frac{k_T}{2\pi}\right)^{1/2} \int_{-\infty}^{\infty} E_0(\vec{y}) \cos \varphi_{xy} \frac{\exp(ik_T|\vec{x} - \vec{y}| - i\pi/4)}{\sqrt{|\vec{x} - \vec{y}|}} \sqrt{1 + p^2} d\xi. \quad (7.1)$$

This solution is for a straight line  $S_i$ ,  $i = 1, 2$ , which is running in the  $\xi$ -direction with the slope  $p$  seen relatively to the  $\xi$ -axis. The time dependence in the expression has been suppressed. The free space wave number is denoted by  $k_T$ ,  $\vec{y}$  is a point on  $S_i$ ,  $n_y$  is the normal to  $S_i$ , directed towards  $\vec{x}$ , and  $H_0^{(1)}$  is the Hankel function of first kind of zeroth order. Finally,  $\varphi_{xy}$  is the angle between the normal  $\vec{n}_y$  to  $S_i$  and the vector  $\vec{x} - \vec{y}$ . The scalar version of the wave equation can be used because the atmosphere is sufficiently tenuous [Tatarski, 1967]. The same equation applies to the magnetic field, and thus it is only necessary to consider the electric field in the following. The solution (7.1) can be used to describe the electric field measured at the LEO.

As the signal propagates in free space from the GPS satellite to the first thin screen  $S_1$ , the electric field  $E_1$  at  $S_1$  will be given as

$$E_1(\xi_1, z_1) = E_G \frac{\exp(ik_T d_{G,1})}{\sqrt{d_{G,1}}} A_1 \exp(ik_T \psi_1(\xi_1)). \quad (7.2)$$

In this equation,  $E_G$  is the electric field transmitted from the GPS, and  $\psi_1$  is the phase modulation due to the atmosphere in the area around  $S_1$ . The factor  $A_1$  is the amplitude modulation which accounts for the attenuation and absorption in the atmosphere in the area around  $S_1$ .

Using the expressions (7.1) and (7.2) the field at the second thin screen can be expressed

$$E_2(\xi_2, z_2) = \left(\frac{k_T}{2\pi}\right)^{1/2} A_2 \exp(ik_T \psi_2(\xi_2)) \int_{-\infty}^{\infty} E_1(\xi_1, z_1) \cos \varphi_{1,2} \frac{\exp(ik_T d_{1,2} - i\pi/4)}{\sqrt{d_{1,2}}} d\xi_1. \quad (7.3)$$

In this case,  $d_{1,2}$  is the distance between the points  $(\xi_1, z_1)$  and  $(\xi_2, z_2)$ , and  $\varphi_{1,2}$  is the angle between the vector  $\vec{d}_{1,2}$  from  $(\xi_1, z_1)$  to  $(\xi_2, z_2)$  and the  $z$ -axis. Finally,  $\psi_2$  is the phase modulation due to the atmosphere in the area around  $S_2$ , and  $A_2$  is the amplitude modulation in the area around  $S_2$ .

Reusing equation (7.1) the field measured by the LEO can be determined as

$$E_L(\vec{x}_L) = \left(\frac{k_T}{2\pi}\right)^{1/2} \int_{-\infty}^{\infty} E_2(\xi_2, z_2) \cos \varphi_{2,L} \frac{\exp(ik_T d_{2,L} - i\pi/4)}{\sqrt{d_{2,L}}} \sqrt{1 + p_2^2} d\xi_2 \quad (7.4)$$

where (7.3) is used for the field  $E_2$ . Here  $d_{2,L}$  is the distance between the points  $(\xi_2, z_2)$  and  $\vec{x}_L$ , and  $\varphi_{2,L}$  is the angle between the vector  $\vec{d}_{2,L}$  from  $(\xi_2, z_2)$  to  $\vec{x}_L$  and the  $z$ -axis. The constant  $p_2$  is the slope of the screen  $S_2$  seen relatively to the  $\xi$ -axis.

The phase modulation  $\psi_l$ ,  $l = 1, 2$  due to the atmosphere is found using a GO approximation and using an assumption of spherical symmetry in the atmosphere. These approximations were

also used for finding the phase modulation in the one thin screen case described in Chapter 3. The GO approximation is not limiting for the results as the approximation is good when the propagation distance, for which it is used, is relatively short. In the case here, it is only used to find the phase modulation due to the atmosphere. The spherical symmetry assumption becomes local, i.e., it must only be valid in the vicinity of each screen. For each screen it can be shown that the phase modulation will be given as (see Appendix A)

$$\psi_l(\xi) = \int_T (n_l - 1) d\tau = \int_{\xi+R_e}^{\infty} (n_l - 1) \frac{n_l r}{\sqrt{n_l^2 r^2 - a_l^2}} dr \quad (7.5)$$

where  $T$  is the actual ray path through the atmosphere,  $n_l$  is the refractive index in the part of the atmosphere corresponding to screen number  $l = 1, 2$ , and  $a_l = n_l(\xi)(\xi + R_e)$  is the impact parameter.  $R_e$  is the radius from the center of refraction for the Earth [Syndergaard, 1998]. Figure 7.4 illustrates the parameters used for calculating the phase modulation  $\psi_l$ . The

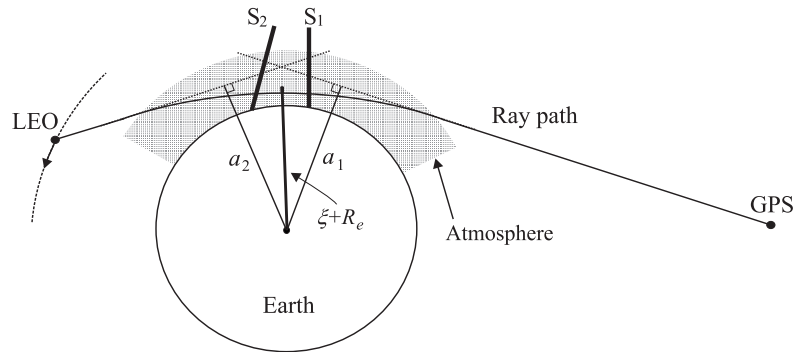


Figure 7.4: *The occultation geometry.*

amplitude modulation factors  $A_1$  and  $A_2$  will be close to unity in the atmosphere. Below the surface of the Earth they will be zero.

### 7.3 Nonlinear Inversion

The expression (7.4) in Section 7.2 is used to find  $E$  from  $n$ . This equation is now inverted. It is obvious to split the inversion into two parts: First, calculation of the phase modulation  $\psi_l$  due to the atmosphere from the measured electric field, and second, calculation of the refractive index  $n_l$  from the phase modulation  $\psi_l$ . In the formulation given in the previous section, both inversions will be nonlinear inversions. Once the refractive index has been determined, the temperature profiles can be derived as described in Section 2.3.

As an occultation measurement gives a one-dimensional data set, some prior information about the horizontal variations in the refractive index is necessary if  $\psi_1 \neq \psi_2$ . To keep the inversion as simple as possible, it has been assumed that the atmosphere is spherically symmetric, i.e.,

$\psi_1 = \psi_2 = \psi$  and  $A_1 = A_2 = A$ . Once the inversion works for a spherically symmetric atmosphere, the extension to  $\psi_1 \neq \psi_2$  will conceptually be a minor extension.

### 7.3.1 Finding the Phase Modulation due to the Atmosphere from the Measured Electric Field

The inversion from measured field to phase modulation is solved by applying a nonlinear iterative inversion algorithm to the discretized version of (7.4). In order to perform the nonlinear iterative inversion, (7.2) is inserted into (7.3) and the resulting expression is inserted into (7.4), giving the expression

$$E_L(\vec{x}_L) = K_L \int_{-\infty}^{\infty} \Psi(\xi_2) \frac{\exp(ik_T d_{2,L})}{\sqrt{d_{2,L}}} \cos \varphi_{2,L} \sqrt{1 + p_2^2} \cdot \int_{-\infty}^{\infty} \Psi(\xi_1) \frac{\exp(ik_T (d_{G,1} + d_{1,2}))}{\sqrt{d_{G,1} d_{1,2}}} \cos \varphi_{1,2} d\xi_1 d\xi_2. \quad (7.6)$$

where  $K_L$  is a complex constant, and  $\Psi(\xi) = A(\xi) \exp(ik_T \psi(\xi))$ . The unknown to be determined is the complex phase modulation  $\Psi$  of which only the phase modulation  $\psi$  is to be used to find the refractive index. The expression (7.6) can be written shortly as an operator equation

$$E_L(\vec{x}_L) = \mathcal{F}[\vec{x}_L, \Psi(\xi)]. \quad (7.7)$$

#### The Discretized Problem

Even though the atmosphere of the Earth is tenuous the horizontal propagation path in an occultation makes the complex phase  $\Psi$  vary rather fast.  $\Psi$  will thus be an oscillating function with the number of oscillations increasing exponentially when the signal is approaching the Earth. It has been chosen to discretize this function by linear interpolation to make the calculation of the expansion functions reasonably simple. Due to the increasing number of oscillations, the step-size in the discretization must be varying with decreasing step-size as the signal gets closer to the Earth. The discrete version of  $\Psi$  is thus

$$\Psi(\xi) = \sum_{l=1}^{l_{max}} \phi_l \Phi_l(\xi) \quad (7.8)$$

with

$$\Phi_l(\xi) = \begin{cases} \frac{1}{\xi_l - \xi_{l-1}} (\xi - \xi_{l-1}) & \text{for } \xi \in [\xi_{l-1}, \xi_l[ \\ \frac{1}{\xi_{l+1} - \xi_l} (\xi_{l+1} - \xi) & \text{for } \xi \in [\xi_l, \xi_{l+1}] \\ 0 & \text{otherwise} \end{cases} \quad (7.9)$$

and  $l_{max}$  is the number of expansion functions. The discretization scheme and the expansion functions are illustrated in Figure 7.5. The unknowns in the discretized problem are the phase modulation factors  $\phi_l$ ,  $l = 1, \dots, l_{max}$ .

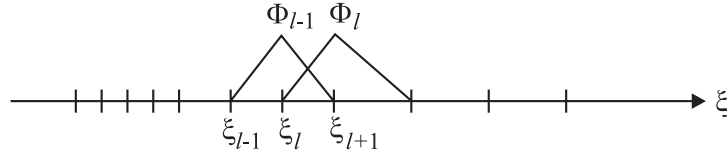


Figure 7.5: *The expansion functions.*

The discrete version (7.8) of  $\Psi$  can be inserted into the equation (7.7). This will give an equation with  $l_{max}$  unknowns  $\phi_l$ . The equation is a function of  $\vec{x}_L$ . By evaluating the equation at  $j_{max}$  points  $\vec{x}_{L,j}$ ,  $j = 1, \dots, j_{max}$  a matrix system is obtained. The evaluation points  $\vec{x}_{L,j}$  are chosen such that the sampling density increases as the Earth is approached. The equations in the discrete version of the nonlinear equation are

$$E_{L,j} = \mathcal{F}_j[\phi] \text{ for } j = 1, \dots, j_{max} \quad (7.10)$$

where  $E_{L,j} = E_L(\vec{x}_{L,j})$ ,  $\phi$  is the column vector  $\{\phi_l\}$  of the phase modulation factors, and  $\mathcal{F}_j$  is the discretized version of  $\mathcal{F}$  in (7.7) evaluated in the points  $\vec{x}_{L,j}$  with the expansion functions for  $\Psi$  inserted, i.e.,

$$\mathcal{F}_j[\phi] = \mathcal{F} \left[ \vec{x}_{L,j}, \sum_{l=1}^{l_{max}} \phi_l \Phi_l(\xi) \right]. \quad (7.11)$$

As the tangent heights in an occultation normally extends from  $\approx 100$  km to around the surface of the Earth, the number of samples in one occultation with 50 Hz sampling rate is large, that is, around 1500. Even with this number of samples, the measured excess phase variation (the measured phase subtracted by the phase due to the direct distance between the satellites) from sample to sample close to the Earth is larger than  $2\pi$ . In order to get a good representation of the signal  $E_{L,j}$  in complex notation, the signal is resampled giving  $\approx 3000$  samples from 100 km down to 4 km, of which only 100 is used in the range from 100 km to 50 km. So far, the signals have not been inverted below 4 km in the tests to avoid memory problems. Inversion down to 4 km is sufficient to perform the initial test of the important properties of the two thin screen inversion method. Because of the increasing density of the atmosphere of the Earth, a large number of expansion functions is also necessary to give an appropriate approximation of the phase modulation factors  $\phi_l$  with the given expansion functions. The number of samples used in the range from 100 km down to 4 km is  $\approx 2500$ .

The expression (7.10) for the measured field will be inverted using Newton's method. The idea in Newton's method is to use an initial guess of the phase modulation factors as an estimate of  $\phi$  to calculate the two thin screen propagation solution (the right hand side of (7.10)). This solution

is compared to the measured field (the left hand side of (7.10)). Then a Taylor expansion of the nonlinear equation (7.10) is used to calculate an updated estimate of the phase modulation factors. The updated estimate of the phase modulation factors can be used to calculate the two thin screen propagation, and the steps can be repeated until the required accuracy is obtained.

The initial phase modulation guess will be denoted by  $\phi^{(1)}$ . From the Taylor expansion of equation (7.10) updated estimates  $\phi^{(2)}, \dots, \phi^{(k)}, \dots$  can be found until convergence to the true solution is reached. After  $k-1$  iterations the updated estimate for the phase modulation factors is  $\phi^{(k)}$ . When this estimate is not the exact  $\phi$ , a correction  $\Delta\phi^{(k)}$  must be found such that the sum  $\phi^{(k)} + \Delta\phi^{(k)}$  is the correct  $\phi$ , i.e.,

$$E_{L,j} = \mathcal{F}_j[\phi^{(k)} + \Delta\phi^{(k)}] \text{ for } j = 1, \dots, j_{max}. \quad (7.12)$$

The truncated Taylor expansion of the right hand side of equation (7.12) is

$$\mathcal{F}_j[\phi^{(k)} + \Delta\phi^{(k)}] \simeq \mathcal{F}_j[\phi^{(k)}] + \sum_{l=1}^{l_{max}} \left( \frac{\partial \mathcal{F}_j}{\partial \phi_l} \right)^{(k)} \Delta\phi_l^{(k)} \text{ for } j = 1, \dots, j_{max}. \quad (7.13)$$

where  $\left( \frac{\partial \mathcal{F}_j}{\partial \phi_l} \right)^{(k)}$  is the partial derivative of  $\mathcal{F}_j$  with respect to  $\phi_l^{(k)}$ , and  $\Delta\phi_l^{(k)}$  is an element in the vector  $\Delta\phi^{(k)}$ . Thus, a correction matrix system, which will be likely to improve the updated estimate  $\phi^{(k)}$ , is [Blok and Oristaglio, 1995, sec. 3.4]

$$E_{L,j} - \mathcal{F}_j[\phi^{(k)}] = \sum_{l=1}^{l_{max}} \left( \frac{\partial \mathcal{F}_j}{\partial \phi_l} \right)^{(k)} \Delta\phi_l^{(k)} \text{ for } j = 1, \dots, j_{max}. \quad (7.14)$$

In this, the partial derivative of  $F_j$  with respect to one of the phase modulation factors  $\phi_l^{(k)}$  is given by

$$\begin{aligned} \left( \frac{\partial \mathcal{F}_j}{\partial \phi_l} \right)^{(k)} = & K_L \left( \int_{-\infty}^{\infty} \Phi_l(\xi_2) \frac{\exp(ik_T d_{2,L})}{\sqrt{d_{2,L}}} \cos \varphi_{2,L} \sqrt{1+p_2^2} \right. \\ & \cdot \int_{-\infty}^{\infty} \Psi(\xi_1) \frac{\exp(ik_T(d_{G,1} + d_{1,2}))}{\sqrt{d_{G,1}d_{1,2}}} \cos \varphi_{1,2} d\xi_1 d\xi_2 \\ & + \int_{-\infty}^{\infty} \Psi(\xi_2) \frac{\exp(ik_T d_{2,L})}{\sqrt{d_{2,L}}} \cos \varphi_{2,L} \sqrt{1+p_2^2} \\ & \left. \cdot \int_{-\infty}^{\infty} \Phi_l(\xi_1) \frac{\exp(ik_T(d_{G,1} + d_{1,2}))}{\sqrt{d_{G,1}d_{1,2}}} \cos \varphi_{1,2} d\xi_1 d\xi_2 \right). \end{aligned} \quad (7.15)$$

where  $\Psi(\xi_1)$  and  $\Psi(\xi_2)$  are obtained from (7.8). The updated estimate for the phase modulation factors becomes

$$\phi^{(k+1)} = \phi^{(k)} + \Delta\phi^{(k)}. \quad (7.16)$$

The matrix system (7.14) can be written in short form as

$$\mathbf{E}_L - \mathbf{F}[\phi^{(k)}] = \left( \frac{\partial \mathbf{F}}{\partial \phi} \right)^{(k)} \Delta \phi^{(k)} \quad (7.17)$$

where  $\mathbf{E}_L = \{E_{L,j}\}$  is the column vector of the measurements in the points  $x_{L,j}$ ,  $\mathbf{F} = \{\mathcal{F}_j\}$  is the column vector of the discrete right hand side in equation (7.10), and  $\left( \frac{\partial \mathbf{F}}{\partial \phi} \right)^{(k)} = \left\{ \left( \frac{\partial \mathcal{F}_j}{\partial \phi_l} \right)^{(k)} \right\}$  is the matrix of the partial derivatives (7.15) (the Jacobian).

The equation (7.7) is a nonlinear Fredholm integral equation of the first kind. This type of problem is ill-posed [Wing, 1991]. Simplified, this means that the solution  $\Psi$  will be very sensitive to noise in the measured quantity  $E_L$  such that the solution will be unstable. According to Hansen [1997], the discrete version (7.10) of (7.7) will also be ill-posed, and so will the correction matrix system (7.17). That (7.17) is ill-posed will be evident when implementing the matrix  $\left( \frac{\partial \mathbf{F}}{\partial \phi} \right)^{(k)}$  in (7.17), as this matrix will have a very high condition number. The ill-posedness must be taken into account when solving the correction matrix system (7.17). A way of solving ill-posed problems is to use the least squares solution to the regularized problem [Hansen, 1997, sec. 1.3]. This can be formulated in a number of ways, but the solution to (7.17) which is used here is given as

$$\min_{\Delta \phi^{(k)}} \left\{ \left\| \left( \mathbf{E}_L - \mathbf{F}[\phi^{(k)}] \right) - \left( \frac{\partial \mathbf{F}}{\partial \phi} \right)^{(k)} \Delta \phi^{(k)} \right\|_2^2 + \lambda_d^2 \left\| \mathbf{L} \Delta \phi^{(k)} \right\|_2^2 \right\} \quad (7.18)$$

where  $\lambda_d$  is the regularization parameter. The quantity  $\mathbf{L}$  is a diagonal matrix containing weighting values  $w_l$ . Due to the unequal sampling density of  $\phi$  a weighting factor must be used to calculate the norm of the correction in the minimization problem (7.18). The chosen expansion functions are not orthonormal, so a direct normalization of the functions cannot be done. Instead the functions have been weighted according to their width to give them all the same influence, i.e.,  $w_l = \sqrt{\xi_{l-1} - \xi_{l+1}}$ .

The solution found from the minimization problem (7.18) may not give the best correction  $\Delta \phi^{(k)}$ . This is because the correction matrix system (7.14) is a Taylor expansion truncated to first order. This expansion is not necessarily a good approximation of the nonlinear equation, particularly if the initial guess  $\phi^{(1)}$  is far from the correct result. Therefore, apart from choosing the optimal solution to (7.18), it is common to use a modified solution  $\alpha \cdot \Delta \phi^{(k)}$ , where  $\alpha$  is found from [e.g., Blok and Oristaglio, 1995, sec. 3.4]

$$\min_{\alpha} \left\{ \left\| \mathbf{E}_L - \mathbf{F}[\phi^{(k)}] + \alpha \cdot \Delta \phi^{(k)} \right\|_2^2 + \lambda_o^2 \left\| \mathbf{L} \alpha \cdot \Delta \phi^{(k)} \right\|_2^2 \right\}. \quad (7.19)$$

where  $\lambda_o$  is the regularization parameter. The quantity  $\alpha$  is a diagonal matrix of scalar parameters  $\alpha_l$ . In the present case, this regularization has been done by trial and error. When taking this trial and error process into account, the updated result for the phase modulation factors becomes

$$\phi^{(k+1)} = \phi^{(k)} + \alpha \cdot \Delta \phi^{(k)} \quad (7.20)$$

Thus, it is assured that  $\phi^{(k+1)}$  is a better estimate of  $\phi$  than  $\phi^{(k)}$ . The procedure is commonly referred to as line search [Blok and Oristaglio, 1995, sec. 3.4].

Due to the large number of measured samples and the large number of unknowns in the least squares minimization problem (7.18), the problem has been solved using the conjugate gradients least squares (CGLS) method. The CGLS method [Hansen, 1997, ch. 6] is an iterative method for solving linear equations. When the CGLS method is used to find the optimal solution to the minimization problem (7.18) the regularization is controlled by the number of iterations. The fewer the iterations the more regularization [Hansen, 1997, sec. 6.3].

### 7.3.2 Finding the Refractive Index from the Phase Modulation due to the Atmosphere

Once the phase modulation  $\psi$  has been found through the nonlinear iteration procedure described in Section 7.3.1, the expression (7.5) for the phase modulation must be used to obtain the refractive index  $n(r)$ . The dependences of  $\psi(\xi)$  on  $n(r)$  is nonlinear, so the inversion must be solved in a manner similar to what has just been described for finding the complex phase modulation  $\Psi$  from the measured field  $E$ .

According to (7.5), the phase modulation due to the atmosphere depends on the refractive index as

$$\psi(\xi) = \int_{\xi+R_E}^{\infty} (n(r) - 1) \frac{n(r)r}{\sqrt{n(r)^2 r^2 - a^2}} dr \quad (7.21)$$

with  $a = n(\xi)(\xi + R_E)$ . The phase modulation  $\psi$  and the refractive index  $n(r)$  are both real functions but the rate of changes in the functions increases exponentially as  $\xi$  decreases. The operator equation corresponding to (7.21) can be written

$$\psi(\xi) = \Omega[\xi, n(r)] \quad (7.22)$$

The refractive index  $n(r)$  has been discretized using linear interpolation with decreasing step-size as  $r$  decreases

$$n(r) = \sum_{l=1}^{l_{max}} \eta_l \Phi_l(r). \quad (7.23)$$

The refractive index factors to be found through the nonlinear inversion is denoted by  $\eta_l$ . The quantity  $l_{max}$  denotes the number of samples. The expansion functions are  $\Phi_l(r)$  given by (7.9) with  $\xi$  replaced by  $r$ .

The discrete version of  $n$  can be inserted into the nonlinear equation (7.22). This will give an equation with  $l_{max}$  unknowns  $\eta_l$ . The equation is a function of  $\xi$ . By evaluating the equation in  $j_{max}$  points  $\xi_j$ ,  $j = 1, \dots, j_{max}$  a nonlinear matrix system is obtained. The evaluation points  $\xi_j$  are chosen such that the sampling density increases as the Earth is approached. The equations in the discrete version of the nonlinear equation (7.22) are

$$\varphi_j = \Omega_j[\boldsymbol{\eta}] \text{ for } j = 1, \dots, j_{max} \quad (7.24)$$

where  $\varphi_j = \psi(\xi_j)$ ,  $\boldsymbol{\eta} = \{\eta_l\}$  is the column vector of the refractive index factors, and  $\Omega_j$  is the discrete version of  $\Omega$  in (7.22) with the expansion functions for  $n$  inserted

$$\Omega_j[\boldsymbol{\eta}] = \Omega \left[ \xi_j, \sum_{l=1}^{l_{max}} \eta_l \Phi_l(r) \right]. \quad (7.25)$$

The number of samples used for approximating  $n$  from 100 km down to 4 km is  $\approx 700$ . The number of samples in  $\psi$  used from 100 km to 4 km is  $\approx 1000$ . It should be noted that the sampling points and the number of samples differ from what was used to find  $\Psi$  from  $E_L$  although the indices have been reused in this section. This is because less samples are required to approximate the real functions  $\psi$  and  $n$ .

As the equation (7.24) is nonlinear it will be solved iteratively using Newton's method as described in Section 7.3.1. After  $k - 1$  iterations the updated estimate of the factors of the discretized refractive index profile is denoted by  $\boldsymbol{\eta}^{(k)}$ . The discrete version of the correction matrix system becomes

$$\varphi_j - \Omega_j[\boldsymbol{\eta}^{(k)}] = \sum_{l=1}^{l_{max}} \left( \frac{\partial \Omega_j}{\partial \eta_l} \right)^{(k)} \Delta \eta_l^{(k)} \text{ for } j = 1, \dots, j_{max} \quad (7.26)$$

where  $\Delta \eta_l^{(k)}$  is the correction. The partial derivative of  $\Omega_j$  with respect to one of the refractive index factors  $\eta_l$  is

$$\left( \frac{\partial \Omega_j}{\partial \eta_l} \right)^{(k)} = \int_{\xi_j + R_e}^{\infty} \Phi_l \left( \frac{nr}{\sqrt{n^2 r^2 - a^2}} + \frac{(n-1)(n(\xi_j + R_e) - a)ar}{(n^2 r^2 - a^2)^{3/2}} \right) dr \quad (7.27)$$

where  $n$  is given by (7.23).

The equation (7.26) can be written compactly as

$$\boldsymbol{\varphi} - \boldsymbol{\Omega}[\boldsymbol{\eta}^{(k)}] = \left( \frac{\partial \boldsymbol{\Omega}}{\partial \boldsymbol{\eta}} \right)^{(k)} \Delta \boldsymbol{\eta}^{(k)} \quad (7.28)$$

where  $\boldsymbol{\varphi} = \{\varphi_j\}$  is the vector of the phase modulation in the points  $\xi_j$ ,  $\boldsymbol{\Omega} = \{\Omega_j\}$  is the vector of the discretized right hand side of equation (7.24),  $\left( \frac{\partial \boldsymbol{\Omega}}{\partial \boldsymbol{\eta}} \right)^{(k)} = \left\{ \left( \frac{\partial \Omega_j}{\partial \eta_l} \right)^{(k)} \right\}$  is the matrix of the partial derivatives (7.27) (the Jacobian), and  $\Delta \boldsymbol{\eta}^{(k)} = \{\Delta \eta_l^{(k)}\}$  is the column vector of the corrections.

The solution to the correction matrix system is again found as the solution to a minimization problem

$$\min_{\Delta \boldsymbol{\eta}} \left\{ \left\| (\boldsymbol{\varphi} - \boldsymbol{\Omega}[\boldsymbol{\eta}]) - \left( \frac{\partial \boldsymbol{\Omega}}{\partial \boldsymbol{\eta}} \right) \Delta \boldsymbol{\eta} \right\|_2^2 + \lambda_d^2 \|\mathbf{L} \Delta \boldsymbol{\eta}\|_2^2 \right\} \quad (7.29)$$

where the superscript  $(k)$  has been dropped and  $\lambda_d$  is the regularization parameter. As the sampling density is unequal the weighting factors are included in  $\mathbf{L}$ , which is a diagonal matrix

containing the weighting values  $w_l$ . These are found in the same way as described for the minimization problem (7.18). The minimization problem (7.29) has been solved using the CGLS method. The result for the updated refractive index factors becomes

$$\boldsymbol{\eta}^{(k+1)} = \boldsymbol{\eta}^{(k)} + \boldsymbol{\beta} \cdot \Delta\boldsymbol{\eta}^{(k)} \quad (7.30)$$

where the diagonal matrix  $\boldsymbol{\beta}$  is used to control the regularization that guarantees the updated refractive index to be a better estimate of  $\boldsymbol{\eta}$  than the previous estimate. This is similar to the minimization problem (7.19) for the case of deriving  $\Psi$  from  $E$ . This regularization has been performed by trial and error as in the case for finding  $\Psi$  from  $E$ .

## 7.4 An Example of the Inversion

The inversion method is tested using a simulated occultation data set. The data set used is the same type of simulated occultation as was used in the examples 3 and 4 in Section 5.1. The one-dimensional forward occultation simulator takes into account diffraction [Kursinski *et al.*, 1997]. The model uses a spherical Earth, spherical satellite orbits, and a piecewise linear temperature profile as atmosphere model. No water vapor or ionosphere is included in the model. Thus, the temperature profile determines the refractive index profile uniquely.

Figure 7.6 shows the temperature profile for the example. As can be seen, the example chosen has

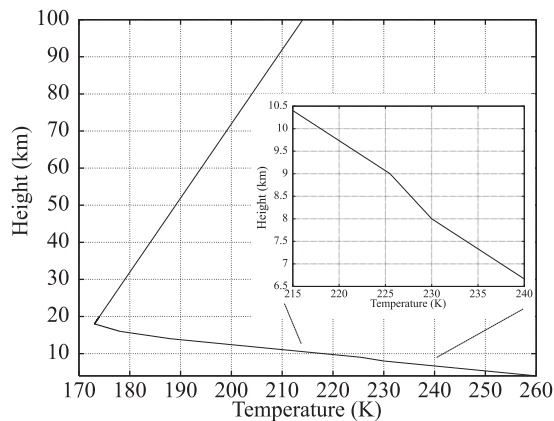


Figure 7.6: *Temperature profile as a function of height for the example used.*

a very smooth profile. Figure 7.7 shows the corresponding simulated occultation measurement as a function of the corresponding height in the atmosphere for the L1 frequency of the GPS signal. As there is no ionosphere included, only one frequency is necessary for the simulation. The measured amplitude is shown relative to the amplitude that would be measured in the absence of the atmosphere. Similarly, the phase due to the direct propagation in the case where there is no atmosphere has been subtracted from the measured phase shown (i.e., the excess phase is shown). It is the excess phase and the relative amplitude which is of importance in the inversion. The electric field measured in the absence of the atmosphere is known from the

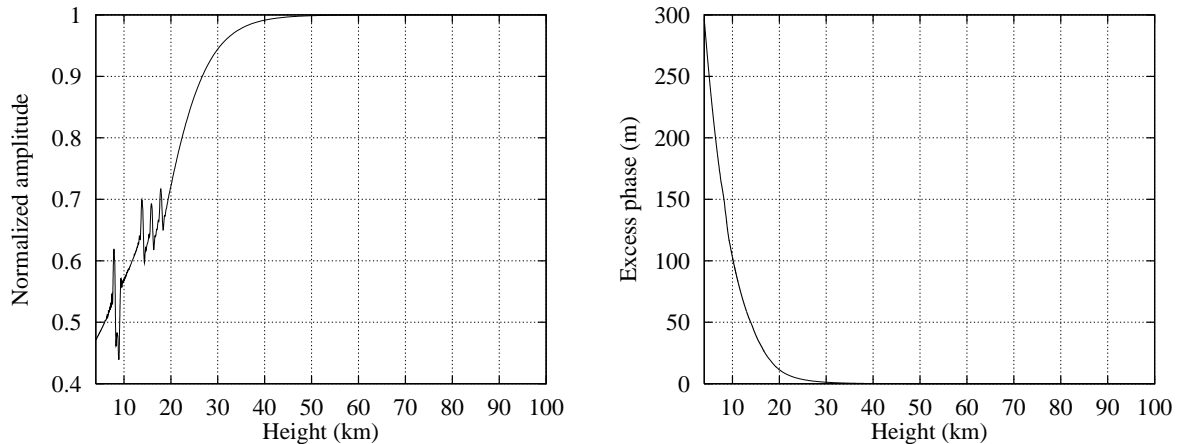


Figure 7.7: Measured amplitude and excess phase for the example used.

satellite positions, and thus the propagation equation (7.6) can be normalized with this factor. The oscillations seen in the amplitude in Figure 7.7 are caused by changes in the temperature gradient. The temperature gradient changes also cause oscillations in the phase, but due to the very fast increase of the phase below 20 km the oscillations cannot be distinguished as easily as in the amplitude. The wavelength at the L1 frequency is approximately 0.2 m so the excess phase shown is equal to  $\approx 1500 \cdot 2\pi$  at the height 4 km.

#### 7.4.1 Inversion Results $E$ to $\Psi$

To perform the inversion, the positions of the thin screens must first be determined. These are parameters of the two thin screen propagation equation. The optimal positions of the thin screens have been determined from tests on simulated occultation data sets where the atmosphere is known, and thus can be used as input for the propagation equation (7.6). This leads to the first screen being placed at the position  $z_1 = -50$  km, and the second screen being placed at the position  $z_2 = 115$  km  $- 0.75\xi$ .

The inversion to the nonlinear equation (7.6) is performed on the discretized problem as was described in Section 7.3. However, in this section all quantities will be written in their continuous version. The continuous versions of the updated estimate of the phase modulation are defined from the discrete phase modulation factors in accordance with (7.8):

$$\Psi^{(k)}(\xi) = \sum_{l=1}^{l_{max}} \phi_l^{(k)} \Phi_l(\xi) \quad (7.31)$$

and similarly  $\Delta\Psi^{(k)}$  is defined from  $\Delta\phi^{(k)}$ .

#### The Initial Phase Guess

When inverting the data shown in Figure 7.7, an initial guess  $\Psi^{(1)}$  of the phase modulation must be obtained. To obtain this guess, the geometrical optics inversion method is used to invert the

occultation data to a refractive index profile, and then the phase modulation is calculated from (7.21). The phase modulation, thus obtained for each of the thin screens for the example used, has a smooth profile which has increased to a value of  $\approx 50$  m at 4 km. In the complex representation this phase modulation will be  $1 \cdot \exp(ik_T \psi)$ . The GO inversion method is very good for smooth profiles, so the initial guess for  $\Psi$  for the two thin screen model should be good.

The difference  $E_L - \mathcal{F}[\Psi^{(1)}]$  between the measured electric field and the two thin screen propagation solution ((7.7) where the  $\vec{x}_L$  dependence has been omitted) is shown in Figure 7.8. Both amplitude and phase differences are shown relative to the amplitude and phase of  $E_L$ ,

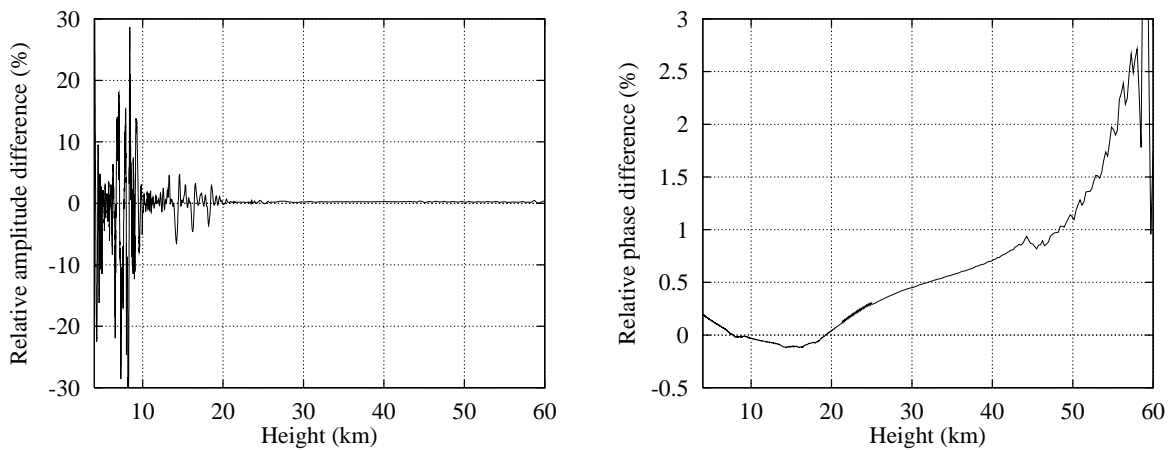


Figure 7.8: *Relative difference to the measured electric field  $E_L$  in amplitude and phase using the initial phase modulation guess.*

respectively. The results are only shown below 60 km. This is due to the fact that the phase decreases exponentially with height, and this gives rise to oscillations in the two thin screen propagation solution for large heights. Normally only results below 30-40 km are considered reliable no matter what inversion method is used. The large heights are used only to initialize the algorithm.

The increasing difference to the measured phase of  $E_L$  above 40 km is not a very big problem although better results should be obtainable. In absolute measures, the difference to the phase below 10 km is a much bigger problem as the phase varies very fast in this area, and even 0.25% difference is several periods of the complex phase of  $E_L$ . At the height 4 km a difference of 0.05% in the phase is equal to a difference of  $\approx 0.75 \cdot 2\pi$ .

The relative difference to the amplitude of  $E_L$  increases as the height decreases. This is because the absolute amplitude decreases. The amplitude of  $E_L$ , which is shown in Figure 7.7, is smooth apart from in the area around the change in the temperature gradients. Thus, the oscillations seen in the amplitude difference in Figure 7.8 are due to unwanted oscillations in the two thin screen propagation result. The large differences seen in the amplitude results, compared to the phase results, are to be expected as any approximation of the wave propagation approximates the phase better than the amplitude.

### The Updated Phase

The differences shown in Figure 7.8 (without the normalization) is used as left hand side in the correction matrix system (7.14) for the first iteration. As mentioned in Section 7.3, the correction matrix system is solved using the CGLS method. Furthermore, a trial and error process is applied to find the updated estimate  $\Psi^{(k)}$ , which also is the optimal solution to the minimization problem (7.19). This process is equal to finding the correction  $\Delta\Psi^{(1)}$  which minimizes the difference  $E_L - \mathcal{F}[\Psi^{(2)}]$  where  $\Psi^{(2)} = \Psi^{(1)} + \Delta\Psi^{(1)}$ . The details of the CGLS solution and the trial and error procedure are described by *Mortensen* [1999].

The resulting updated phase modulation  $\psi^{(2)}$  is shown on the left in Figure 7.9. The amplitude

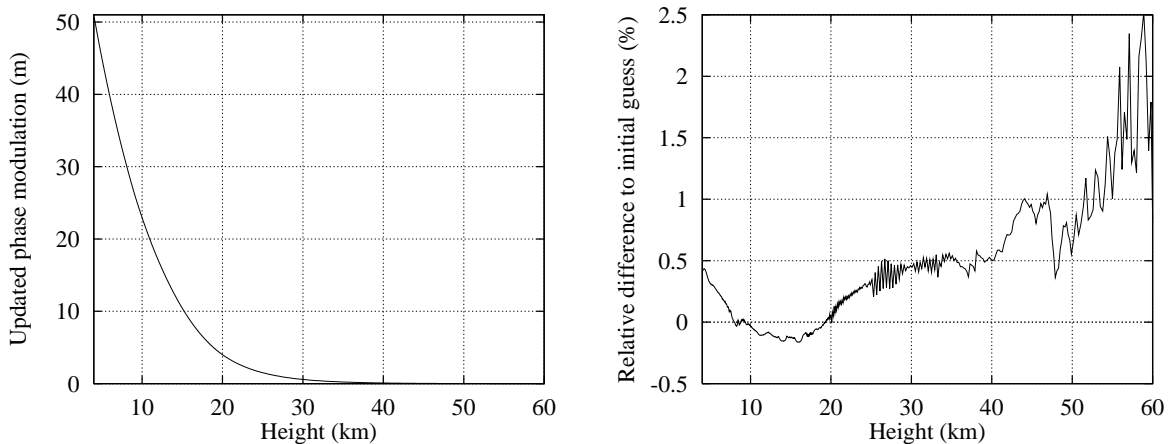


Figure 7.9: On the left, the phase modulation after addition of initial data with the correction, i.e.,  $\psi^{(2)}$ . On the right, the relative difference between  $\psi^{(2)}$  and  $\psi^{(1)}$ .

of the updated complex phase modulation has been set equal to 1. On the right in Figure 7.9, the relative difference between the updated phase modulation and the initial phase modulation guess  $(\psi^{(2)} - \psi^{(1)})/\psi^{(2)}$  is shown. The initial phase modulation guess  $\psi^{(1)}$  is found from the refractive index profile obtained using the geometrical optics inversion method. Thus, the initial phase modulation guess is very smooth. The relative difference shown on the right in Figure 7.9 therefore shows, that the updated phase modulation has a tendency of oscillating. This is particularly significant for large heights just as the relative difference to the initial guess is largest for large heights.

Figure 7.10 shows the difference  $E_L - \mathcal{F}[\Psi^{(2)}]$  where the updated complex phase modulation is given by  $\Psi^{(2)} = 1 \cdot \exp(ik_T\psi^{(2)})$ . Both the amplitude and the phase of the difference  $E_L - \mathcal{F}[\Psi^{(2)}]$  are shown relative to the amplitude and phase of  $E_L$ , respectively. Both the amplitude difference and the phase difference shown in Figure 7.10, using the updated complex phase modulation, are reasonably low. When comparing the phase difference of the updated result to the phase difference obtained using the initial phase modulation guess a significant improvement is seen in the entire area shown. From 30 km and downwards the relative difference  $\arg(E_L - \mathcal{F}[\Psi^{(2)}])/\arg(E_L)$  is less than 0.05%, whereas the initial result shows differences up to 0.5% in

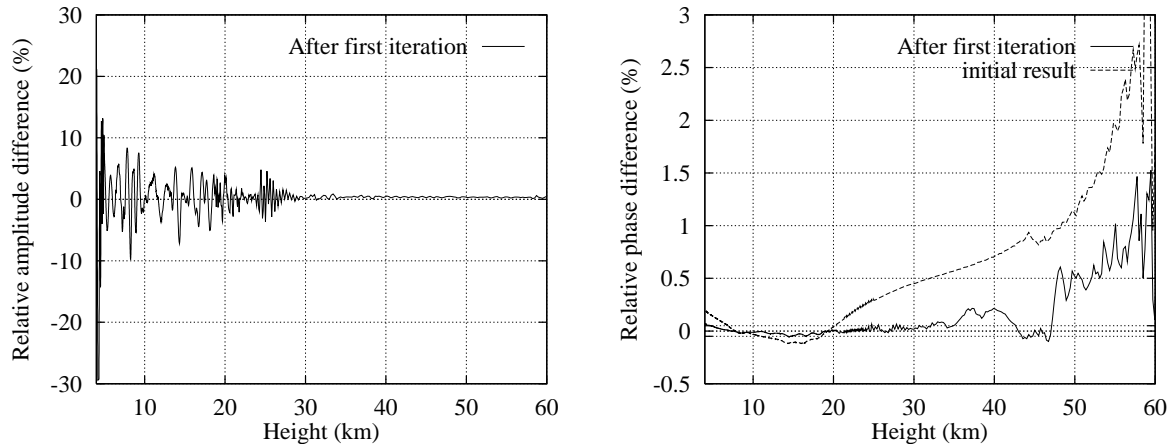


Figure 7.10: *The relative difference to the measured electric field  $E_L$  after first iteration using the updated phase modulation. In the plot of the phase difference on the right, the dashed line shows the relative difference to  $E_L$  after using the initial phase modulation guess.*

this area. The initial amplitude result has not been included in Figure 7.10. This is because the amplitude difference is rather noisy due to the oscillations in the two thin screen propagation solution. When comparing the amplitude difference to the initial result, which is shown in Figure 7.8, it can be seen that the updated phase modulation estimate lowers the amplitude difference below 10 km, but the improvement is not as significant as for the phase difference. Furthermore, the noise in the amplitude difference is increased a little for heights above 10 km.

Even though the updated phase difference shown in Figure 7.10 is low, a close look at the result shows that the oscillations seen in the amplitude difference also are apparent in the phase difference result. The reason, why the updated result is less smooth than the initial result, is that the updated phase modulation  $\Psi^{(2)}$  contains oscillations. The oscillations in the updated phase modulation were shown in Figure 7.9. The oscillations in  $\Psi^{(2)}$  are an artifact of the correction matrix system and the way this is solved to derive  $\Delta\Psi^{(1)}$ . The main problem in the solution to the correction matrix system is that the complex problem has a fast varying phase.

The difference shown in Figure 7.10 could be used as right hand side for the correction matrix system in a new iteration of the Newton method. In the test here, the iteration procedure is stopped after the first iteration. As the first iteration introduces unwanted oscillations in the result, it is not expected that a second iteration will be able to both remove the oscillations and lower the difference to  $E_L$  further. If good results are to be achieved in a second iteration the solution of the correction matrix system through the minimization problems (7.18) and (7.19) must be modified to produce a solution that does not introduce artificial oscillations in the result. Furthermore, the phase difference after the first iteration is already low. The difference to the phase of  $E_L$  is less than 0.05% in the height range from 4 km to 30 km which is the area of main interest for the inversion here. As mentioned 0.05% difference at the height 4 km is  $\approx 0.75 \cdot 2\pi$ , i.e., less than one period. The absolute difference will be largest at 4 km because the measured phase will be largest at this height. For comparison the difference using the initial phase modulation guess is  $\approx 3 \cdot 2\pi$  at 4 km. Thus, the phase modulation  $\Psi^{(2)}$  is considered

sufficiently close to the correct  $\Psi$ , for the initial test which is shown here. The difference from  $\Psi^{(2)}$  to the final converged phase modulation result  $\Psi$  can be estimated to  $< 0.15\%$  at 4 km, i.e., the total difference from the initial guess to the converged  $\Psi$  at 4 km is  $\approx 0.55\%$ . This estimate is based on a judgment of the correspondence between  $\arg(E_L)$  and  $\psi$  being only slightly nonlinear.

#### 7.4.2 Inversion Results $\psi$ to $n$

The updated phase modulation  $\psi^{(2)}$  shown in the left panel in Figure 7.9 is the phase modulation that must be inverted to obtain the refractive index through (7.21) as this is the estimate for  $\psi$  (the left hand side of (7.21)).

Again the inversion is performed on the discretized problem, but the quantities involved will be written in their continuous form. The continuous versions of the updating refractive index solutions are defined from the discrete refractive index factors in accordance with (7.23)

$$n^{(k)}(r) = \sum_{l=1}^{l_{max}} \eta_l^{(k)} \Phi_l(r) \quad (7.32)$$

and similarly  $\Delta n^{(k)}$  is defined from  $\Delta \boldsymbol{\eta}^{(k)}$ .

To perform the inversion, an initial guess  $n^{(1)}$  of the refractive index must be obtained. This guess is obtained using the geometrical optics inversion method to invert the occultation data to a refractive index profile. This refractive index profile is then used to calculate the phase modulation from the right hand side of (7.22) and the difference  $\psi - \Omega[n^{(1)}]$ , which is (7.22) where the  $\xi$  dependence has been omitted, can be obtained. The guess  $n^{(1)}$  is identical to the refractive index profile that was used to obtain the initial phase modulation guess  $\psi^{(1)}$ , and thus  $\Omega[n^{(1)}] = \psi^{(1)}$ . The initial normalized difference  $(\psi - \Omega[n^{(1)}])/\psi$  is equal to the difference shown in the right panel of Figure 7.9 because the phase modulation was derived from  $E_L$  through only one iteration.

The difference  $\psi - \Omega[n^{(1)}]$  is used as left hand side of the correction matrix system (7.26). The correction matrix system is solved using the CGLS method. Furthermore, a trial and error process is applied to find the correction matrix system which minimizes the differences  $\psi - \Omega[n^{(2)}]$ , where  $n^{(2)} = n^{(1)} + \Delta n^{(1)}$  is the updated refractive index estimate, and  $\Delta n^{(1)}$  is the correction. This process is similar to the process of finding the optimal correction  $\Delta \Psi^{(1)}$ , which was described in Section 7.4.1.

Figure 7.11 shows the difference  $\psi - \Omega[n^{(2)}]$  together with the initial difference  $\psi - \Omega[n^{(1)}]$ . Both results are shown relative to  $\psi$ . As described previously the phase modulation  $\psi$  is rather noisy. The refractive index guess  $n^{(1)}$  which is found from using the geometrical optics inversion method on the other hand is smooth. The correction  $\Delta n^{(1)}$  has been chosen relatively smooth - particularly for large heights. Thus, as can be seen from Figure 7.11 the result of the updating is primarily to lower the average difference. As the noise in  $\psi$  is a result of problems with the inversion from  $E_L$  to  $\psi$  there seems to be no reason to transfer this noise to the refractive index

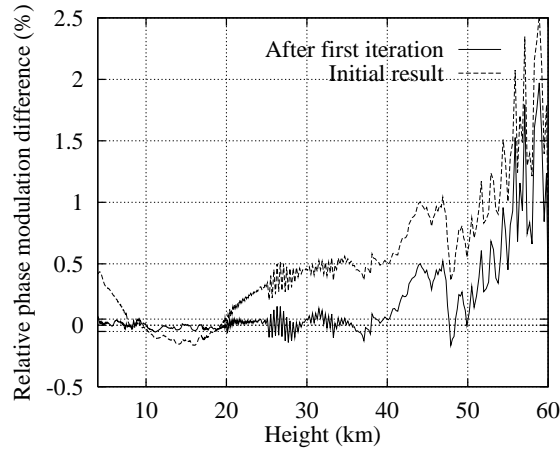


Figure 7.11: *The relative error after first iteration using the updated refractive index shown together with the relative error after using the initial refractive index guess.*

profile, although this means that some structure in the refractive index profile may be lost. The noise is primarily significant above  $\approx 25$  km whereas the primary interest in the inversion tests in this thesis is heights below 30 km, so the smoothing at large heights has no significant impact on the results of interest.

From 25 km down to the height 4 km the relative difference  $(\psi - \Omega[n^{(2)}])/\psi$  is less than 0.05%. From 25 km to  $\approx 35$  km the average difference is less than 0.05%. This difference is small enough that the result can be considered to be converged for this initial test. The relative refractive index error, when the result  $n^{(2)}$  is used as  $n$ , is shown in Figure 7.12. The relative error is

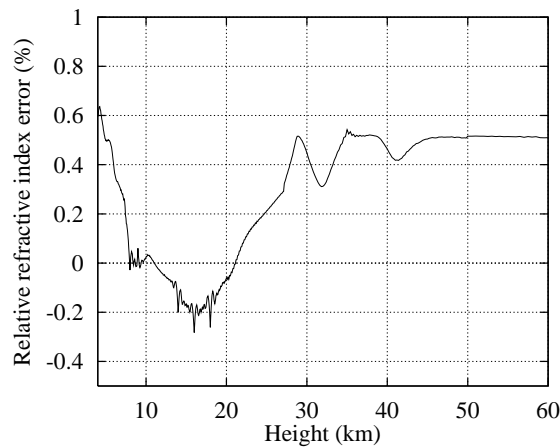


Figure 7.12: *The relative error in the obtained refractive index profile.*

defined as  $(n - n_{model})/n_{model}$  where  $n_{model}$  is the refractive index of the model profile used for the occultation simulation. When judging this result, it should be taken into account that the inversion procedures both from  $E_L$  to  $\psi$  and from  $\psi$  to  $n$  are not completely converged. At 4 km where the error is largest, the total error when taking the residual contributions into account can be estimated to  $< 0.75\%$ . This takes into account both the residual error from the inversion

to  $\psi$  and from the inversion to  $n$ . The estimate is based on a judgment of the inversion from  $\psi$  to  $n$  to be only slightly nonlinear. Above the height  $\approx 35$  km the refractive index error is underestimated. The efforts have been focused on the inversion below 30 km, and thus there has been made little attempt of getting the nonlinear inversions to converge above 30 km.

In the height range corresponding to the changes in the temperature gradients (see Figure 7.6), it can be seen that the obtained refractive index profile is too smooth. This is a result of the initial guess  $n^{(1)}$  being a little too smooth, and the updating at the present state being unable to improve this.

## 7.5 Discussion

From the obtained refractive index profile a temperature profile can be derived as described in Section 2.3. In the simulated example there is no additional errors introduced by this derivation, as the simulation contains no water vapor and no ionosphere. The conversion is only performed to put the results on a form comparable to the results shown in Chapter 5 and Chapter 6. The error of the temperature profile obtained with the two thin screen inversion method is shown in Figure 7.13. The error is defined as the model temperature subtracted by the temperature found through the inversion. The dashed line in Figure 7.13 shows for comparison the error

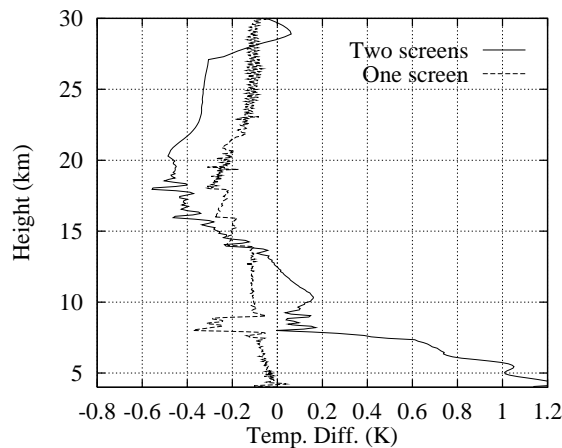


Figure 7.13: *Temperature error - one and two screen results compared.*

obtained using the Fresnel transform inversion method, which is a one thin screen method, on the simulated occultation data set. As can be seen from Figure 7.13 the result obtained with only one screen is generally significantly better than the results obtained with the two thin screen method so far.

In Figure 7.14 a small area around the temperature disturbance at 8 km is shown. The temperature profile obtained with the two thin screen inversion method has been plotted with the linear back-ground temperature slope subtracted such that the temperature gradient in areas away from the disturbance is zero. The dashed line in the plot is the model atmosphere temperature profile. The figure illustrates that there is no height bias in the two thin screen inversion

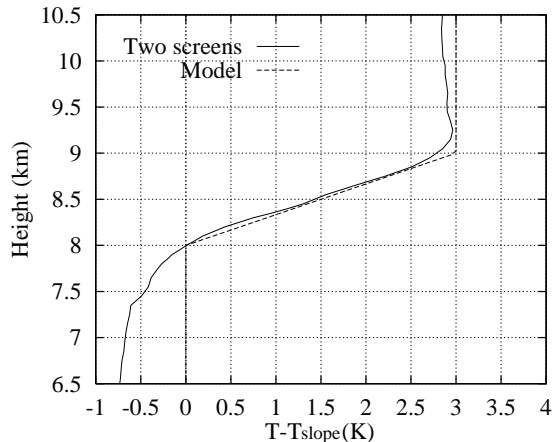


Figure 7.14: *The obtained temperature profile with the background temperature slope subtracted. Comparison with model data.*

result, i.e., the temperature disturbance is retrieved at the correct height. As mentioned in the introductory discussion of the two thin screen inversion method in Section 7.1, the integration height is a parameter of the method alongside the positions of the thin screens. As the problem has been formulated in this chapter, there has been introduced no height bias. In this way, the height bias, which was seen for the Fresnel transform inversion method formulation of the one thin screen inversion method in Chapter 3, is avoided. Introducing a height bias could improve the average accuracy of the inversion result, but the improvement is not sufficiently large to be worth the cost of introducing a height bias.

The primary problem with the result of the two thin screen inversion method is the current lack of average accuracy. The Fresnel transform inversion method is the optimal solution to the one thin screen inversion problem. In the implementation of this it was found, that not only was the position of the thin screen very important for the result, the shape of the screen also had a significant impact on the results [Mortensen and Høeg, 1998b]. In the one thin screen case the thin screen must be shaped to follow the tangent point, i.e., the thin screen must be bend, as the tangent point moves  $\approx 200$  km during an occultation (see Section 3.2.1). In the two thin screen case, the thin screens should be placed symmetrically around the tangent point to obtain the best approximation of the signal propagation path length. The initial attempt to solve this problem has been to introduce a slope of one of the thin screens. This is not a particularly good approximation close to the surface of the Earth where the tangent point moves rather quickly (see Section 3.2.1). The error profile seen in Figure 7.13 with a negative error for large heights, which changes to a positive, fast increasing error for small heights, can easily be attributed to the effect of using a straight line with a constant slope to approximate the movement of the tangent point during an occultation (see Figure 3.4). Thus, the implementation of the two thin screen inversion method should be modified to have bend screens.

A reasonable expectation for the effect of introducing bend screens in the two thin screen implementation is that the error will be lowered to at least half of the error of the Fresnel inversion method. This seems to be a reasonable expectation even though the height bias of the Fresnel in-

version method is avoided. The reason for this positive estimate is that a significant improvement of the result was the experience in the Fresnel transform inversion method when introducing a bend screen [Mortensen and Høeg, 1998b]. The improvement in the Fresnel transform inversion method was to lower the error by a factor of  $\approx 8$  close to the Earth, i.e., going from an error of 5-10 K below the height 5 km to less than 1 K.

The reason why the bend screens was not included from the beginning is the complexity of the two thin screen inversion method. With only one thin screen the inversion can be performed analytically, while the two thin screen inversion method is a nonlinear inversion method. This causes the inversion to be heavily based on numerical algorithms. Calculation of the solution to the correction matrix system in Newton's method is computationally demanding and complicated because the occultation problem is a complex problem with a fast varying phase, i.e., the problem is highly oscillating.

The example shows that the the two thin screen inversion method is a feasible inversion method when implemented as explained in this chapter. With this knowledge as basis, it is now possible to continue with optimizing first the two thin screen model to include bend screens, and next improving the numerical algorithms for the iterative solutions of the two inversion problems involved. Fully optimized, the method is expected to give very good results with the important potential of including horizontal information by changing the phase modulation from the first to the second screen.

Further improvements of the horizontal information and the average accuracy can be achieved by introducing more thin screens. Before the two thin screen method has been fully optimized there seems to be no reason to attempt this, as the two thin screen method seems promising with regards to the achievable accuracy so far. The complexity of the inversion method and thereby the computationally demands will be increased with every extra thin screen included. However, the increase in complexity will not be large compared to the complexity jump from one thin screen to two thin screens. So, three to four screens may well be a future goal.

## 7.6 Summary

The two thin screen inversion method has been introduced. The method is an extension of the Fresnel transform inversion method. When fully implemented and optimized the method can take horizontal variations into account. However, this will require more than one occultation or prior information from another source. The main problem of the method is that with two thin screens the inversion process becomes nonlinear. This causes the implementation of the method to be complicated and computationally demanding compared to the Fresnel transform inversion method. The method shows promising results although the implementation is far from optimized. The primary problem in the current implementation is that bend screens must be included to obtain accurate results.

# Chapter 8

## Conclusions

This thesis has two parts: The first part, consisting of Chapter 2 to Chapter 6, is a study of high vertical resolution methods for inversion of radio occultation data. The second part of the thesis, which is presented in Chapter 7, contains a description of a new inversion method. Below, a summary of the findings will be given and conclusions will be drawn. Finally, suggestions for future continuations of this research will be presented.

### 8.1 High Vertical Resolution Inversion Methods

Two high vertical resolution inversion methods are described in this thesis: The Fresnel transform inversion method and the back-propagation inversion method.

The Fresnel transform inversion method achieves high vertical resolution through the use of Fresnel diffraction theory. A thin screen, which moves along the tangent point of the occultation, approximates the atmosphere of the Earth. This thin screen approximation is too simple in the troposphere and limits the accuracy of the method. The temperature error of the obtained profiles exceeds 1 K below the height  $\approx 4$  km. Furthermore, the temperature results have a small height bias of  $\approx 100$  m in the troposphere. However, the results are quite good seen in relation to the simplicity of the approximation.

In the back-propagation inversion method a solution to the 2-D Helmholtz equation is used to back-propagate the measured electromagnetic field. The back-propagation has the effect of focusing the measured field. As the field is back-propagated to a virtual measurement line close to the tangent point of the occultation, high vertical resolution is achieved. At the virtual measurement line the geometrical optics approximation is applied to invert the field to refractive index profiles. The accuracy in smooth areas is as good as the geometrical optics inversion method and furthermore, large vertical gradients in the refractive index are resolved with high accuracy.

Common to the back-propagation inversion method and the Fresnel transform inversion method is, that the lower limit of the vertical resolution is  $\approx 100$  m, and that the methods can overcome most multipath problems. Also common to the two high vertical resolution inversion methods is, that a high level of thermal and atmospheric noise can lower the vertical resolution. None of the methods can take horizontal variations into account. This results in a low horizontal resolution of about 250 km. Furthermore, deviations from spherical symmetry on a smaller scale will affect the measurement and can seriously degrade the vertical resolution.

Through a series of examples of inversions of both simulated occultation data sets and GPS/MET occultation data sets the results of the two inversion methods are compared to each other, to the results obtained with the geometrical optics inversion method, and to ECMWF data. The back-propagation inversion results are at least as good as the geometrical optics inversion results. In areas with large gradients the back-propagation inversion method is clearly superior. The Fresnel transform inversion method has better vertical resolution than the geometrical optics inversion method, but the bias in the average result and the height bias significantly lowers the value of the results compared to the results of both the geometrical optics inversion method and the back-propagation inversion method. Both the back-propagation inversion method and the Fresnel transform inversion method can resolve multipath problems to a large extent. Horizontal variations cause similar problems for the two methods and for the geometrical optics inversion method. That is, even for a very smooth model atmosphere, the horizontal variation causes detectable errors in the temperature profiles. The results of inversion of GPS/MET occultation data with both the back-propagation inversion method and the Fresnel transform inversion method compare well with ECMWF data. As the ECMWF data have low vertical resolution, it cannot be determined if some of the variations in the inversion results are due to horizontal variations that has been mapped into the vertical profiles. However, the results are in accordance with the expectations with an average difference to the ECMWF data less than  $\pm 2$  K in most of the height range from the surface to 30 km.

The influence on the inversion results from severe horizontal gradients in the atmosphere has not been assessed in this thesis. This may in many cases show up to constitute a significant problem for achieving accurate refractive index profiles and temperature profiles with the existing inversion methods. Furthermore, the high vertical resolution methods described in this thesis cannot account for all multipath problems. That is, vertical gradients larger than  $\approx 8.5 \cdot 10^{-8} \text{ m}^{-1}$  cannot be resolved. How often this situation will occur in the atmosphere and limit the occultation inversion results has not been assessed.

High vertical resolution inversion methods will be of interest for tropopause studies. Around the tropopause the horizontal variations are expected to be limited and thus, the full potential of the vertical resolution can be exploited. GPS radio occultation data can therefore become an important contributor of data to studies of the small scale structure of the tropopause. In the lower troposphere, particularly where there is water vapor, horizontal variations are likely to degrade the resolution and the accuracy of the inversion methods. On the other hand, water vapor is expected to be the most frequent contributor to larger gradients that cause multipath

propagation.

Indeed, small scale variations in the atmosphere causing multipath propagation is a frequent phenomenon. This statement seems to be justified from the analysis of GPS/MET data and from simulation experiments. Thus, even in situations where high vertical resolution is not important, it must be recommended to use an inversion method that can take multipath propagation into account. The back-propagation inversion method is more accurate than the Fresnel transform, and both methods have the same limitations with respect to horizontal resolution. This indicates that among the currently existing inversion methods, the back-propagation inversion method is to be preferred.

## 8.2 A new Inversion Method

The two thin screen inversion method is a new method for inversion of radio occultation measurements which is described for the first time in this thesis. The method has been developed on the basis of the results presented in the first part of the thesis. The two thin screen inversion method is based on the same principles as the Fresnel transform inversion method. Only, two thin screens are used to model the atmosphere instead of one. Thus, by combination of several occultation measurements or use of information from other measurement methods, it will be possible to enhance the horizontal resolution by a factor of two compared to the currently used inversion methods. The vertical resolution will be the same as for the Fresnel transform inversion method, that is, very high.

When two thin screens are used to approximate the atmosphere in the model for the occultation measurement, the resulting inversion process becomes nonlinear. This causes the implementation of the two thin screen inversion method to be complicated and computationally demanding compared to the other inversion methods that have been described in this thesis. The method as it is described in this thesis is far from optimized. The primary problem in the current implementation is, that bend screens must be included to obtain accurate results. However, the results shown in this thesis are promising: The error of the temperature result is less than 1 K from 30 km down to  $\approx 5$  km in the current implementation, and it seems realistic to expect that this result can be improved to be less than 1 K error down to the surface in the optimal implementation with two bend screens. This expectation is based on the experience from the implementation of the Fresnel transform inversion method.

Whether the expected outcome matches the effort of implementing the two thin screen inversion method will of course depend on what the inversion results are to be used for. In order to explore the full information content in an occultation measurement, however, it is necessary to explore new inversion methods. The analytical inversion schemes, which can be derived for all the methods described in the first part of the thesis, are tied to the assumption of spherical symmetry in the atmosphere. Thus, any inversion method trying to circumvent this assumption

will become significantly more complex. The basic methodology of the two thin screen inversion method has been developed and proved to be working by the example shown in this thesis. Future work on this method is a question of optimization and exploration of the limitations of the method. Seen in this perspective the implementation and use of the two thin screen inversion method is a moderate task.

### 8.3 Future Research

The work presented in this thesis only concerns a small part of the research going on in the area of radio occultation measurements of the atmosphere of the Earth. However, to continue in line with the subject of this thesis, i.e., inversion methods, there are two subjects that seems to be of primary interest for future research.

First of all, the impact on the inversion results from horizontal gradients should be studied more carefully. Particularly, the high vertical resolution inversion methods have not been investigated very thoroughly in this respect. The impact on the inversion results from severe horizontal gradients, both along the signal propagation path and perpendicular to this, is not known. If this area is explored it will be easier to judge the extent of the need for using inversion methods with better horizontal resolution.

Secondly, the two thin screen inversion method should be optimized, and the limitations of its applicability should be studied. The optimization needed is both in the sense of implementing the method to achieve the most accurate results, but also in the sense of optimization of the numerical algorithm to decrease the computational effort. Once this has been done, the limits of the horizontal resolution with the two thin screen inversion method should be investigated.

## Appendix A

# The Phase Modulation in a Spherically Symmetric Atmosphere

The phase modulation  $\psi_l$ ,  $l = 1, 2$  is defined from the refractive index  $n_l$  as

$$\psi_l(\xi) = \int_T (n_l - 1) d\tau, \quad (\text{A.1})$$

where  $T$  denotes the propagation path of the ray through the atmosphere, and  $d\tau$  is the infinitesimal length along the path. It is assumed that the ray path  $T$  starts outside the atmosphere of the Earth. The ray path stops at the tangent point since the phase modulation  $\psi_l$  covers half of the atmosphere.

The parameters describing the ray path propagation in a spherically symmetric atmosphere are illustrated in Figure A.1. In the figure,  $\hat{T}$  is the unit direction vector of the ray path,  $\vec{r}$  is the position vector,  $\theta$  is the angle between the direction vector of the  $x$ -axis and  $\vec{r}$ , and  $a$  is the impact parameter.

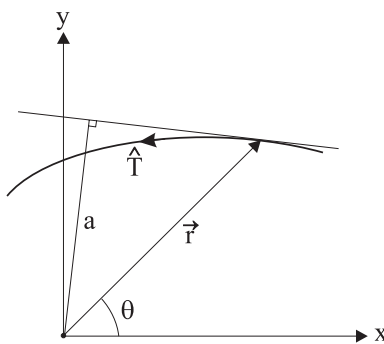


Figure A.1: *Ray path in a spherically symmetric atmosphere.*

The position vector  $\vec{r}$  can be expressed in polar coordinates  $(r, \theta)$  as

$$\vec{r} = (x, y) = (r \cos \theta, r \sin \theta). \quad (\text{A.2})$$

In a spherically symmetric atmosphere the differential relation between  $\theta$  and  $r$  is given by [Born and Wolf, 1993, sec. 3.2]

$$\frac{d\theta}{dr} = \frac{a}{r\sqrt{r^2 n_l^2 - a^2}}. \quad (\text{A.3})$$

Thus, the position vector of the ray path  $T$  can be expressed in polar coordinates (A.2) as a function of the radius, i.e.,  $\vec{r}(r)$ . By use of this, the expression for the phase modulation can be rewritten to

$$\psi_l(\xi) = \int_T (n - 1) d\tau = \int_{\xi+R_e}^{\infty} (n_l(r) - 1) \cdot \|\vec{r}'(r)\| dr \quad (\text{A.4})$$

where  $\xi + R_e$  is the tangent height, which is connected to the impact parameter as  $a = n_l(\xi + R_e)$ .

The derivative of  $\vec{r}(r)$  is given by

$$\vec{r}'(r) = \left( \cos \theta - r \sin \theta \frac{d\theta}{dr}, \sin \theta + r \cos \theta \frac{d\theta}{dr} \right), \quad (\text{A.5})$$

and the norm of this is given by

$$\|\vec{r}'(r)\| = \sqrt{1 + r^2 \left( \frac{d\theta}{dr} \right)^2} = \frac{r n_l}{\sqrt{r^2 n_l^2 - a^2}} \quad (\text{A.6})$$

in which the relation (A.3) has been used.

Finally, the expression for the phase modulation becomes

$$\psi_l(\xi) = \int_{\xi+R_e}^{\infty} (n_l(r) - 1) \cdot \frac{r n_l}{\sqrt{r^2 n_l^2 - a^2}} dr \quad (\text{A.7})$$

which is the expression given in Section 7.2. The atmosphere is only required to be locally spherically symmetric as  $\psi_l$ ,  $l = 1, 2$  can be calculated individually for each half of the atmosphere.

## Appendix B

### Papers

#### **Inversion of GPS occultation measurements using Fresnel diffraction theory**

By M. D. Mortensen and P. Høeg  
*Geophysical Research Letters*, 25, 2441-2444, 1998.



# Vertical resolution approaching 100 m for GPS occultations of the Earth's atmosphere

By M. D. Mortensen, R. P. Linfield, and E. R. Kursinski  
*Radio Science*, accepted for publication, 1999.



# References

- Ahmad, B., Accuracy and resolution of atmospheric profiles obtained from radio occultation measurements, Ph.D. thesis, Center for Radar Astronomy, Stanford University, 1998.
- Ahmad, B., and G. L. Tyler, Systematic errors in atmospheric profiles obtained from abelian inversion of radio occultation data: Effects of large-scale horizontal gradients, *Journal of Geophysical Research - Atmospheres*, 1998a, submitted.
- Ahmad, B., and G. L. Tyler, The two-dimensional resolution kernel associated with retrieval of ionospheric and atmospheric refractivity profiles by abelian inversion of radio occultation phase data, *Radio Science*, *33*, 129–142, 1998b.
- Belloul, M., and A. Hauchecorne, Effect of periodic horizontal gradients on the retrieval of atmospheric profiles from occultation measurements, *Radio Science*, *32*, 469–478, 1997.
- Bevis, M., S. Businger, S. Chiswell, T. A. Herring, R. A. Anthes, C. Rocken, and R. H. Ware, GPS meteorology: Mapping zenith wet delays onto precipitable water, *Journal of Applied Meteorology*, *33*, 379–386, 1994.
- Blok, H., and M. Oristaglio, Wavefield imaging and inversion in electromagnetics and acoustics, *Tech. Rep. Rep. nr. Et/EM 1995-21*, Centre for Technical Geoscience, Delft University of Technology, 1995.
- Born, M., and E. Wolf, *Principles of Optics*, 6th ed., Pergamon Press, Oxford, England, 1993.
- Chew, W. C., *Waves and Fields in Inhomogeneous Media*, IEEE PRESS series on Electromagnetic Waves, IEEE Press, New York, 1995.
- Collin, R. E., *Antennas and Wave Propagation*, McGraw-Hill series in Electrical Engineering, McGraw-Hill Book Company, Singapore, 1985.
- Fälthammar, C.-G., Space physics, *Tech. rep.*, Department of Plasma Physics, Alfvén Laboratory, Royal Institute of Technology, Stockholm, Sweden, 1994.
- Fischback, F. F., A satellite method for pressure and temperature below 24 km, *Bulletin American Meteorological Society*, *46*, 528–532, 1965.
- Fjeldbo, G., and V. R. Eshleman, The bistatic radar-occultation method for the study of planetary atmospheres, *Journal of Geophysical Research*, *70*, 3217–3225, 1965.

- Fjeldbo, G., and V. R. Eshleman, The atmosphere of Mars analyzed by integral inversion of the Mariner IV occultation data, *Planet. Space Sci.*, *16*, 1035–1059, 1968.
- Fjeldbo, G., J. Kliore, and V. Eshleman, The neutral atmosphere of Venus as studied with the Mariner V radio occultation experiments, *The Astronomical Journal*, *76*, 123–140, 1971.
- Goodman, *Introduction to Fourier Optics*, Classic Textbook Reissue Series, McGraw-Hill, New York, USA, 1986.
- Gorbunov, M., Accuracy of the refractometric method in a horizontally non-uniform atmosphere, *Atmos. and Ocean. Phys.*, *24*, 1988.
- Gorbunov, M., and A. S. Gurvich, Microlab-1 experiment: Multipath effects in the lower troposphere, *Journal of Geophysical Research*, *103*, 13,819–13,826, 1998a.
- Gorbunov, M., and A. S. Gurvich, Algorithms of inversion of Microlab-1 satellite data including effects of multipath propagation, *Int. J. Remote Sensing*, *19*, 2283–2300, 1998b.
- Gorbunov, M., A. Gurvich, and L. Bengtsson, Advanced algorithms of inversion of GPS/MET satellite data and their application to reconstruction of temperature and humidity, *Tech. Rep. 211*, Max-Planck-Institute for Meteorology, Hamburg, 1996.
- Grimault, C., A multiple phase screen technique for electromagnetic wave propagation through random ionospheric irregularities, *Radio Science*, *33*, 595–605, 1998.
- Gurvich, A., and S. V. Sokolovskiy, Reconstruction of a pressure field by remote refractometry from space, *Izvestiya, Atmospheric and Oceanic Physics*, *21*, 7–13, 1985.
- Hajj, G. A., E. Kursinski, W. Bertinger, and L. Romans, Assessment of GPS occultations for atmospheric profiling, in *Proceedings of the 7th conference on satellite meteorology and oceanography*, 1994, j4.9.
- Hansen, P. C., *Rank-Deficient and Discrete Ill-Posed Problems: Numerical Aspects of Linear Inversion*, SIAM monographs on mathematical modeling and computation, SIAM, Philadelphia, USA, 1997.
- Hardy, K. R., D. P. Hinson, G. L. Tyler, and E. Kursinski, Atmospheric profiles from active space-based radio measurements, in *Proceedings of the 6th conference on satellite meteorology and oceanography*, 1992.
- Hardy, K. R., G. A. Hajj, and E. Kursinski, Accuracies of atmospheric profiles obtained from GPS occultations, *International Journal of Satellite Communications*, *12*, 463–473, 1994.
- Harris, F. J., On the use of windows for harmonic analysis with the discrete Fourier transform, *Proceedings of the IEEE*, *66*, 51–83, 1978.
- Haugstad, B. S., Effects of the inhomogeneous background on radiation propagating through turbulent planetary atmospheres, *Radio Science*, *13*, 435–440, 1978.

- Hedin, A. E., Extension of the MSIS thermosphere model into the middle and lower atmosphere, *Journal of Geophysical Research*, *96*, 1159–1172, 1991.
- Hinson, D., and J. Magalhaes, Equatorial waves in the stratosphere of Uranus, *Icarus*, *94*, 64–91, 1991.
- Hinson, D. P., F. M. Flasar, A. J. Kliore, P. J. Schinder, J. D. Twicken, and R. G. Herrera, Jupiter's ionosphere: Results from the first Galileo radio occultation experiment, *Geophysical Research Letters*, *24*, 2107–2110, 1997.
- Hinson, D. P., J. D. Twicken, and E. T. Karayel, Jupiter's ionosphere: New results from Voyager 2 radio occultation measurements, *Journal of Geophysical Research*, *103*, 9505–9520, 1998.
- Hocke, K., Inversion of GPS meteorology data, *Annales Geophysicae*, *15*, 443–450, 1997.
- Hocke, K., A. G. Pavelyev, O. I. Yakovlev, L. Barthes, and N. Jakowski, Radio occultation data analysis by the radioholographic method, *Journal of of Atmospheric and Solar-Terrestrial Physics*, 1999, submitted.
- Høeg, P., and C. Ø. Jensen, Global tropopause distribution as a climate change indicator, in *ESTEC Radio Occultation Studies 1996-1998*, TERMA electronics AS, Denmark, 1998, ESA Contracts Nos. 11930/96/NL/CN, 11818/96/NL/CN, 12025/96/NL/CN.
- Høeg, P., A. Hauchecorne, G. Kirhcengast, S. Syndergaard, B. Belloul, R. Leitinger, and W. Rothleitner, Derivation of atmospheric properties using radio occultation technique, *Scientific Report 95-4*, Danish Meteorological Institute, 1995.
- Hofmann-Wellenhof, B., H. Lichtenegger, and J. Collins, *GPS Theory and Practice*, 2nd ed., Springer-Verlag, Wien, 1993.
- Holtan, J. R., *An Introduction to Dynamic Meteorology*, 3rd ed., Academic Press, Inc., San Diego, California, 1992.
- Hubbard, W., J. Jokipii, and B. Wilking, Stellar occultations by turbulent planetary atmospheres: A wave-optical theory including a finite scale height, *Icarus*, *34*, 374–395, 1978.
- Karayel, E. T., and D. P. Hinson, Sub-fresnel-scale vertical resolution in atmospheric profiles from radio occultation, *Radio Science*, *32*, 411–423, 1997.
- Kliore, A., P. Woiceshyn, and W. Hubbard, Temperature of the atmosphere of Jupiter from Pioneer 10/11 radio occultations, *Geophysical Research Letters*, *3*, 113–116, 1976.
- Kuo, Y., X. Xou, and W. Huang, The impact of GPS data on the prediction of an extratropical cyclone: An observing system simulation experiment, *J. Dyn. Atmos. Ocean*, *27*, 439–470, 1997.
- Kuo, Y., X. Xou, S. Chen, W. Huang, Y. Guo, R. Anthes, M. Exner, D. Hunt, C. Rocken, and S. Sokolovskiy, A GPS/MET sounding through an intense upper-level front, *Bull. of Amer. Meteor. Society*, *79*, 616–626, 1998.

- Kursinski, E., G. Hajj, W. I. Bertiger, S. S. Leroy, T. Meehan, L. Romans, J. Schofield, J. Schofield, D. McCleese, W. Melbourne, C. Thornton, T. Yunck, J. Eyre, and R. Nagatani, Initial results of radio occultation observations of Earth's atmosphere using the Global Positioning System, *Science*, *271*, 1107–1110, 1996.
- Kursinski, E., G. Hajj, K. Hardy, J. Schofield, and R. Linfield, Observing Earth's atmosphere with radio occultation measurements using GPS, *J. Geophys. Res.*, *102*, 23,429–23,465, 1997.
- Kursinski, E. R., The GPS radio occultation concept: Theoretical performance and initial results, Ph.D. thesis, California Institute of Technology, 1997.
- Leroy, S. S., Measurement of geopotential heights by GPS radio occultation, *Journal of Geophysical Research*, *102*, 6971–6986, 1997.
- Lindal, G. F., The atmosphere of Neptune: An analysis of radio occultation data acquired with Voyager 2, *The Astronomical Journal*, *103*, 967–982, 1992.
- Marouf, E. A., G. Tyler, and P. Rosen, Profiling Saturn's rings by radio occultation, *Icarus*, *68*, 120–166, 1986.
- McIlveen, R., *Basic Meteorology a physical outline*, Van Nostrand Reinhold, Berkshire, England, 1986.
- Melbourne, W., E. Davis, C. Duncan, G. Hajj, K. Hardy, E. Kursinski, T. Meehan, L. Young, and T. Yunck, The application of spaceborne GPS to atmospheric limb sounding and global change monitoring, *JPL Publication 94-18*, JPL, Pasadena, CA, USA, 1994.
- Mortensen, M. D., The back-propagation method for inversion of radio occultation data, *DMI Scientific Report 98-14*, Dan. Meteorol. Inst., Copenhagen, Denmark, 1998.
- Mortensen, M. D., Non-linear high resolution inversion of radio occultation data, *DMI Scientific Report 99-5*, Dan. Meteorol. Inst., Copenhagen, Denmark, 1999.
- Mortensen, M. D., and P. Høeg, Inversion of GPS occultation measurements using Fresnel diffraction theory, *Geophysical Research Letters*, *25*, 2441–2444, 1998a.
- Mortensen, M. D., and P. Høeg, Resolution properties in atmospheric profiling with GPS, *DMI Scientific Report 98-4*, Dan. Meteorol. Inst., Copenhagen, Denmark, 1998b.
- Mortensen, M. D., R. Linfield, and E. Kursinski, Vertical resolution approaching 100m for GPS occultations of the Earth's atmosphere, *Radio Science*, 1999, accepted, paper no. 1999RS900093.
- Phinney, R. A., and D. L. Anderson, On the radio occultation method for studying planetary atmospheres, *Journal of Geophysical Research*, *73*, 1819–1827, 1968.
- Rocken, C., R. Anthes, M. Exner, D. Hunt, S. Sokolovskiy, R. Ware, M. Gorbunov, W. Schreiner, D. Feng, B. Herman, Y. Kuo, and X. Zou, Analysis and validation of GPS/MET data in the neutral atmosphere, *Journal of Geophysical Research*, *102*, 29,849–29,866, 1997.

- Shaw, D. B., P. Lönnberg, A. Hollingsworth, and P. Undén, Data assimilation: The 1984/85 revisions of the ECMWF mass and wind analysis, *Q. J. R. Meteorol. Soc.*, *113*, 533–566, 1987.
- Skolnik, M. I., *Introduction to Radar Systems*, 2nd ed., McGraw-Hill Book Company, 1980.
- Sokolovskiy, S., and D. Hunt, Statistical optimization approach for GPS/MET data inversions, *URSI GPS/MET Workshop*, 1996, Tucson, Arizona.
- Steiner, A. K., High resolution sounding of key climate variables using the radio occultation technique, Ph.D. thesis, IMG/UoG, University of Graz, Austria, 1998.
- Steiner, A. K., and G. Kirchengast, Gravity wave spectra from GPS/MET occultation observations, *Journal of Atmospheric and Oceanic Technology*, 1999, in press.
- Steiner, A. K., G. Kirchengast, and H. P. Ladreiter, Inversion, error analysis, and validation of GPS/MET occultation data, *Annales Geophysicae*, *17*, 122–138, 1999.
- Syndergaard, S., Modeling the impact of the Earth's oblateness on the retrieval of temperature and pressure profiles from limb sounding, *Journal of Atmospheric and Solar-Terrestrial Physics*, *60*, 171–180, 1998.
- Syndergaard, S., On the ionosphere calibration in GPS radio occultation measurements, *Radio Science*, 1999a, submitted.
- Syndergaard, S., Retrieval analysis and methodologies in atmospheric limb sounding using the GNSS radio occultation technique, Ph.D. thesis, Niels Bohr Institute for Astronomy, Physics and Geophysics, Faculty of Science, University of Copenhagen, Denmark, 1999b.
- Tatarski, V. I., *Wave Propagation in a Turbulent Medium*, Dover Publications, Inc., New York, N. Y., 1967, 299 pp.
- Tyler, G. L., Radio propagation experiments in the outer Solar system with Voyager, *Proceedings of the IEEE*, *75*, 1404–1431, 1987.
- Tyler, G. L., D. N. Sweetnam, J. D. Anderson, S. E. Borutzki, J. K. Campbell, V. R. Eshleman, D. L. Gresh, E. M. Gurrola, D. P. Hinson, N. Kawashima, E. R. Kursinski, G. S. Levy, G. F. Lindal, J. R. Lyons, E. A. Marouf, P. A. Rosen, R. A. Simpson, and G. E. Wood, Voyager radio science observations of Neptune and Triton, *Science*, *246*, 1466–1473, 1989.
- Vorob'ev, V. V., and T. G. Krasi'nikova, Estimation of the accuracy of the atmospheric refractive index recovery from Doppler shift measurements at frequencies used in the NAVSTAR system, *Physics of the Atmosphere and Ocean*, *29*, 602–609, 1994.
- Ware, R., M. Exner, D. Feng, M. Gorbunov, K. Hardy, B. Herman, Y. Kuo, T. Meehan, W. Melbourne, C. Rocken, W. Schreiner, S. Sokolovskiy, F. Solheim, X. Zou, R. Anthes, S. Businger, and K. Trenberth, GPS sounding of the atmosphere from low Earth orbit: Preliminary results, *Bull. of the American Meteorological Society*, *77*, 19–40, 1996.

- 
- Wing, G. M., *A primer on integral equations of the first kind: The problem of deconvolution and unfolding*, SIAM, Philadelphia, USA, 1991.
- Zou, X., F. Vandenberghe, B. Wang, M. E. Gorbunov, Y.-H. Kou, S. Sokolovskiy, J. C. Chang, J. G. Sela, and R. Anthes, Direct assimilation of GPS/MET refraction angle measurements: Part I: Concept and results of raytracing, *Journal of Geophysical Research*, 1998a, submitted.
- Zou, X., B. Wang, F. Vandenberghe, M. E. Gorbunov, Y.-H. Kou, S. Sokolovskiy, J. C. Chang, J. G. Sela, and R. Anthes, Direct assimilation of GPS/MET refraction angle measurements: Part II: Variational assimilation using adjoint techniques, *Journal of Geophysical Research*, 1998b, submitted.